Search for Associated Production of Dark Matter with a Higgs Boson at CMS

arXiv:1703.05236

Shin-Shan Eiko Yu
Department of Physics, National Central University

3 October 2017
HEP Seminar, Chung Yuan Christian University

Outline

- Why search for dark matter at LHC?
- Why mono Higgs?
- Searches for dark matter via the mono-Higgs channel at CMS
- Connection with other dark matter searches
- Conclusion and Outlook

Why Dark Matter?

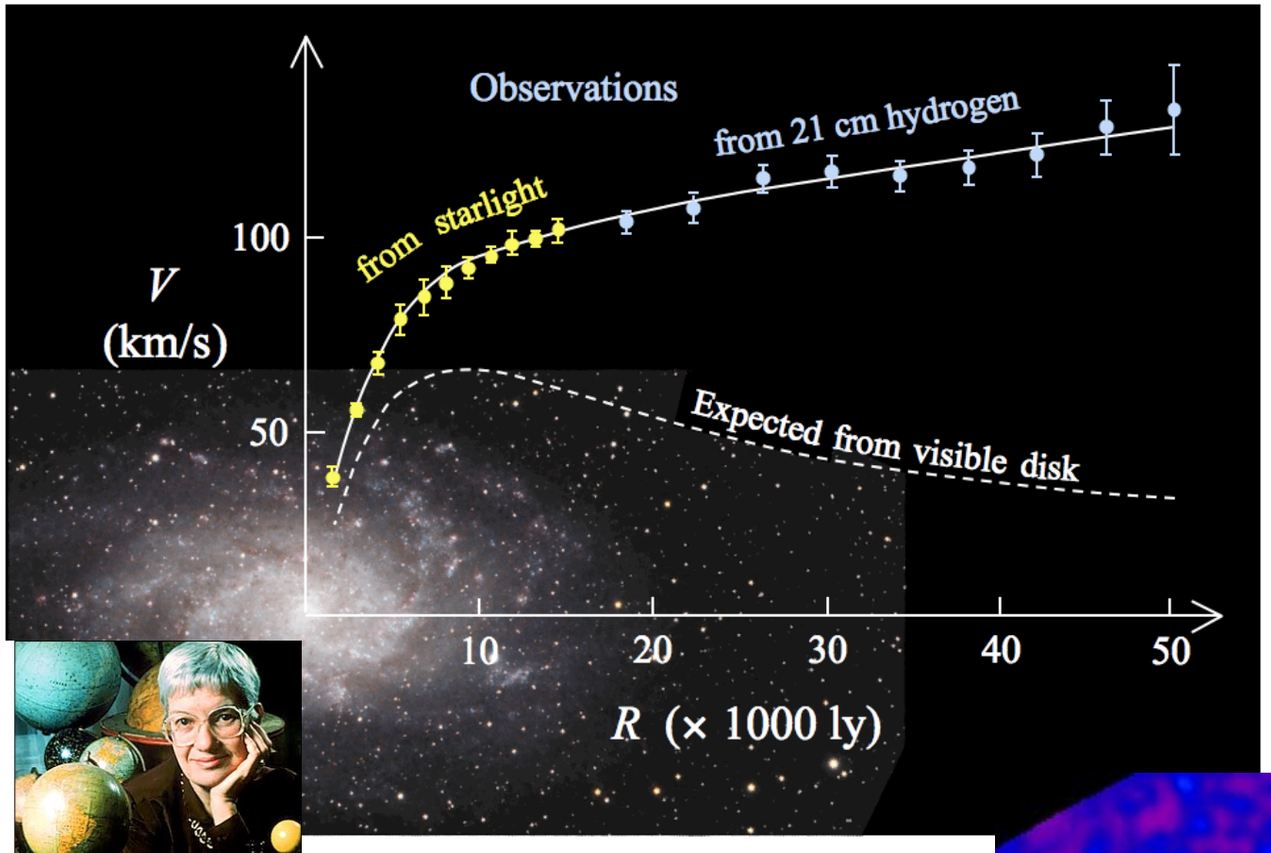

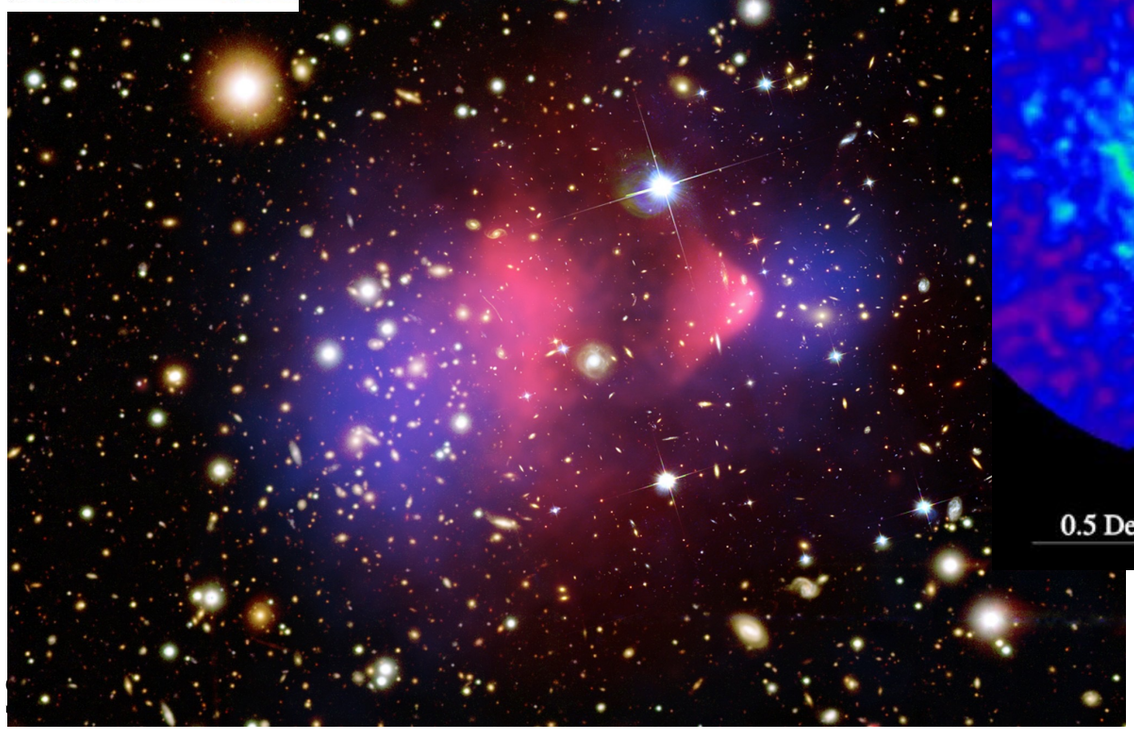

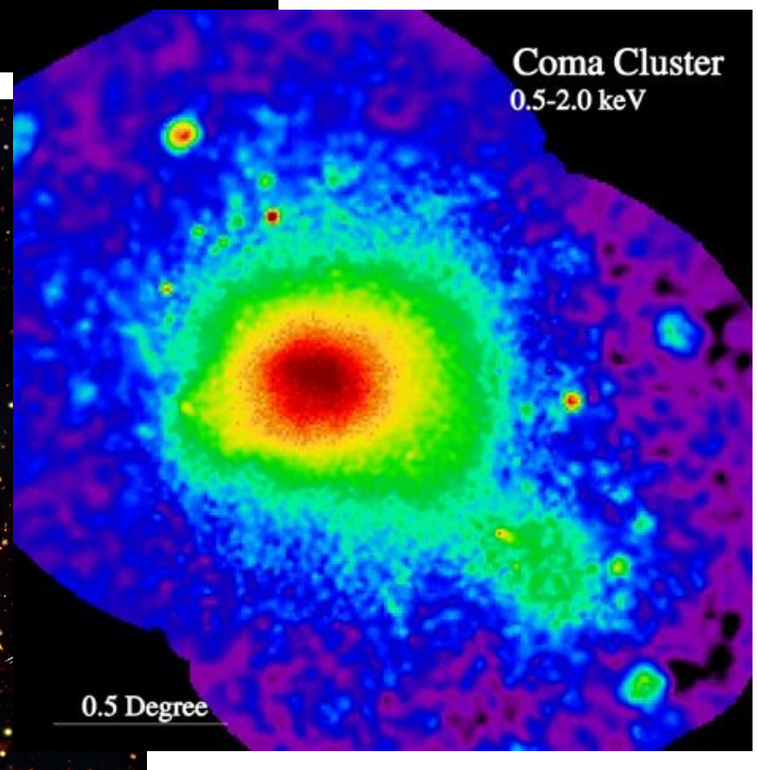

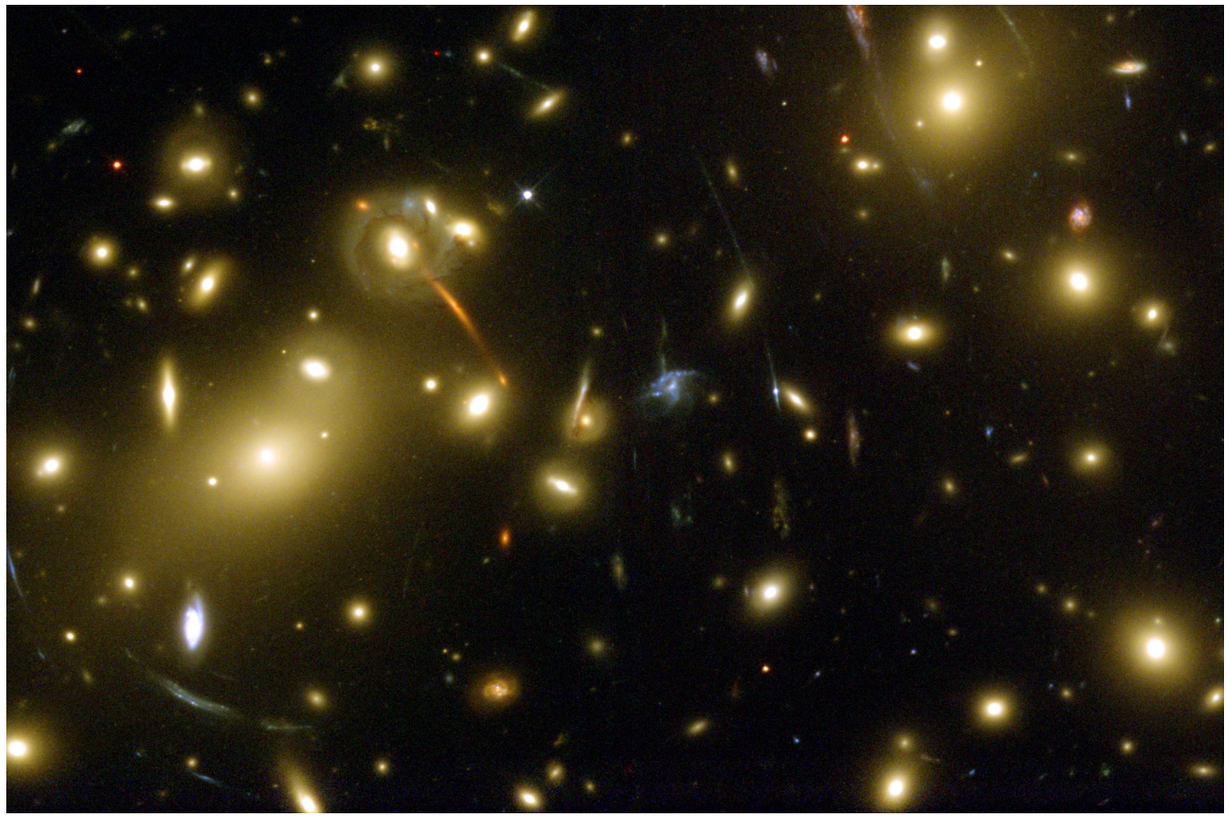

Why Dark Matter at LHC?

- Evidence of dark matter well established from astrophysical observations
  - The exact nature of DM is still unknown
- LHC provides a prime laboratory for production of DM
  - Can probe a wide range of DM/SM interaction types

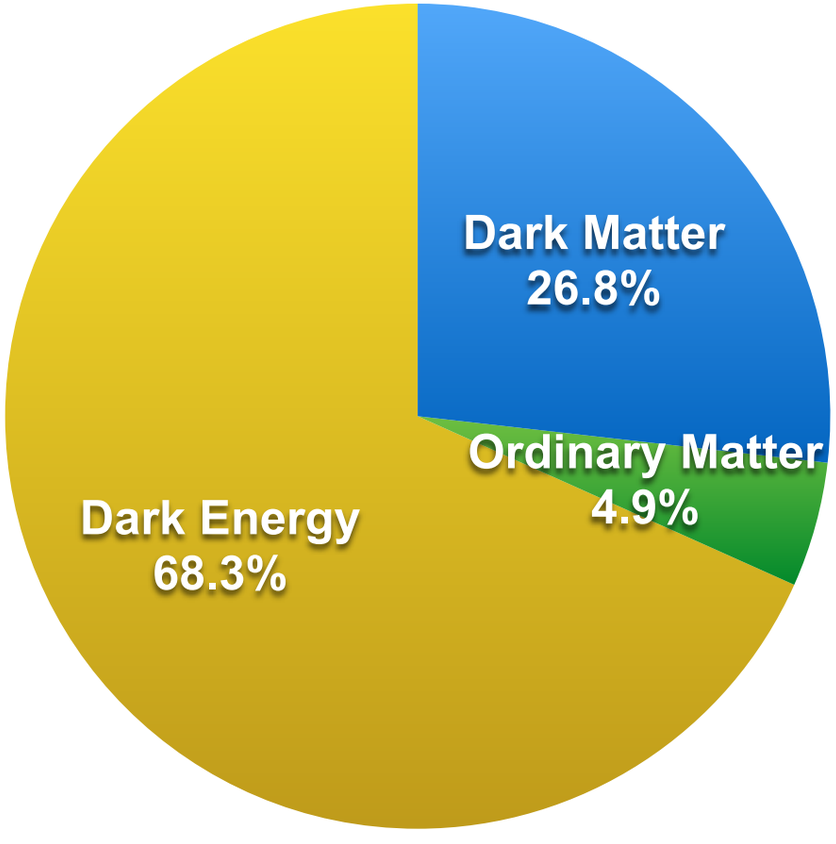

Matter/Energy Today

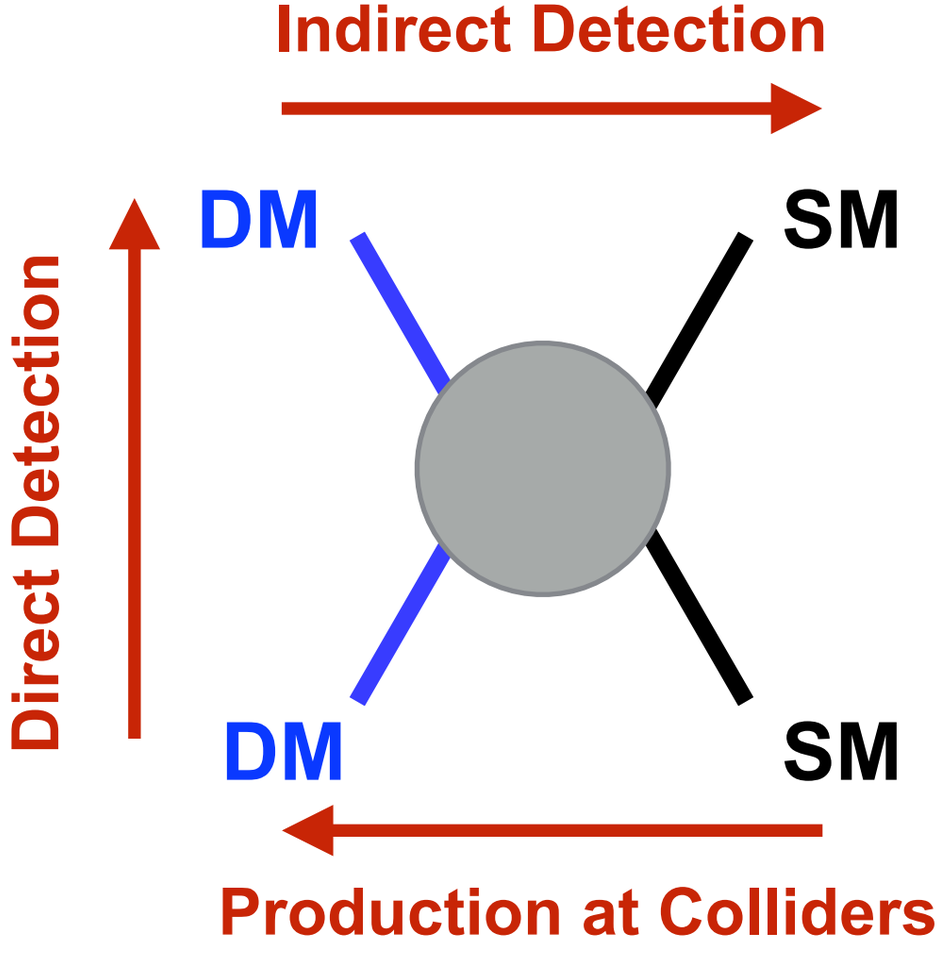

What Is Dark Matter at Colliders?

- Neutral, weakly-interactive, massive, and stable on the distance-scales of tens of meters
  - Dark matter appears as missing transverse momentum in collider detectors

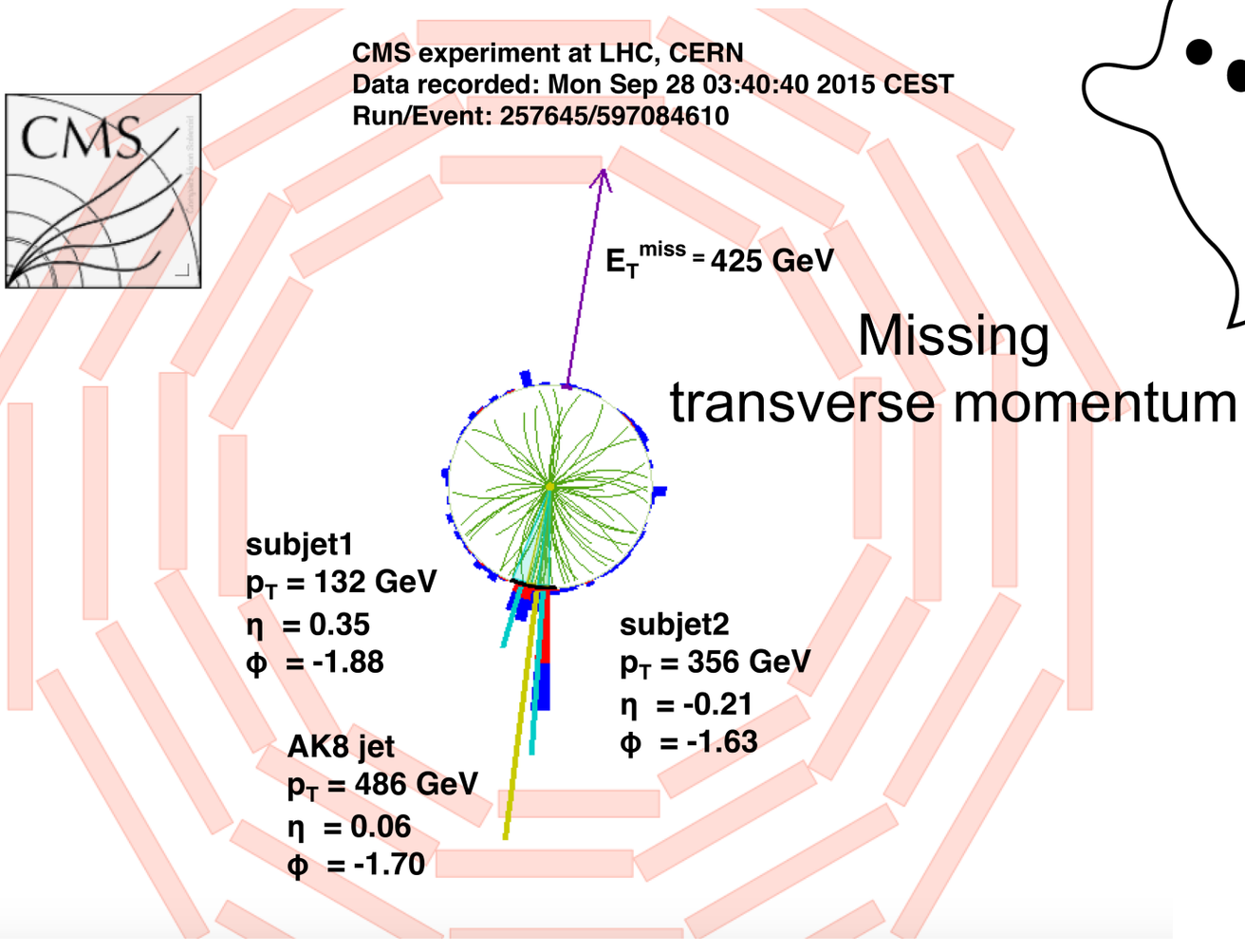

Missing transverse momentum

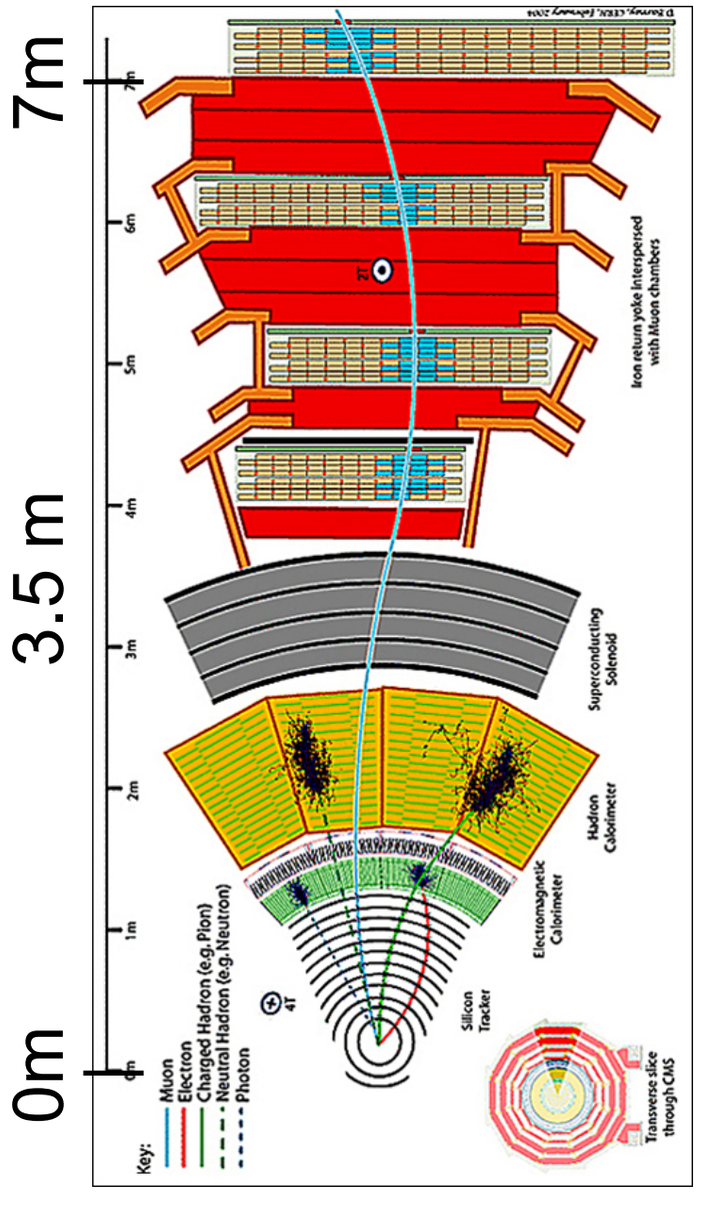

Searches for Dark Matter at LHC

- Typically look for E_T^{miss} + X
  - X= jet (g, q), γ, W, Z, H, tt, bb, t
- Use simplified models to interpret results (arXiv: 1507.00966)
  - DM particle is a Dirac fermion
  - DM particles are pair-produced
  - A new massive particle mediates the DM-SM interaction
  - Minimal flavor violation
  - Mediator has minimal decay width
- Minimal set of parameters
  - coupling structure, M_{MED}, m_{DM}, g_{SM}, g_{DM}

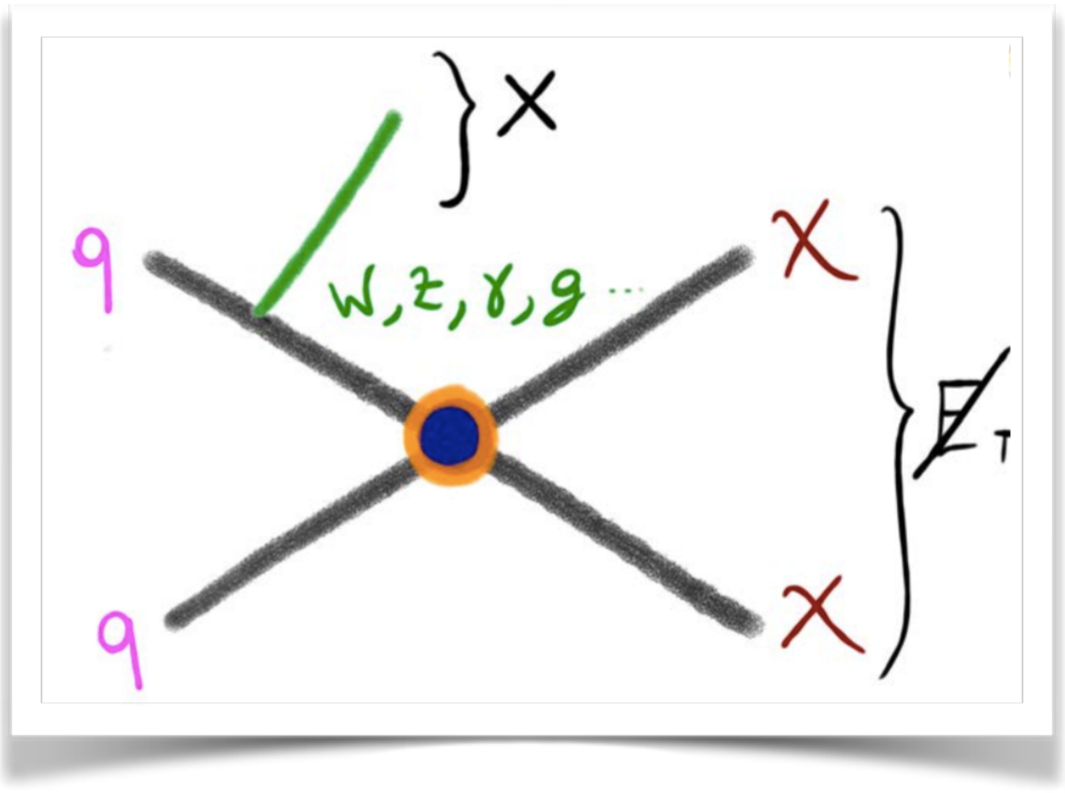

Evolution of Models for Direct DM Production

Effective Field Theory

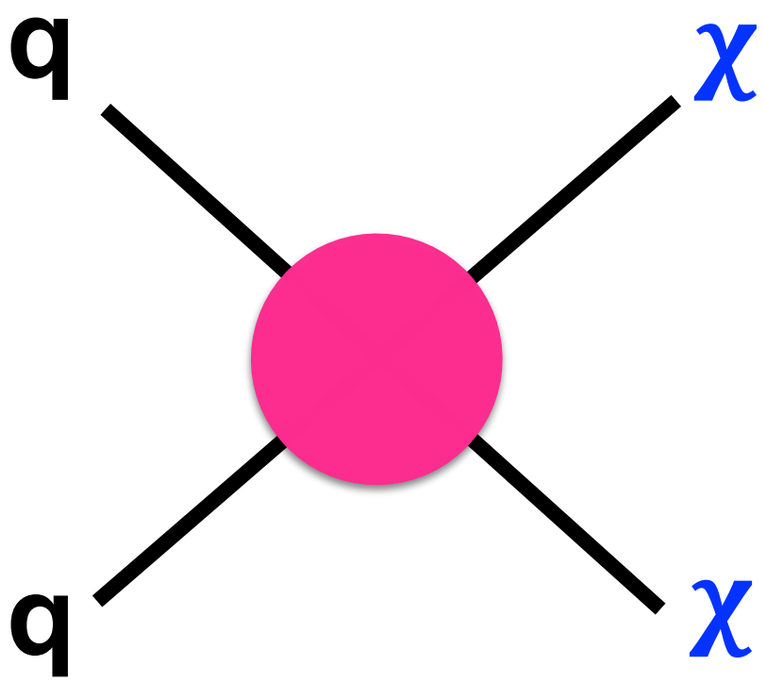

$$\frac{g_\chi g_q}{Q_{\rm tr}^2 - M^2} = -\frac{g_\chi g_q}{M^2}\left(1 + \frac{Q_{\rm tr}^2}{M^2} + \mathrm{O}\left(\frac{Q_{\rm tr}^4}{M^4}\right)\right)$$

$$\simeq -\frac{g_\chi g_q}{M^2} = -\frac{1}{M_*^2}$$

$$M_* \equiv \frac{M}{\sqrt{g_\chi g_q}}$$

- m_{DM}, M_*, underlying coupling type, DM types

- Valid when $Q_{tr}^2 \ll M^2$

Evolution of Models for Direct DM Production

Effective Field Theory

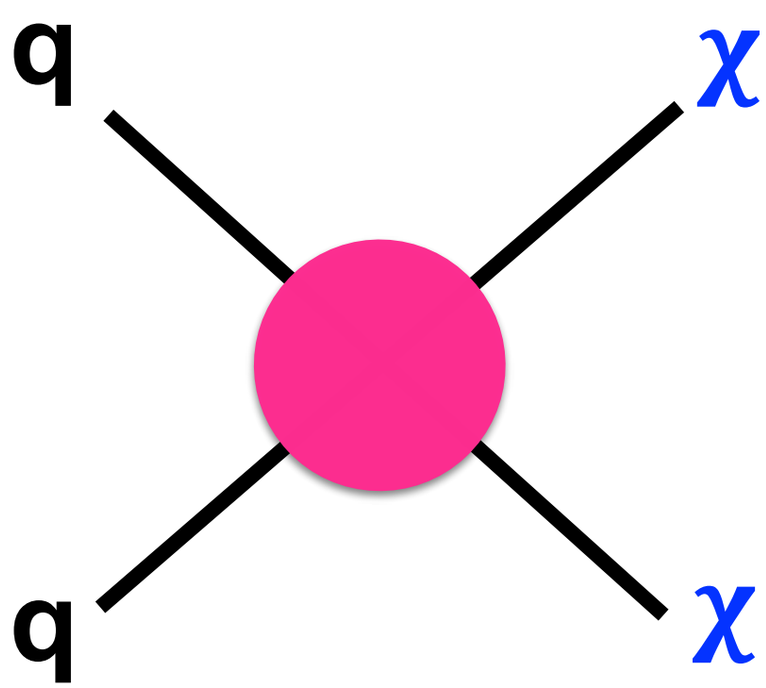

- m_{DM}, M_*, underlying coupling type, DM types
- Valid when $Q_{tr}^2 \ll M^2$

Simplified Model

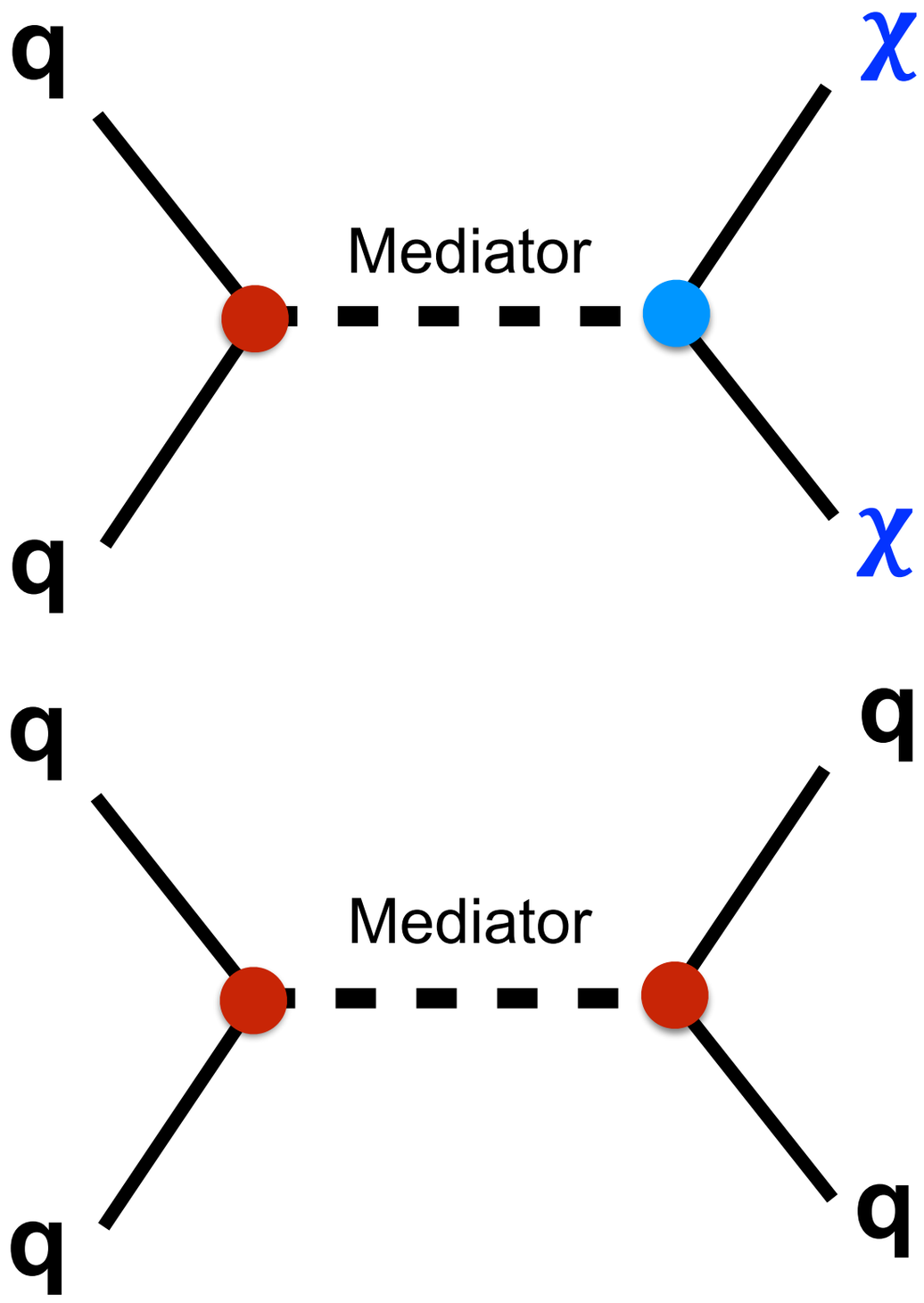

Why Mono-Higgs?

- DM searches at LHC have been performed with various mono-X + missing Et signatures (where X=W, Z, jet, or γ).
- Here, X could be emitted directly from a quark as ISR or as part of new effective vertex coupling of DM to SM
- Unlike W, Z, jet, or γ, Higgs ISR is highly suppressed→mono-Higgs signal could probe directly the structure of the effective DM-SM coupling

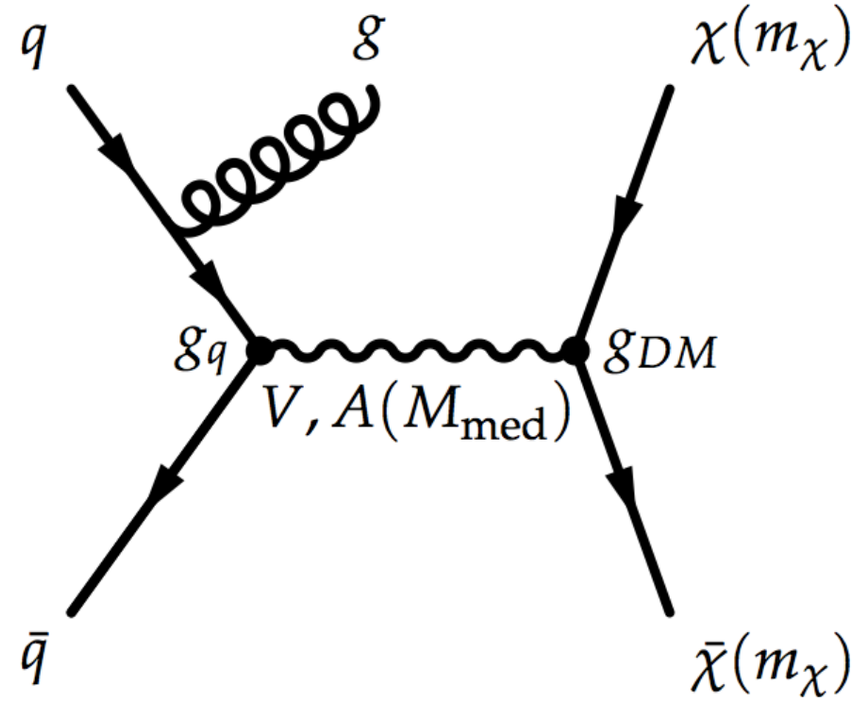

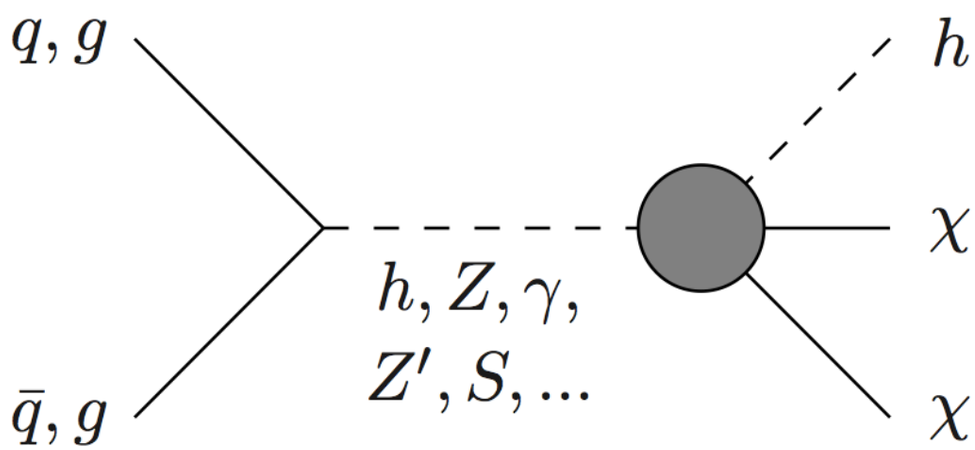

Mono-Higgs Models on the Market

arXiv:1312.2592
axXiv:1402.7074

- Effective Field Theory: DM couples directly to Higgs via n-dimensional operator, valid at energies below cutoff scale Λ. →6 EFTs

- Simplified Models: New massive particle mediates Higgs-DM interaction, including baryonic Z', Z' from hidden sector, pseudo scalar A^0 from 2HDM, and scalar mediator

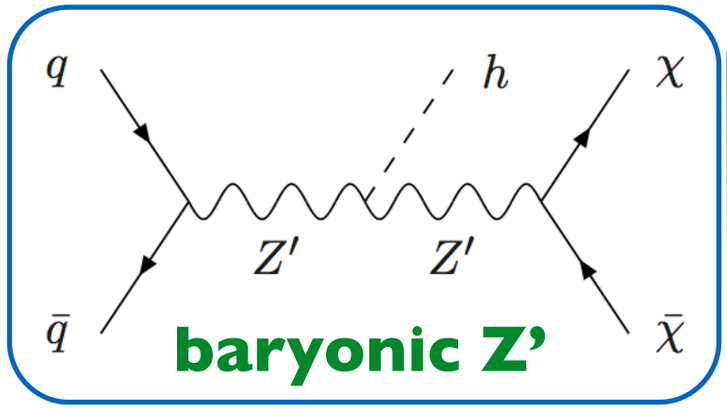

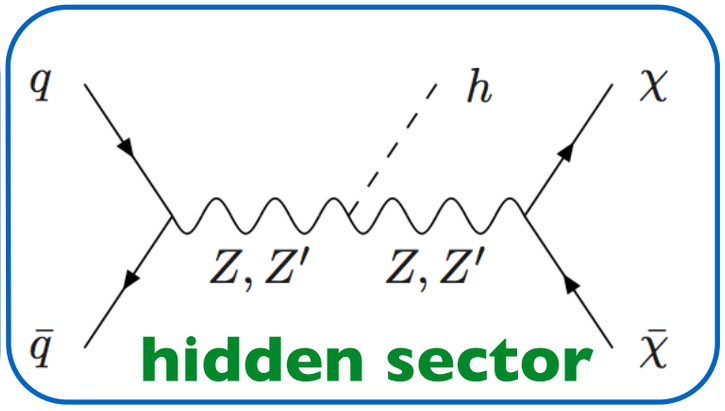

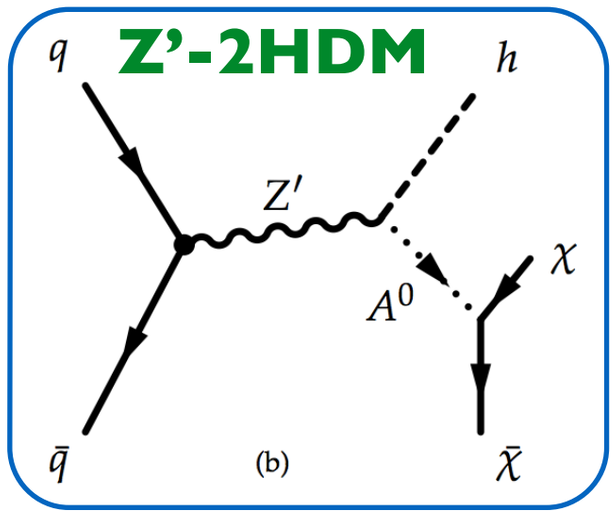

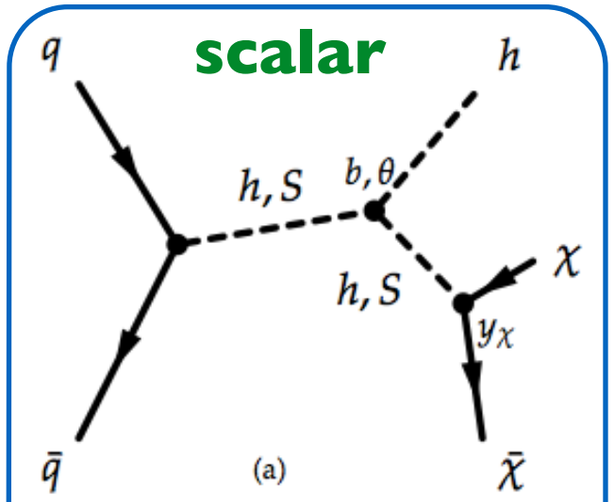

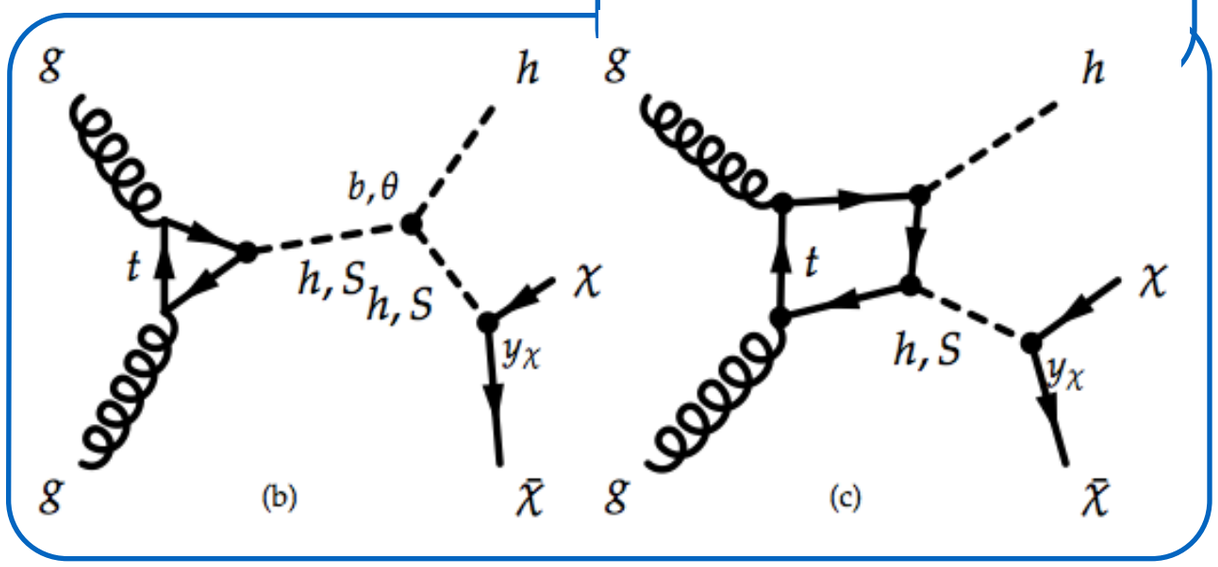

Our Benchmark Model: Z'-2HDM

M_{MED}=100 GeV

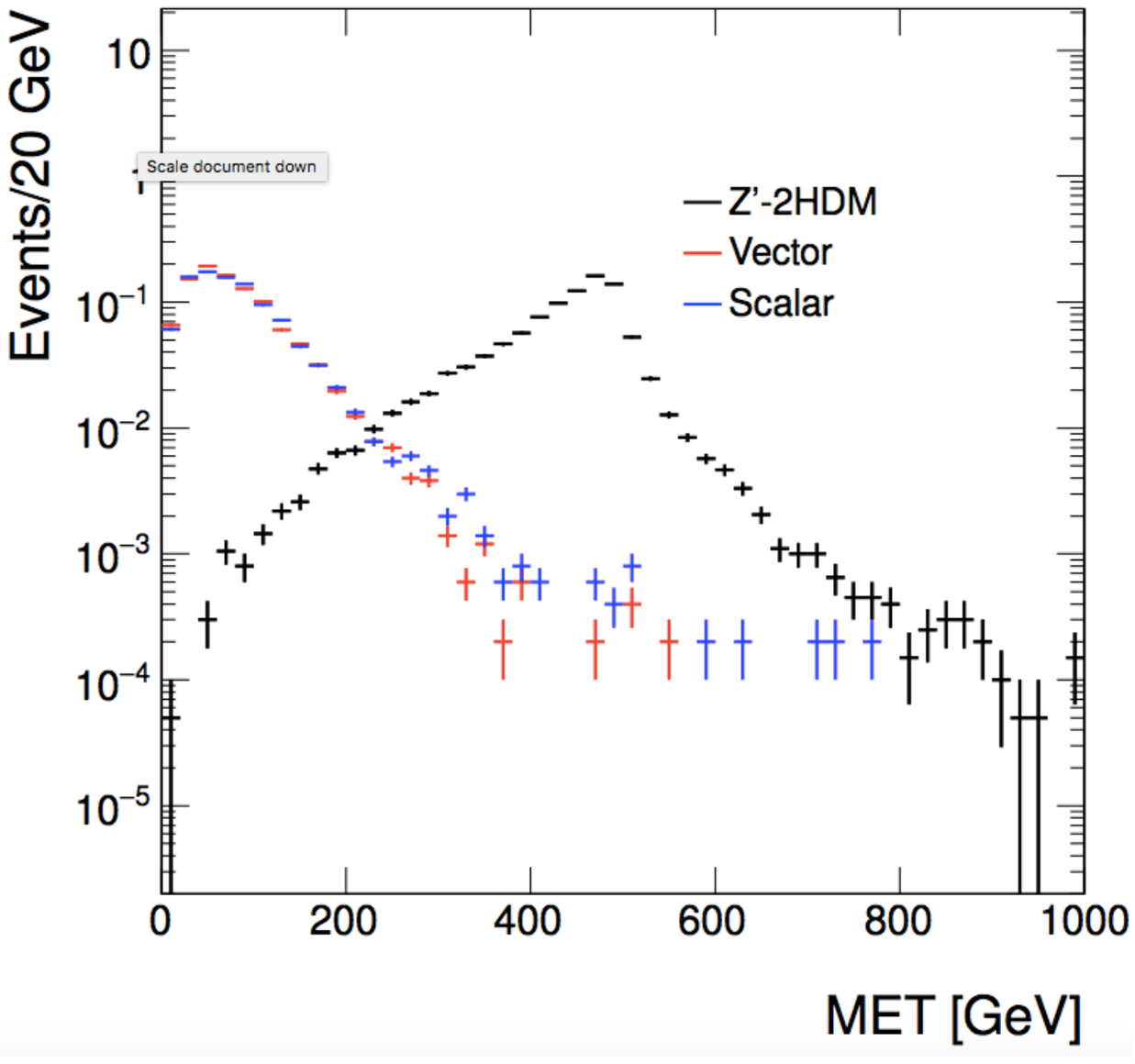

M_{MED}=1TeV

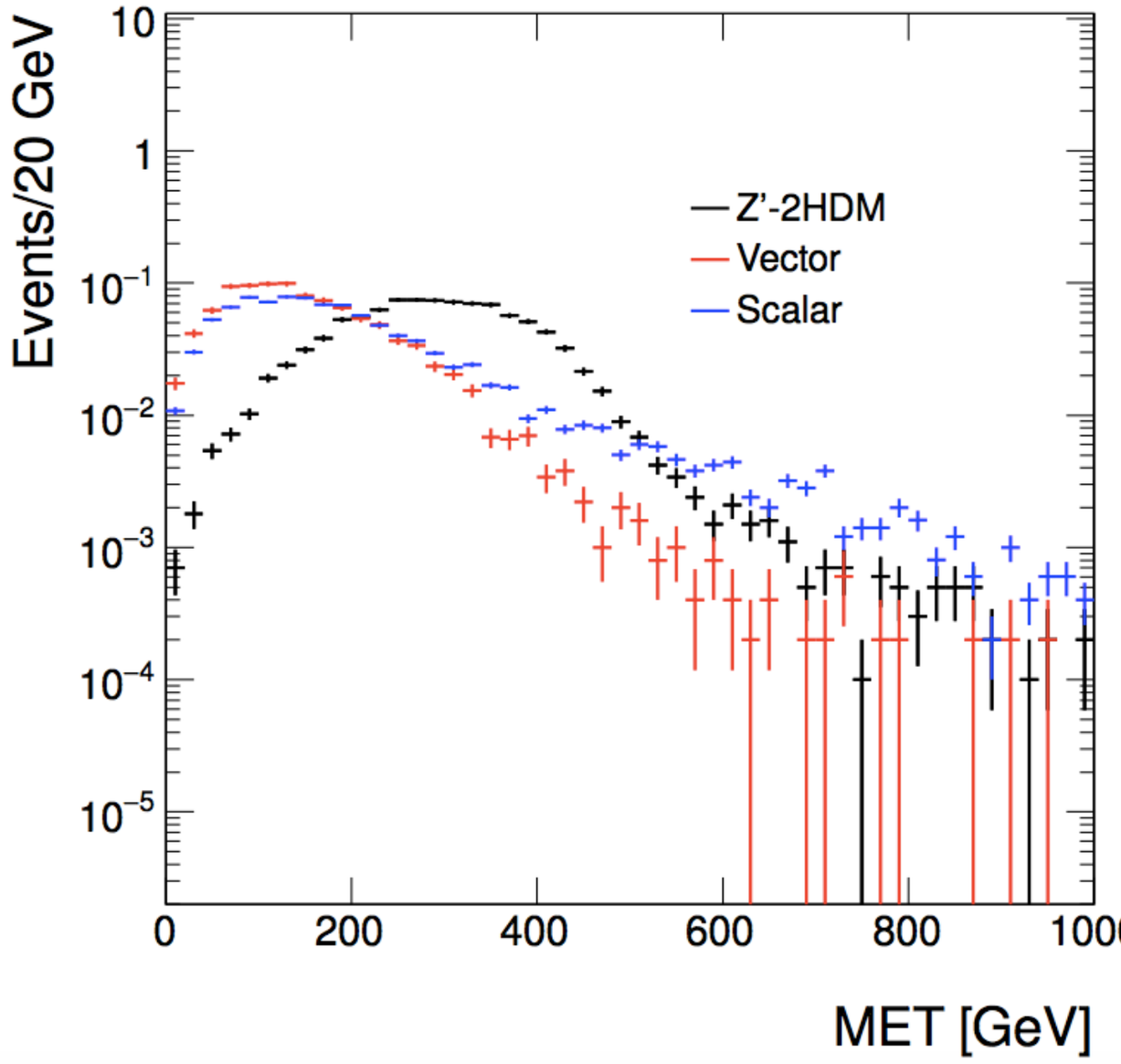

Model Parameters We Considered

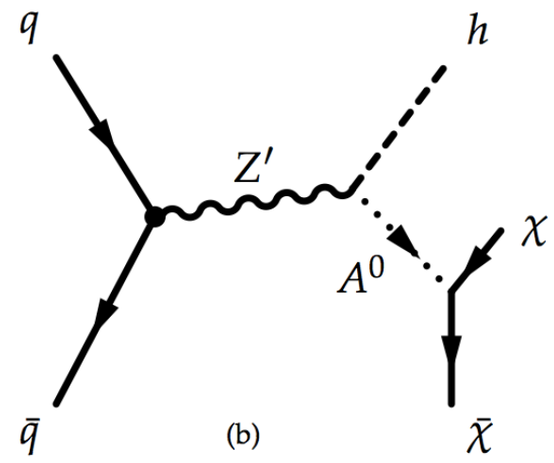

- Higgs sector: Type-II 2HDM with Φ_u and Φ_d
- Gauge sector: extended by a U(1)z' group
- mDM: mass of dark matter particles, mDM≤ 100 GeV
- mA: mass of the pseudo-scalar boson A, 300 ≤ mA ≤ 800 GeV
- mZp: mass of Z', 600 ≤ mZp ≤ 2500 GeV
- gDM: coupling of A with DM particles, gDM=1
- gZ': coupling of Z', gZ'=0.8
- tanβ: ratio of the vacuum expectation values, tanβ=1

Generator-Level Kinematic Distributions

$$p_{\mathrm{COM}}^{A} = p_{\mathrm{COM}}^{h} = \frac{\left[\left(M_{Z'}^{2} - \left(m_A + m_h\right)^2\right)\left(M_{Z'}^{2} - \left(m_A - m_h\right)^2\right)\right]^{1/2}}{2M_{Z'}}$$

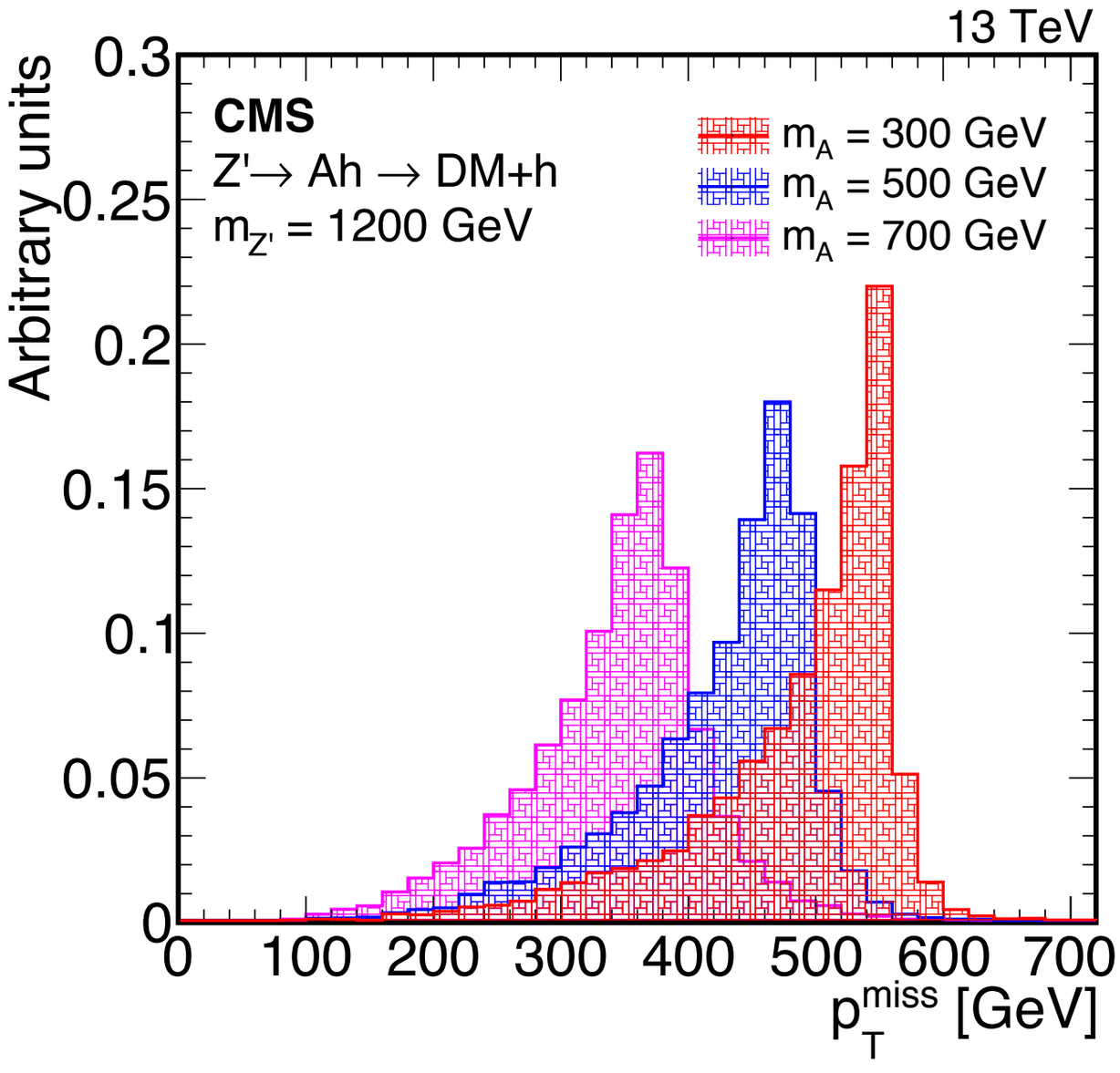

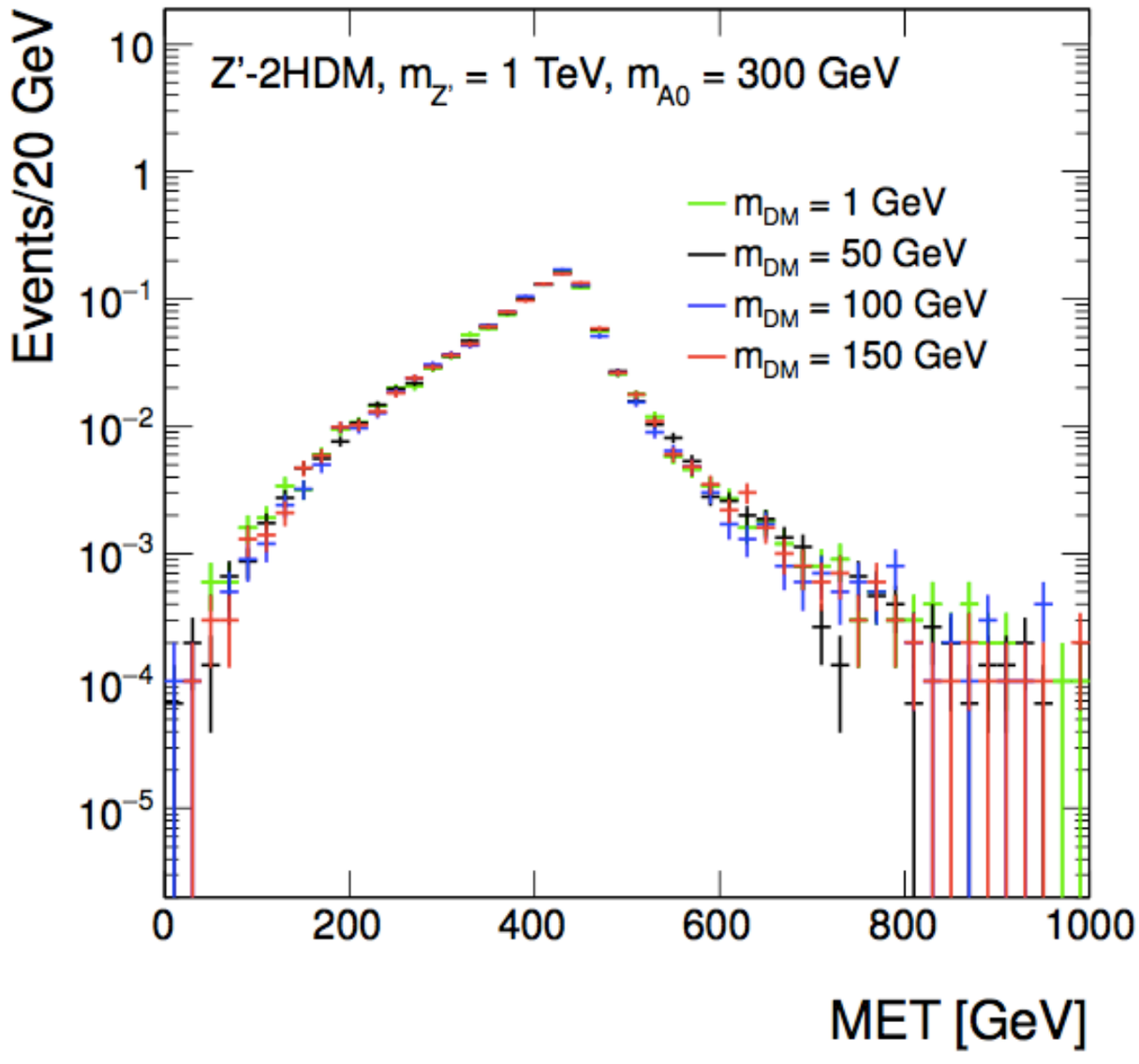

Generator-Level Kinematic Distributions

- MET distributions have little dependence on model parameters

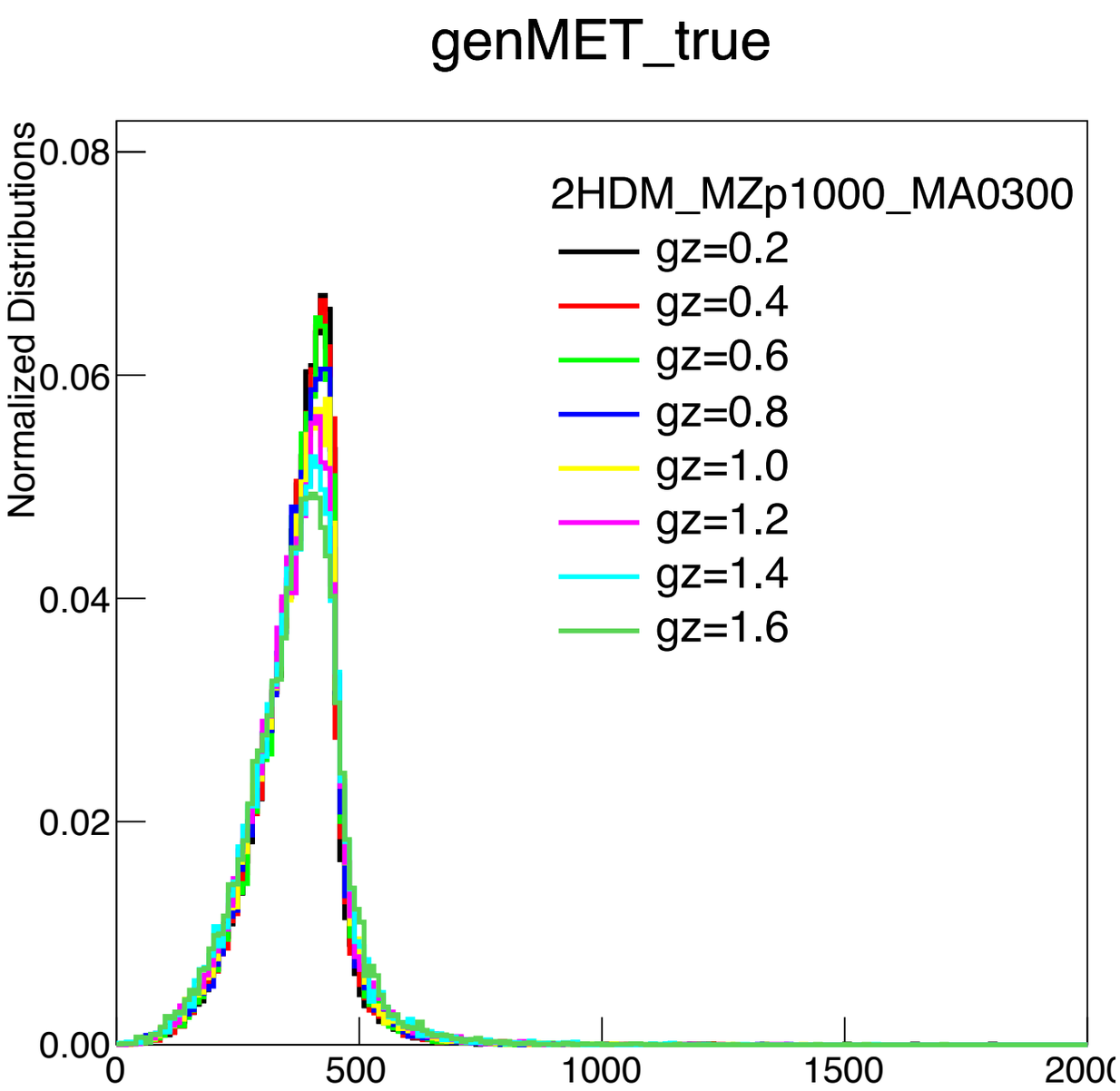

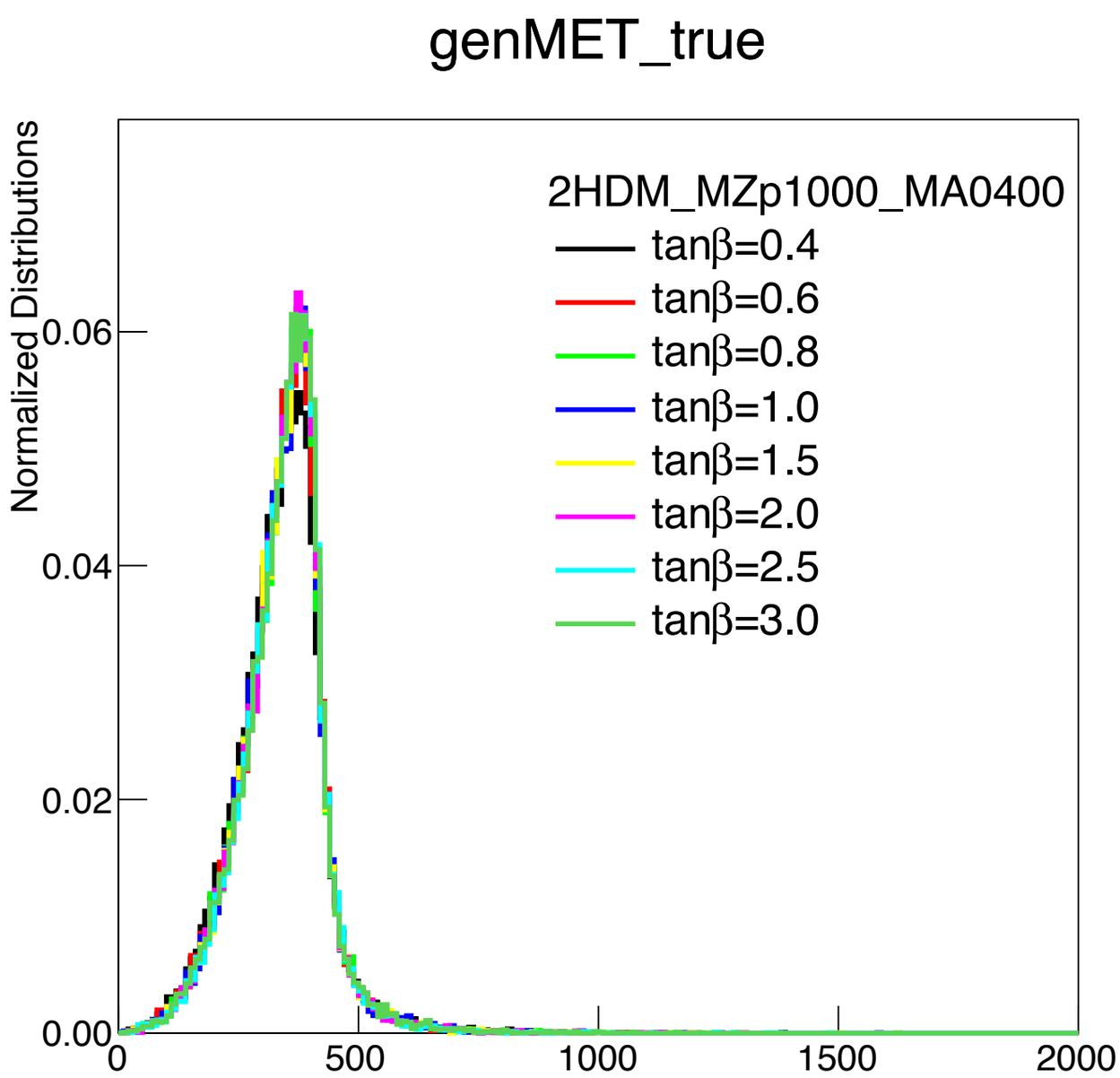

The Large Hadron Collider (LHC)

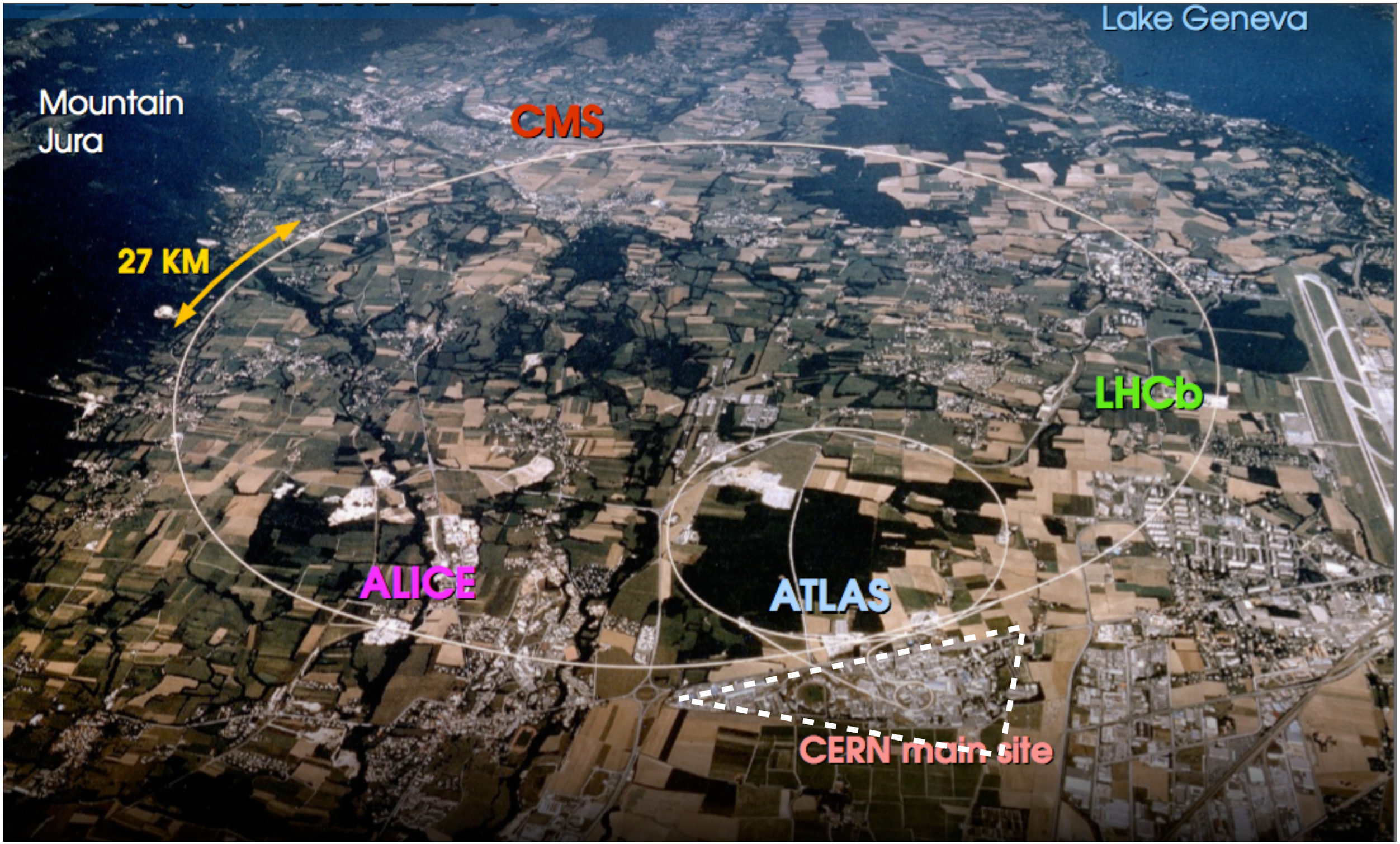

Overall view of the LHC experiments.

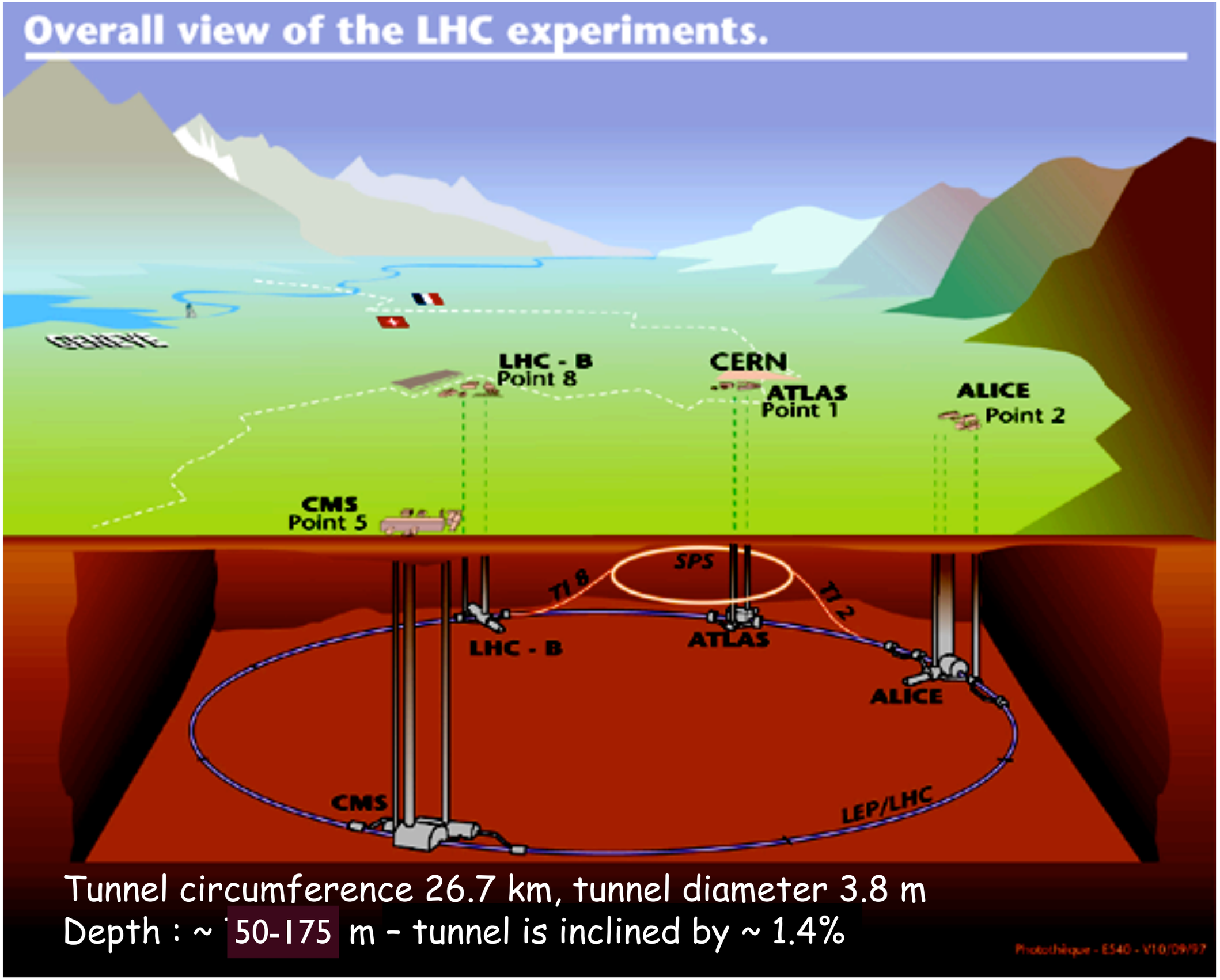

Tunnel circumference 26.7 km, tunnel diameter 3.8 m
Depth : ~ 50-175 m – tunnel is inclined by ~ 1.4%

Compact Muon Solenoid Experiment

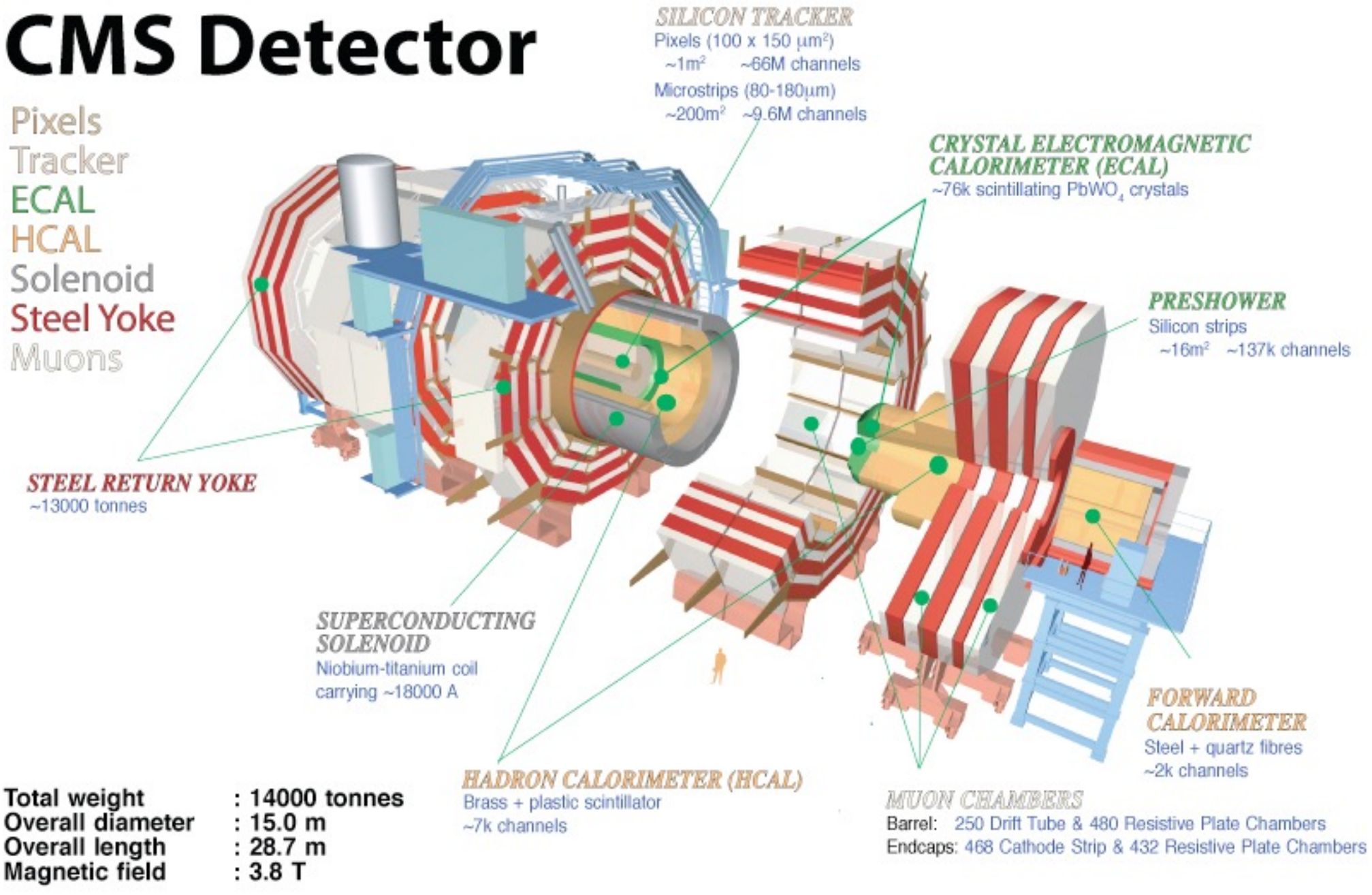

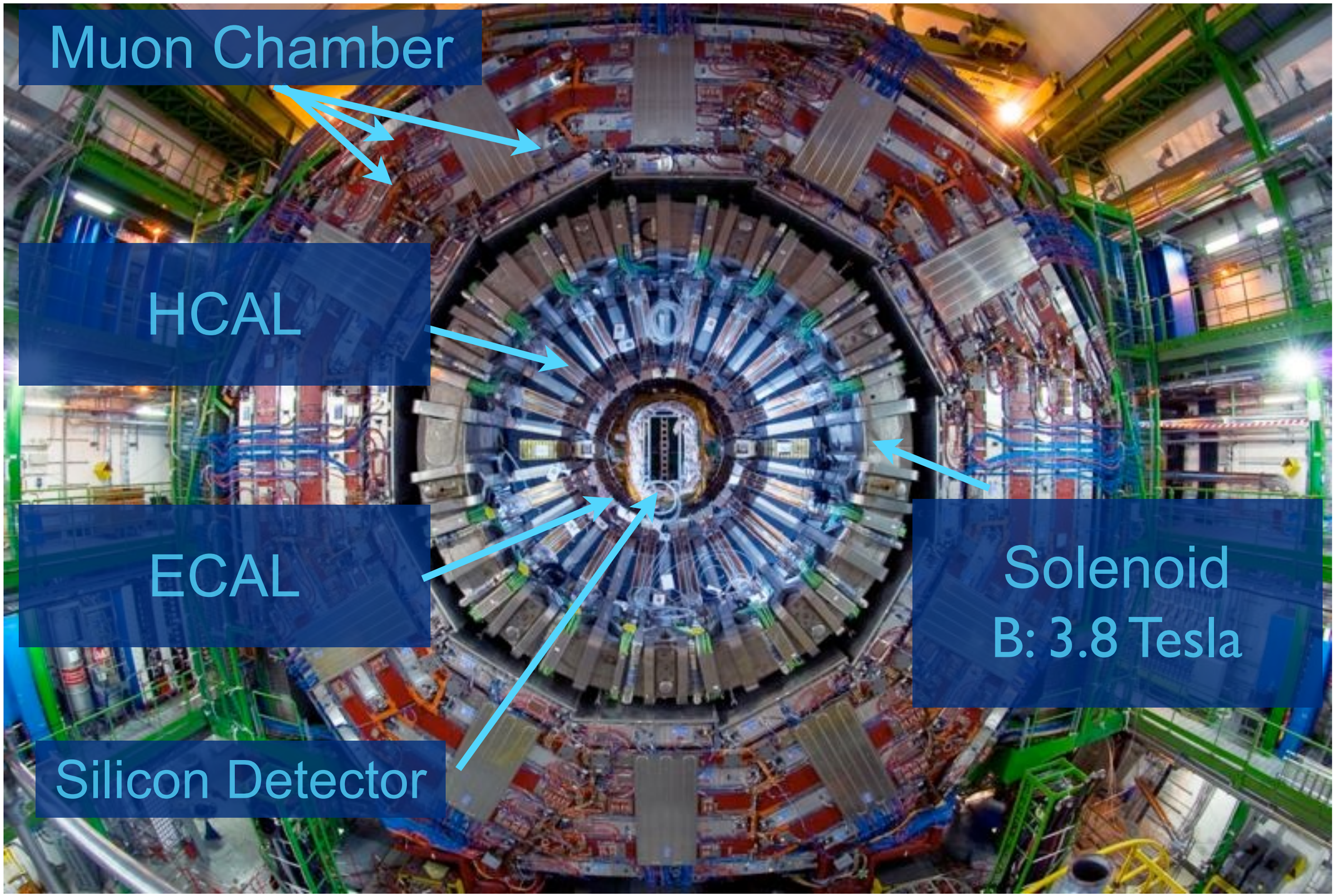
Muon Chamber
HCAL
ECAL
Silicon Detector
Solenoid
B: 3.8 Tesla

Standard Collider Variables

$$\vec{p}_T = \left(p_x, p_y\right)$$

Pseudo-rapidity

$$\eta = -\ln\left[\tan\left(\frac{\theta}{2}\right)\right]$$

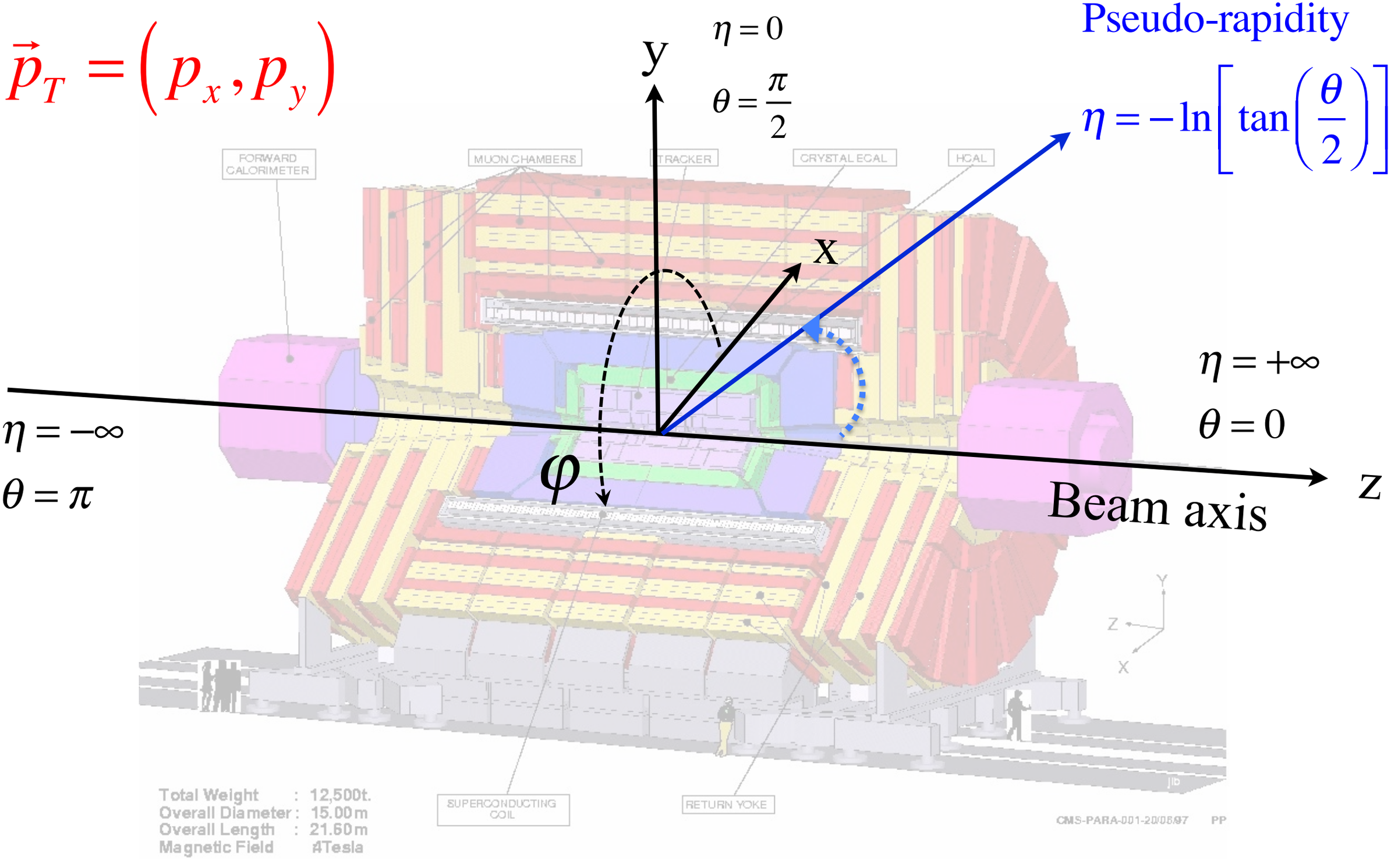

Missing Transverse Momentum

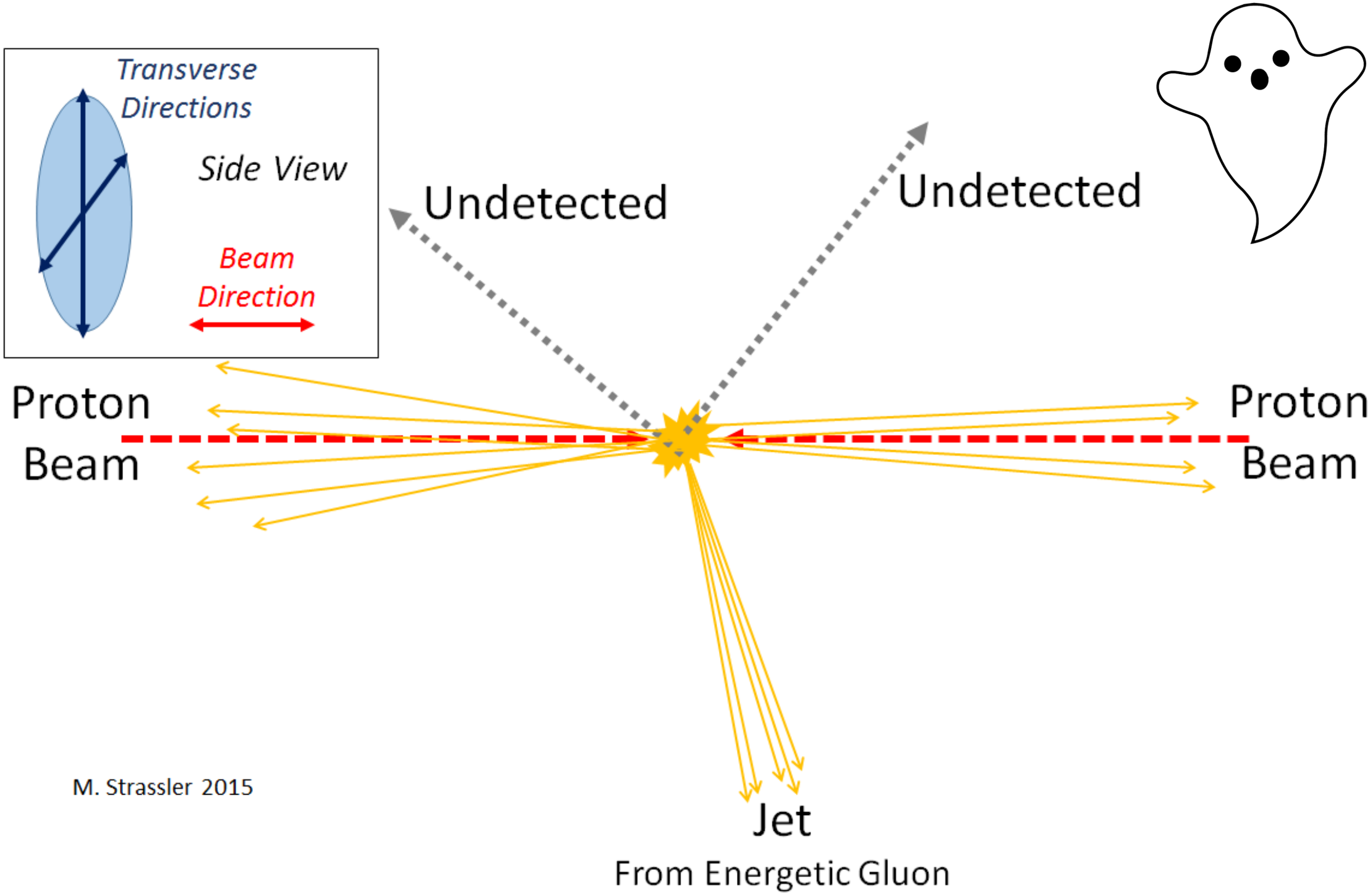

CMS Data Used in This Analysis

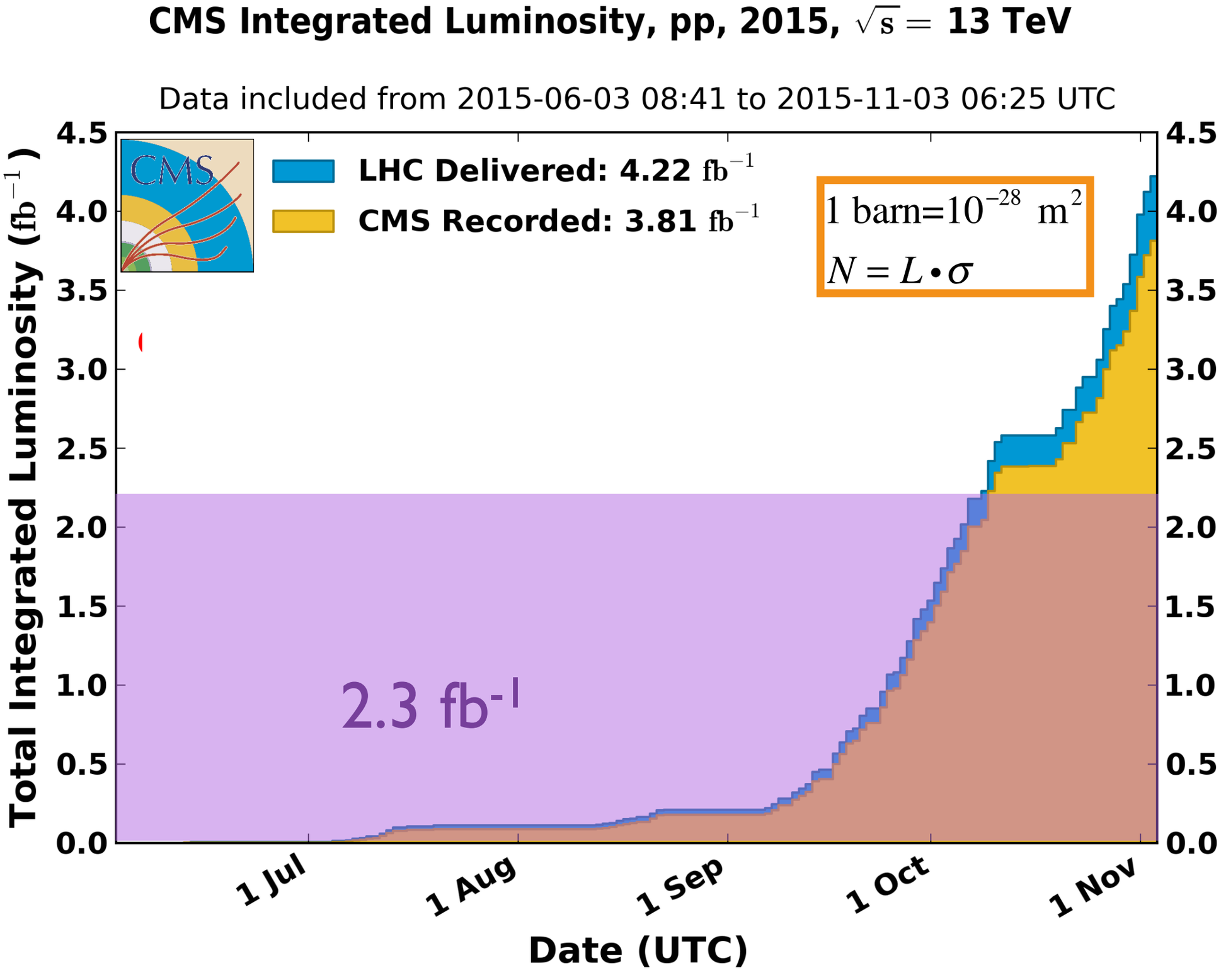

Why H→bb And H→γγ?

- H→bb
  - Wide mass peak (10%), with highest branching ratio (58%)
  - In general, this decay dominates the search sensitivity
- H→γγ
  - Narrow mass peak (1-2% mass resolution), but lower branching ratio (0.2%)
  - Not limited by the MET trigger, can probe models which predict lower MET

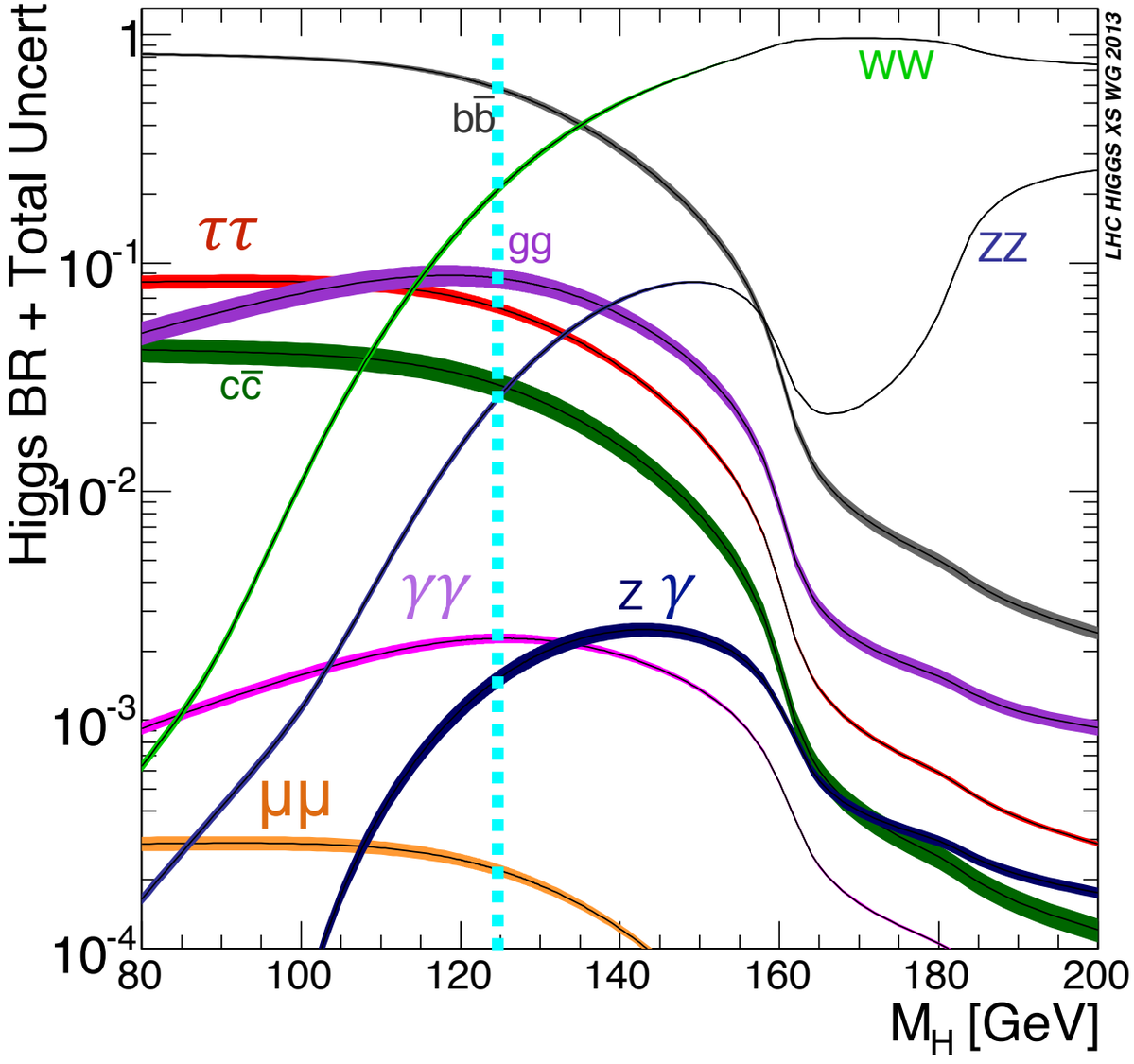

Mono-Higgs Team at CMS

H→bb

Shin-Shan Yu

Raman Khurana

Fang-Ying Tsai

H→bb

Ching-Wei Chen

Shu-Xiao Liu

Michele de Gruttola

H→γγ

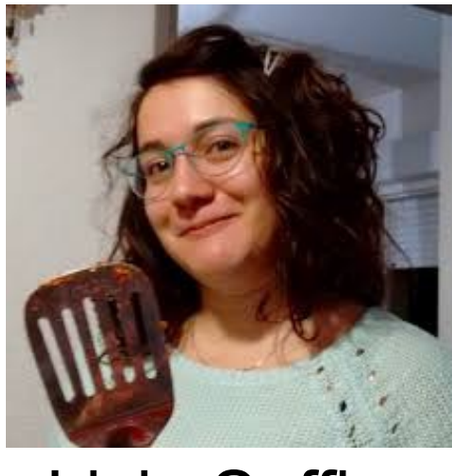

Livia Soffi

Margaret Zientek

Peter Wittich

Mono H→bb: Jet Reconstruction

- Anti-k_T (a= -2), k_T (a=2), CA (a=0) jet reconstruction algorithms

- Sequential clustering algorithms ： Assuming that each particle within jet has different p_T.

$$d_{ij} = min\,(p_{ti}^a, p_{tj}^a) \times \frac{R_{ij}^2}{R^2} \qquad\qquad d_{iB} = p_{ti}^a$$

- p_{ti} : the distance in momentum space between particle i and beam axis.
- a ：An exponent parameter determined by the algorithm actually used.
- R_{ij} ： $\sqrt{(\eta_i^2 - \eta_j^2) + (\phi_i^2 - \phi_j^2)}$
- R ：Radius of jet cone.

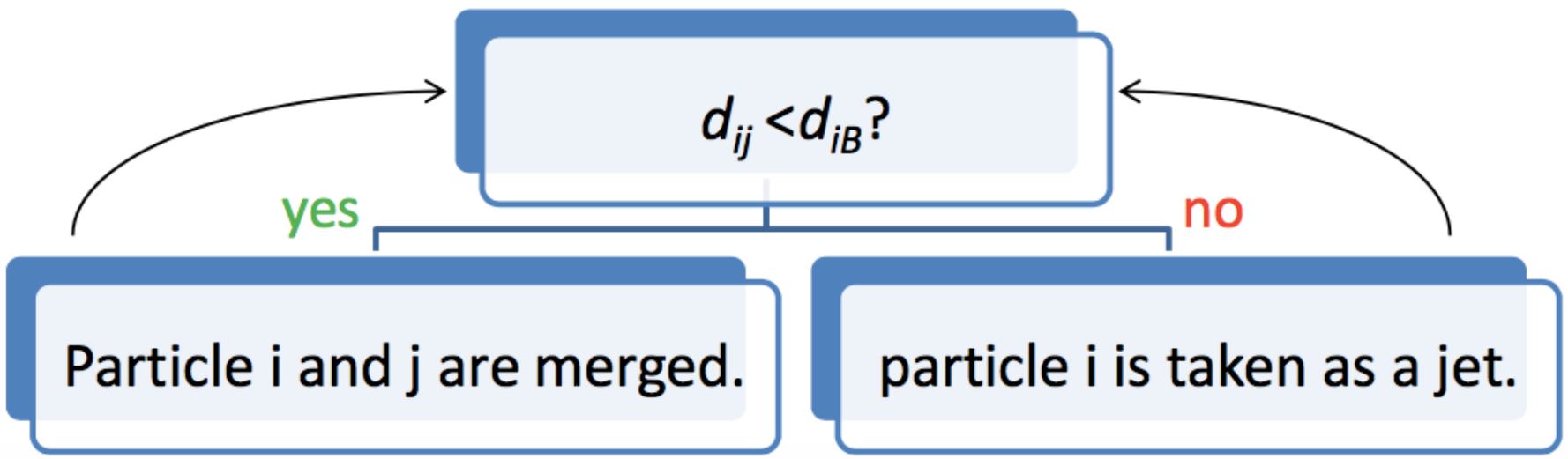

Mono H→bb: Resolved and Boosted Jets

- Our average Higgs pT spans from 120 GeV to 1200 GeV
- Two different jet cone sizes are used: 0.4 (AK4) and 0.8 (AK8)

$$\Delta R_{\min} \approx 2\frac{M_B}{p_B}$$

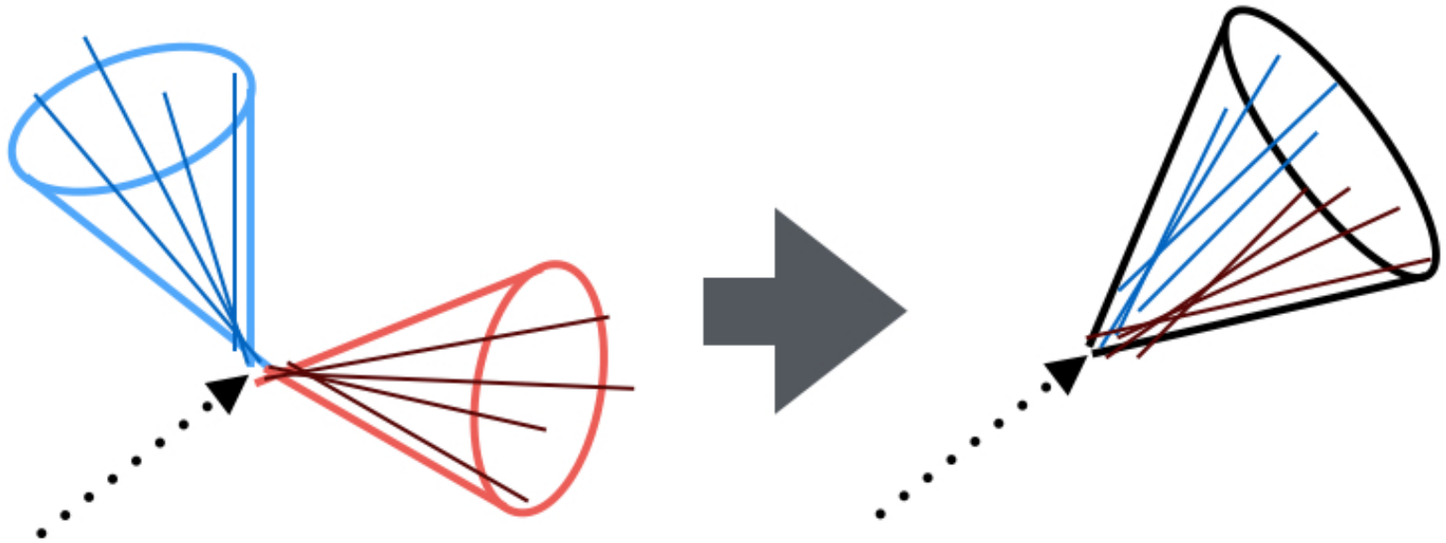

$$\text{Anti-K}_\text{T}\ \Delta R = 0.4 \rightarrow \Delta R = 0.8$$

Mono H→bb: Resolved and Boosted Jets

- Our average Higgs pT spans from 120 GeV to 1200 GeV
- Two different jet cone sizes are used: 0.4 (AK4) and 0.8 (AK8)

$$\Delta R_{\min} \approx 2\frac{M_B}{p_B}$$

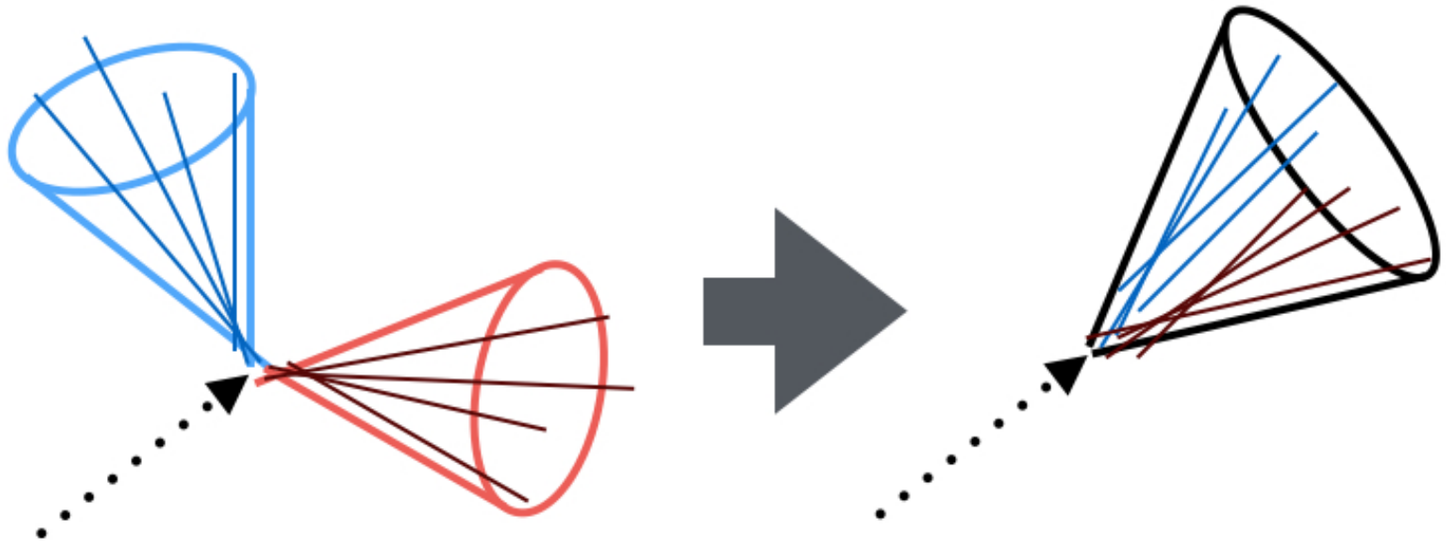

$$\text{Anti-K}_\text{T}\ \Delta R = 0.4 \rightarrow \Delta R = 0.8$$

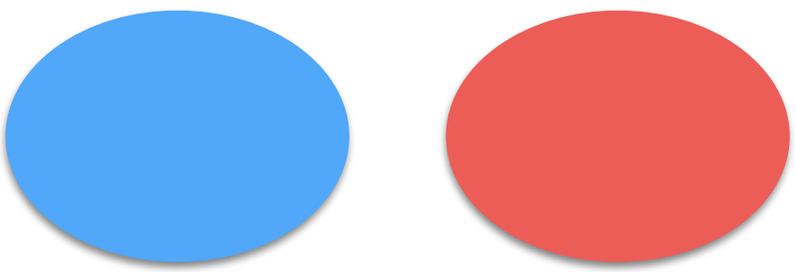

Mono H→bb: Resolved and Boosted Jets

- Our average Higgs pT spans from 120 GeV to 1200 GeV
- Two different jet cone sizes are used: 0.4 (AK4) and 0.8 (AK8)

$$\Delta R_{\min} \approx 2\frac{M_B}{p_B}$$

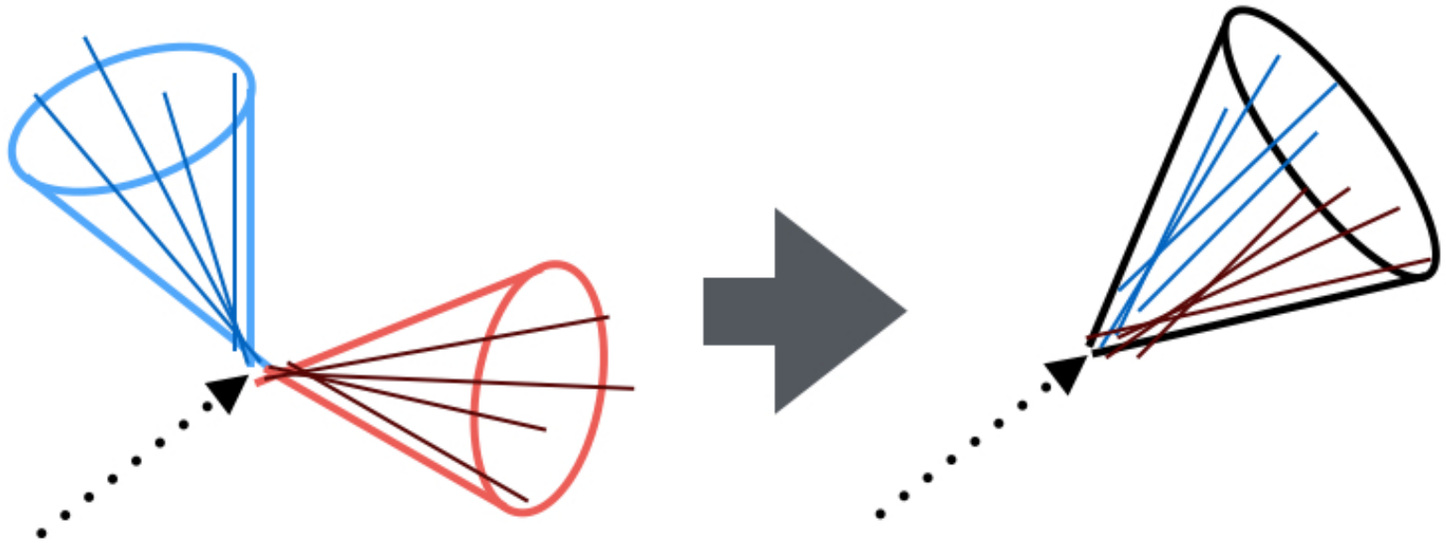

$$\text{Anti-K}_\text{T}\ \Delta R = 0.4 \rightarrow \Delta R = 0.8$$

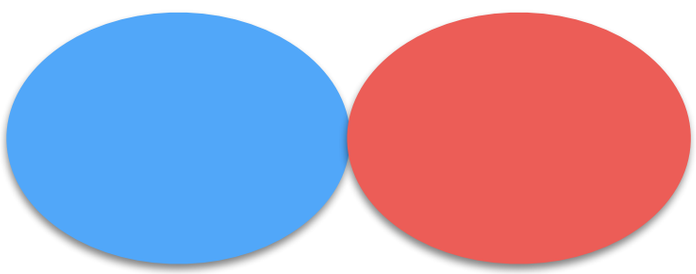

Mono H→bb: Resolved and Boosted Jets

- Our average Higgs pT spans from 120 GeV to 1200 GeV
- Two different jet cone sizes are used: 0.4 (AK4) and 0.8 (AK8)

$$\Delta R_{\min} \approx 2\frac{M_B}{p_B}$$

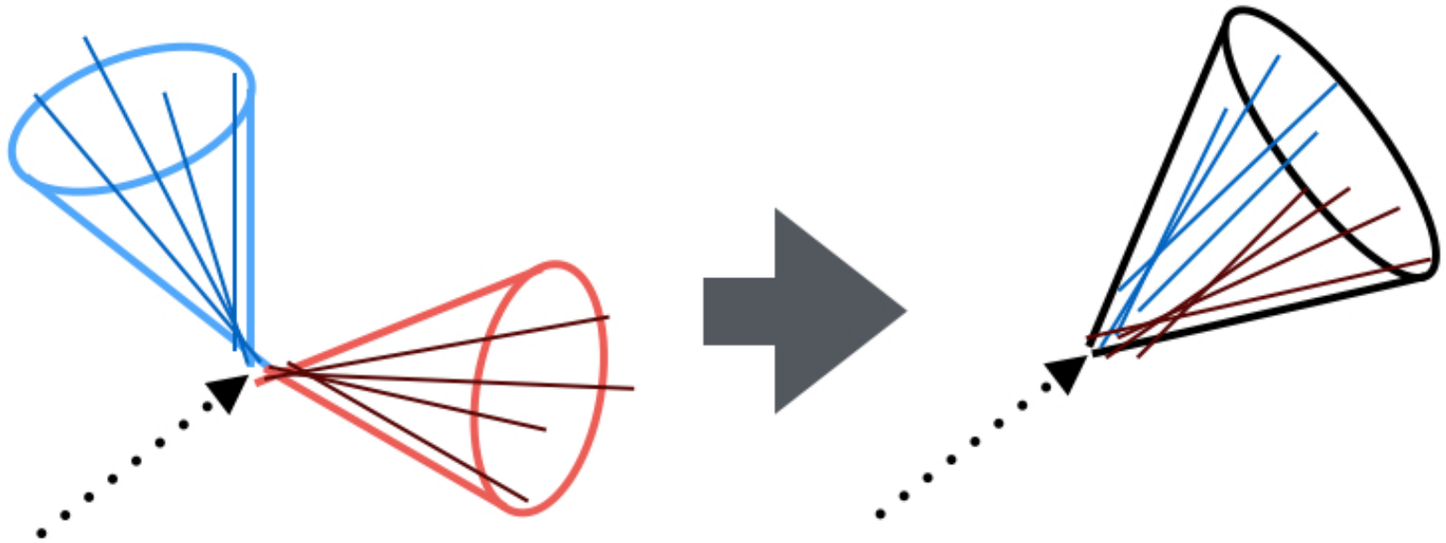

$$\text{Anti-K}_\text{T}\ \Delta R = 0.4 \rightarrow \Delta R = 0.8$$

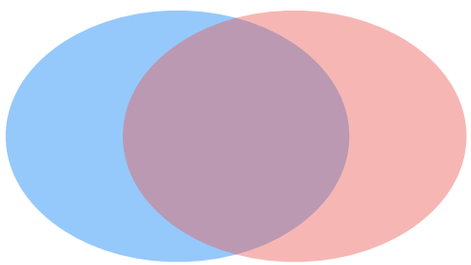

Mono H→bb: Resolved and Boosted Jets

- Our average Higgs pT spans from 120 GeV to 1200 GeV
- Two different jet cone sizes are used: 0.4 (AK4) and 0.8 (AK8)

$$\Delta R_{\min} \approx 2\frac{M_B}{p_B}$$

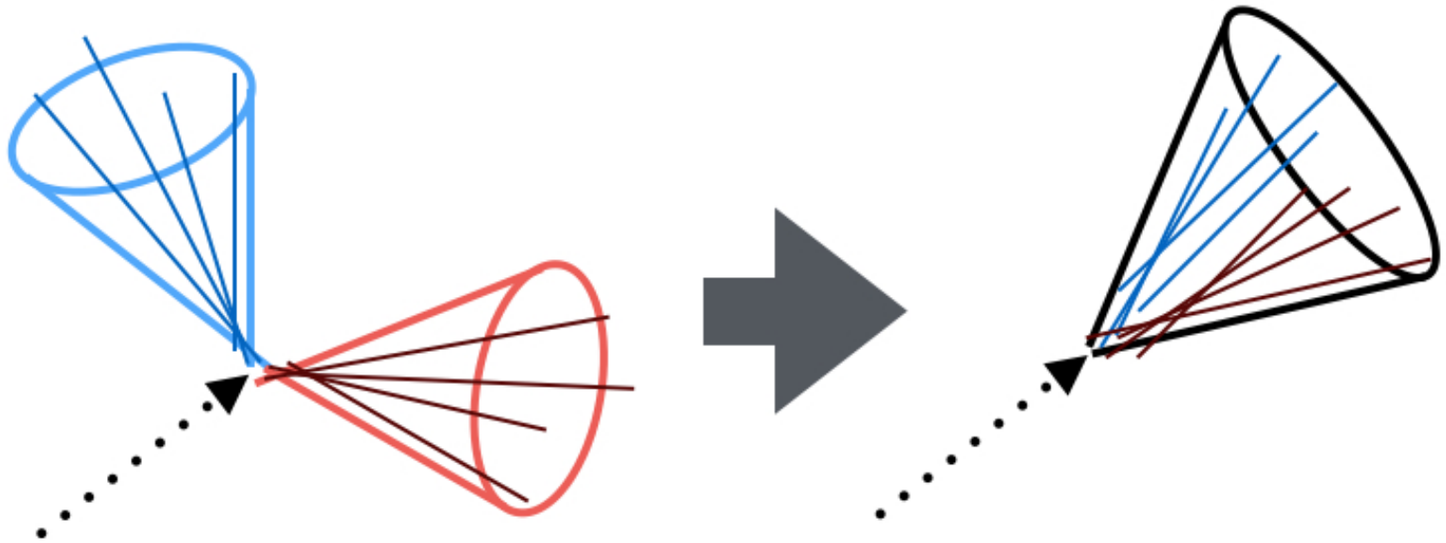

$$\text{Anti-K}_\text{T}\ \Delta R = 0.4 \rightarrow \Delta R = 0.8$$

Mono H→bb: Signal Selection

Cut Variable	Resolved	Boosted
AK4 Jet Kinematics	2 jets with $p_T > 30$ GeV and $\|\eta\| < 2.4$	-
AK8 Jet Kinematics	-	$p_T > 200$ GeV, $\|\eta\| < 2.4$
E_T^{miss}	> 170 GeV	> 200 GeV
p_T^{bb}	> 150 GeV	-
b tagging	Medium WP for both jets	Loose WP for two subjets
$m_{corrected}^{pruned}$	-	100 to 150 GeV
m_{bb}	100 to 150 GeV	-
$\Delta\phi$(AK4 Jet,E_T^{miss})	> 0.4	> 0.4
$\Delta\phi(\vec{p}_T^{miss}, E_T^{miss})$	< 0.7	-
additional isolated lepton (e, μ, τ_h)	0	0
additional AK4 jet	not more than one	not more than one
additional AK4 b jet	0	0

Mono H→bb: Signal Selection

Cut Variable	Resolved	Boosted
AK4 Jet Kinematics	2 jets with $p_T > 30$ GeV and $\|\eta\| < 2.4$	-
AK8 Jet Kinematics	-	$p_T > 200$ GeV, $\|\eta\| < 2.4$
E_T^{miss}	> 170 GeV	> 200 GeV
p_T^{bb}	> 150 GeV	-
b tagging	Medium WP for both jets	Loose WP for two subjets
$m_{corrected}^{pruned}$	-	100 to 150 GeV
m_{bb}	100 to 150 GeV	-
$\Delta\phi$(AK4 Jet,E_T^{miss})	> 0.4	> 0.4
$\Delta\phi(\vec{p}_T^{miss}, E_T^{miss})$	< 0.7	-
additional isolated lepton (e, μ, τ_h)	0	0
additional AK4 jet	not more than one	not more than one
additional AK4 b jet	0	0

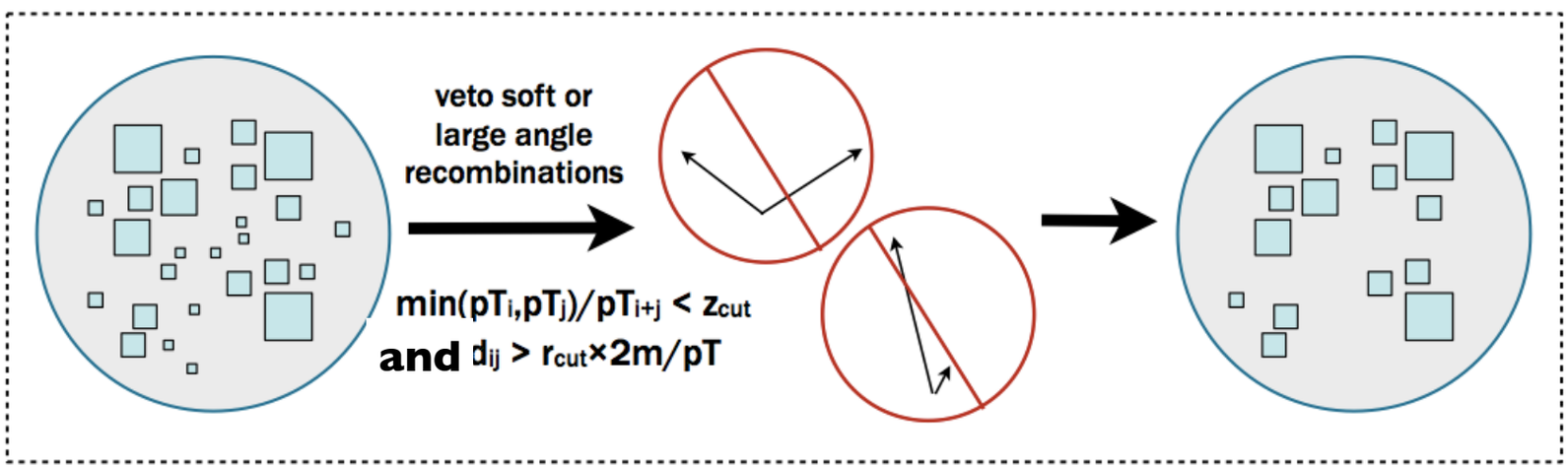

Jet pruning
default:
$z_{cut} = 0.1$
$r_{cut} = 0.5$

Mass Distribution of Pruned Jets

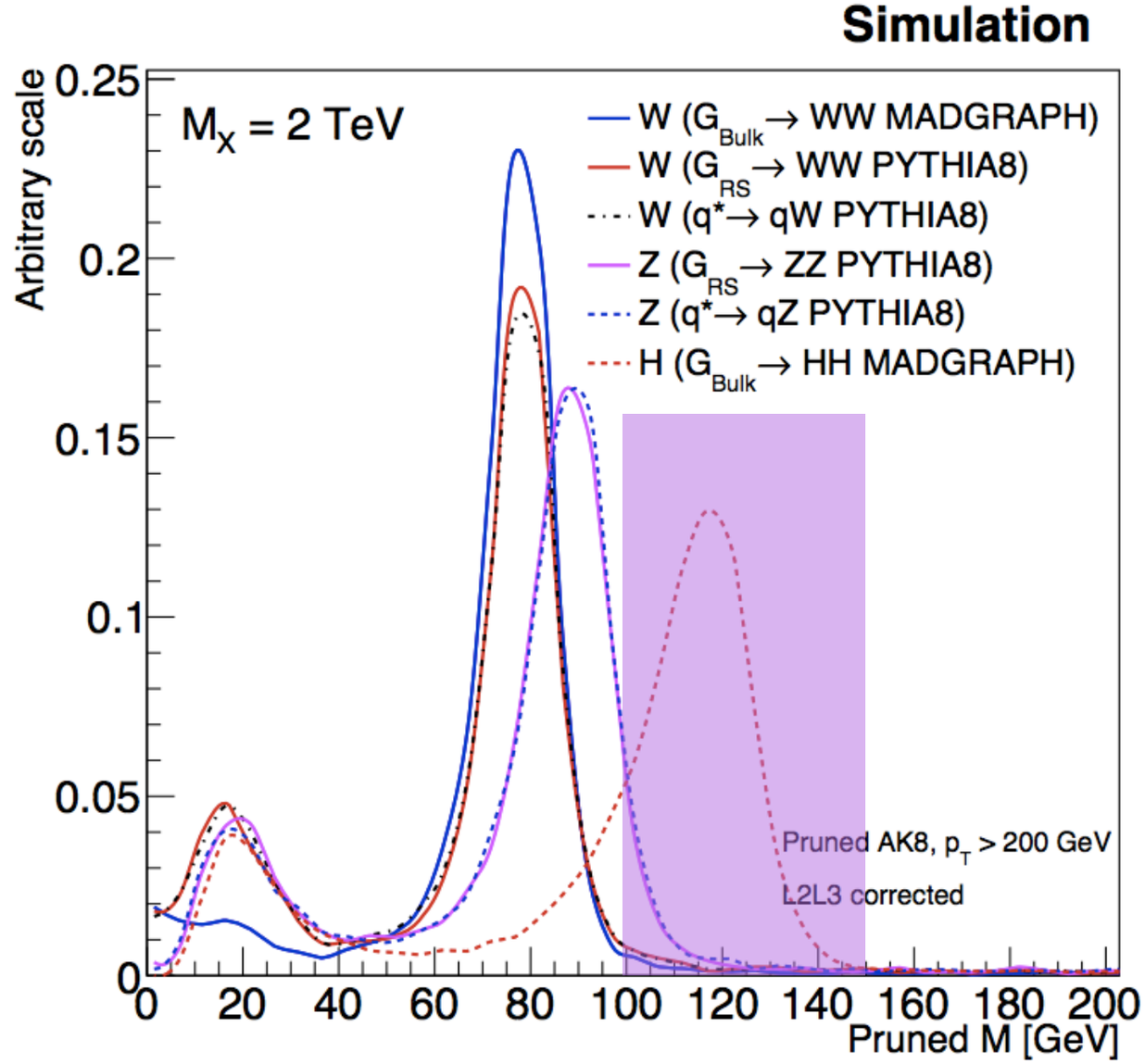

Mass Distribution of Pruned Jets

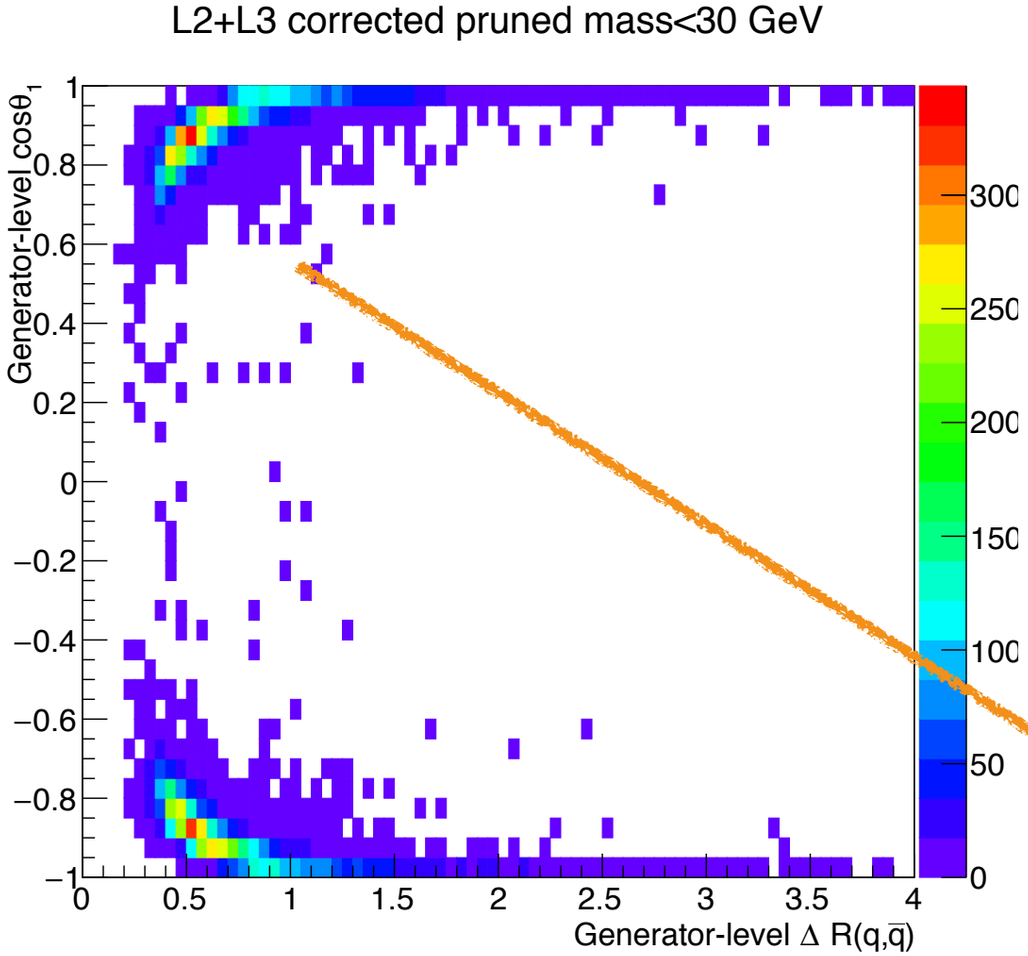

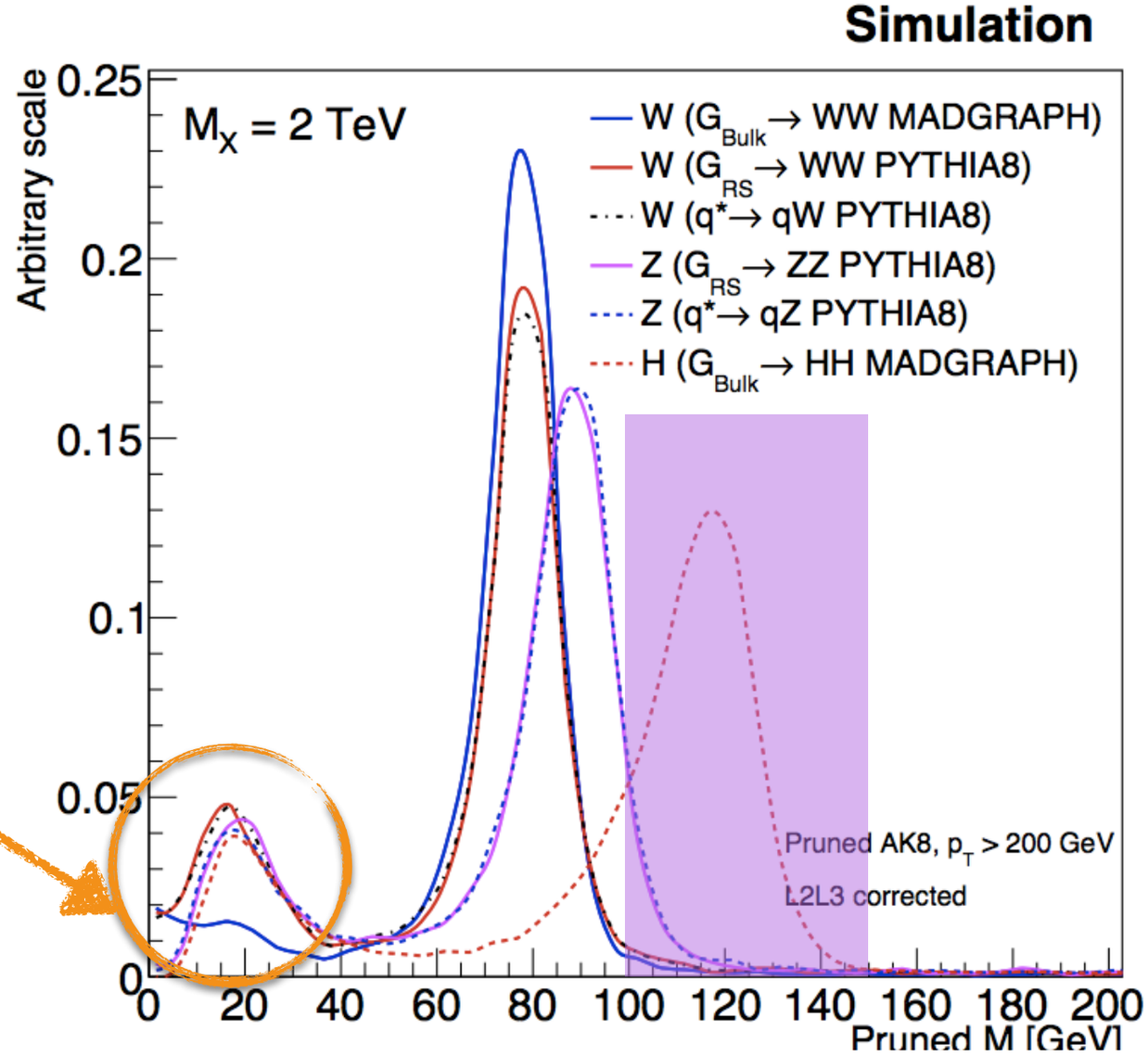

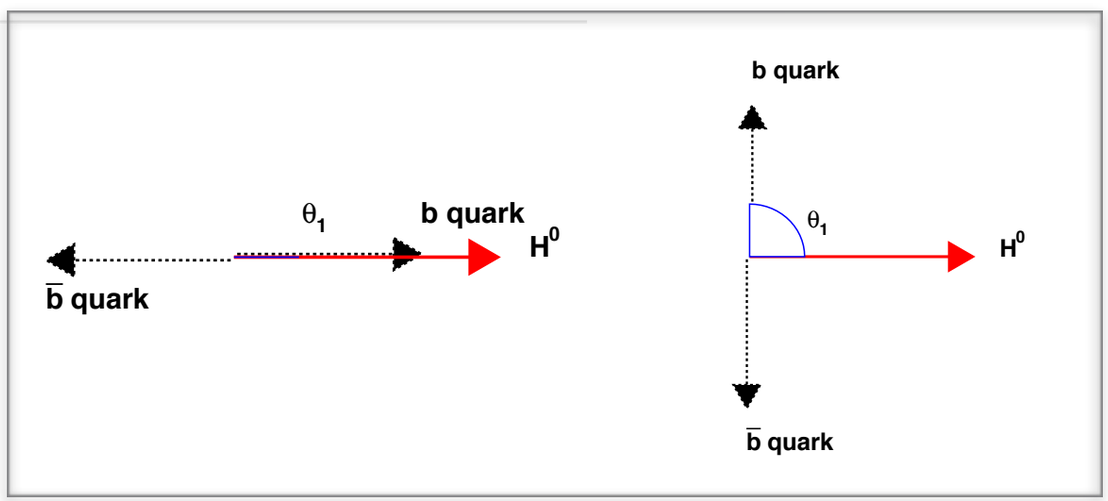

Subjet b-Tagging for Higgs Jet

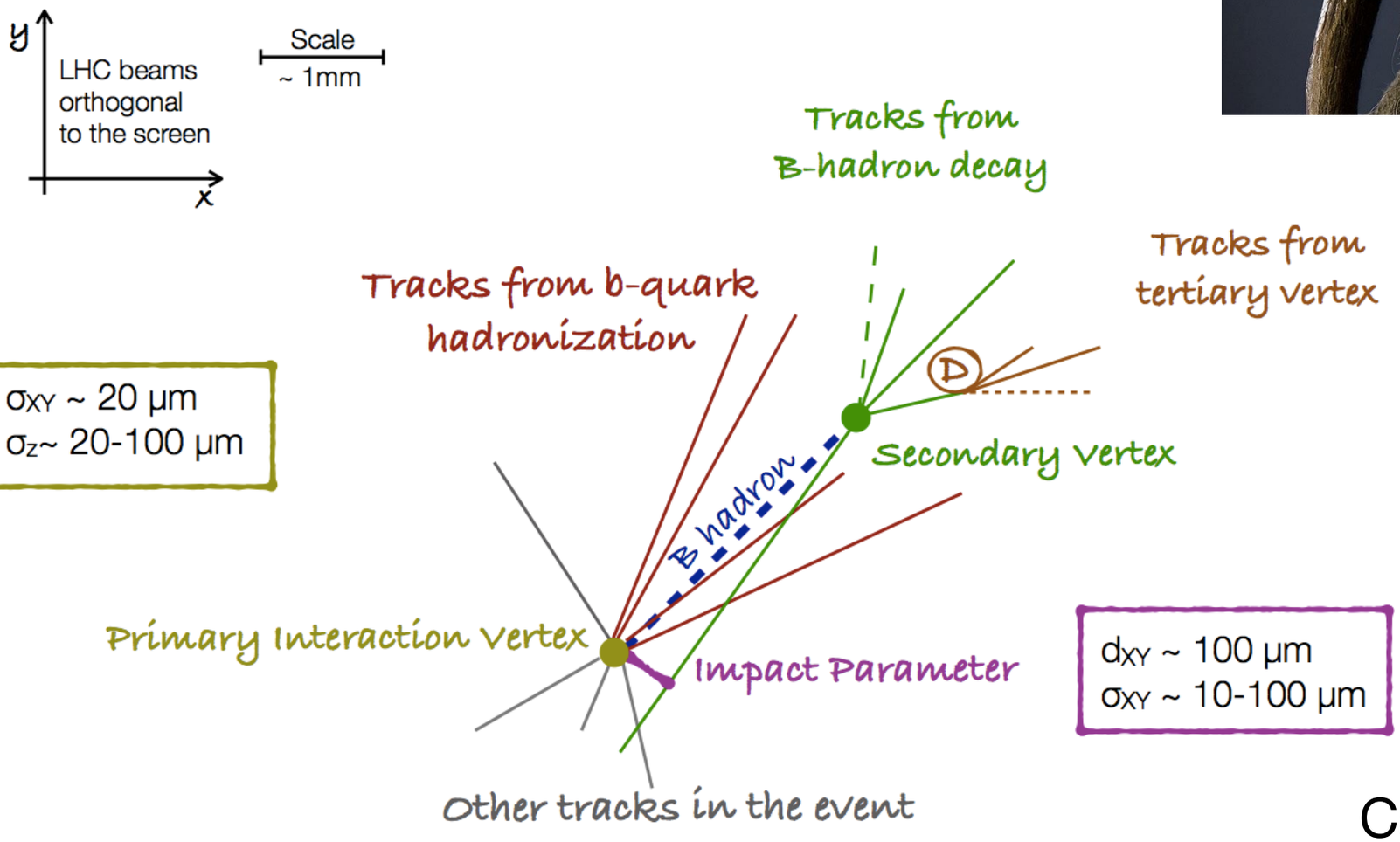

Caterina Vernieri (Boost 2015)

Subjet b-Tagging for Higgs Jet

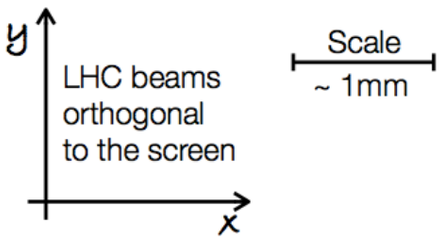

Scale
~ 1mm

σ_{XY} ~ 20 μm
σ_z~ 20-100 μm

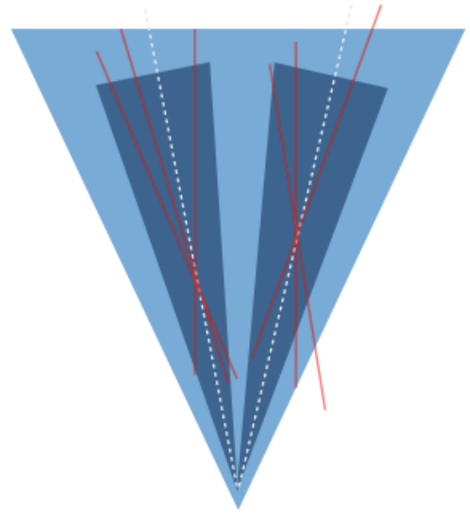

sub-jets

Defines sub-jets
b-tagging observables for each sub-jet
explicit jet track association

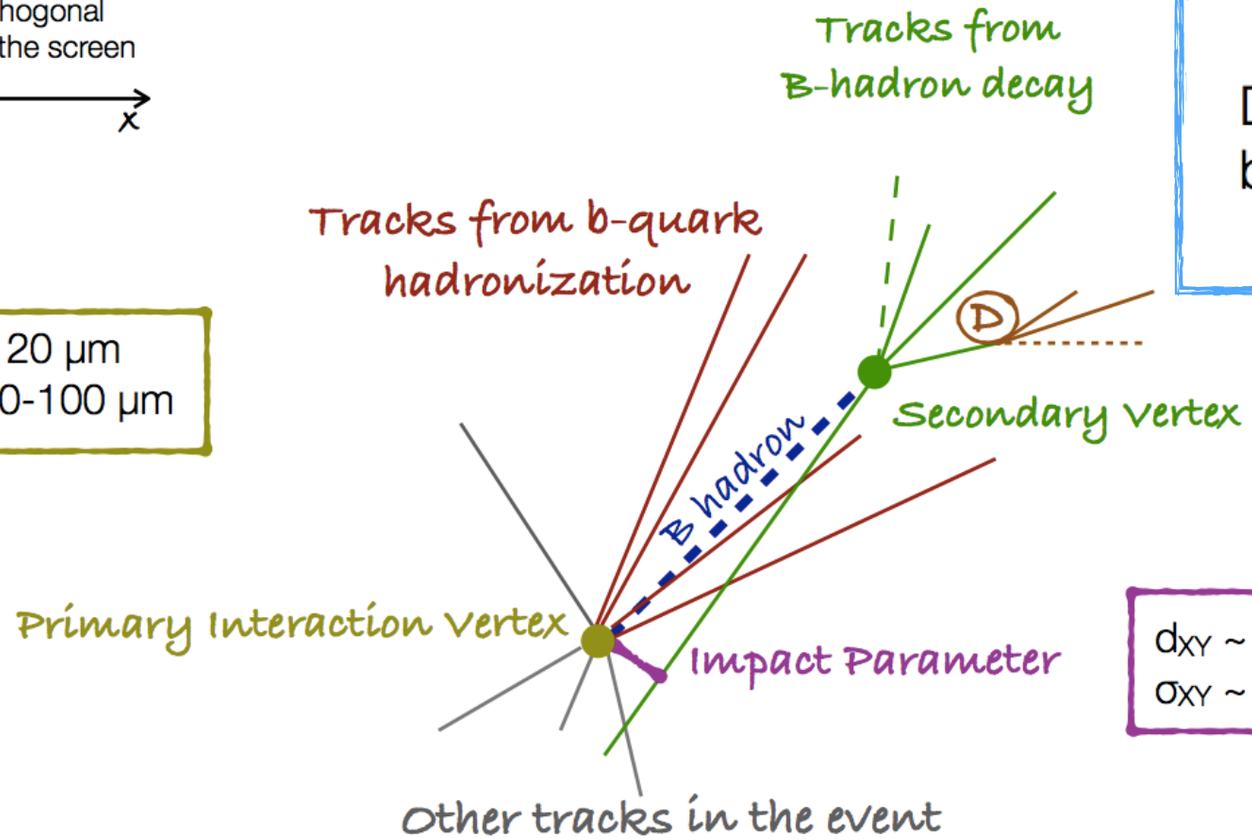

d_{XY} ~ 100 μm
σ_{XY} ~ 10-100 μm

Caterina Vernieri (Boost 2015)

Subjet b-Tagging for Higgs Jet

AK8 subjet and AK4 b-tagging:

efficiency 83% with a mis-tag rate 10%

(loose working point)

efficiency 69% with a mis-tag rate of 1%

(medium working point)

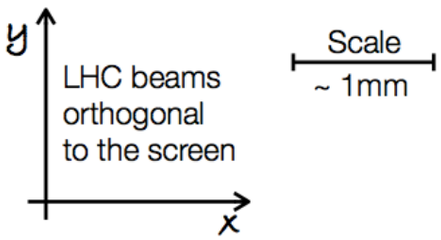

Scale
~ 1mm

σ_{XY} ~ 20 μm
σ_z~ 20-100 μm

d_{XY} ~ 100 μm
σ_{XY} ~ 10-100 μm

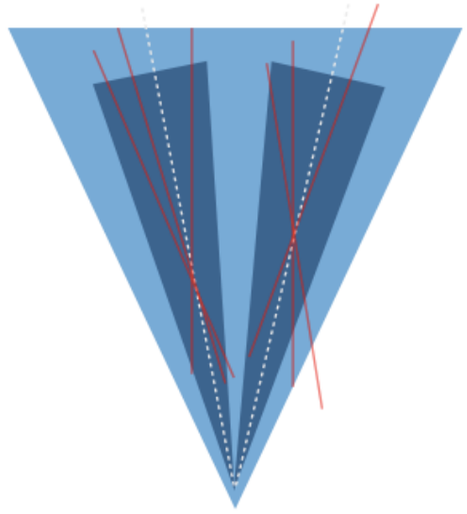

sub-jets

Defines sub-jets
b-tagging observables for each sub-jet
explicit jet track association

Caterina Vernieri (Boost 2015)

Mono H→bb: Acceptance, Efficiency

- Product of acceptance and efficiency is about 1-20%

m_A [GeV]	300	400	500	600	700	800
$m_{Z'}$ [GeV]	$h \to b\bar{b}$					
600	0.058 ± 0.003	0.013 ± 0.003	—	—	—	—
800	0.132 ± 0.003	0.117 ± 0.003	0.083 ± 0.003	0.040 ± 0.003	—	—
1000	0.245 ± 0.004	0.218 ± 0.003	0.167 ± 0.002	0.123 ± 0.003	0.181 ± 0.003	0.066 ± 0.003
1200	0.282 ± 0.003	0.272 ± 0.004	0.262 ± 0.003	0.238 ± 0.004	0.195 ± 0.003	0.126 ± 0.003
1400	0.286 ± 0.003	0.287 ± 0.003	0.283 ± 0.003	0.279 ± 0.003	0.285 ± 0.003	0.249 ± 0.003
1700	0.280 ± 0.003	0.284 ± 0.003	0.283 ± 0.003	0.284 ± 0.003	0.285 ± 0.004	0.284 ± 0.003
2000	0.269 ± 0.005	0.271 ± 0.003	0.275 ± 0.003	0.273 ± 0.003	0.276 ± 0.003	0.279 ± 0.004
2500	0.248 ± 0.003	0.246 ± 0.003	0.250 ± 0.004	0.251 ± 0.003	0.255 ± 0.003	0.256 ± 0.003

Mono H→bb: Major Background

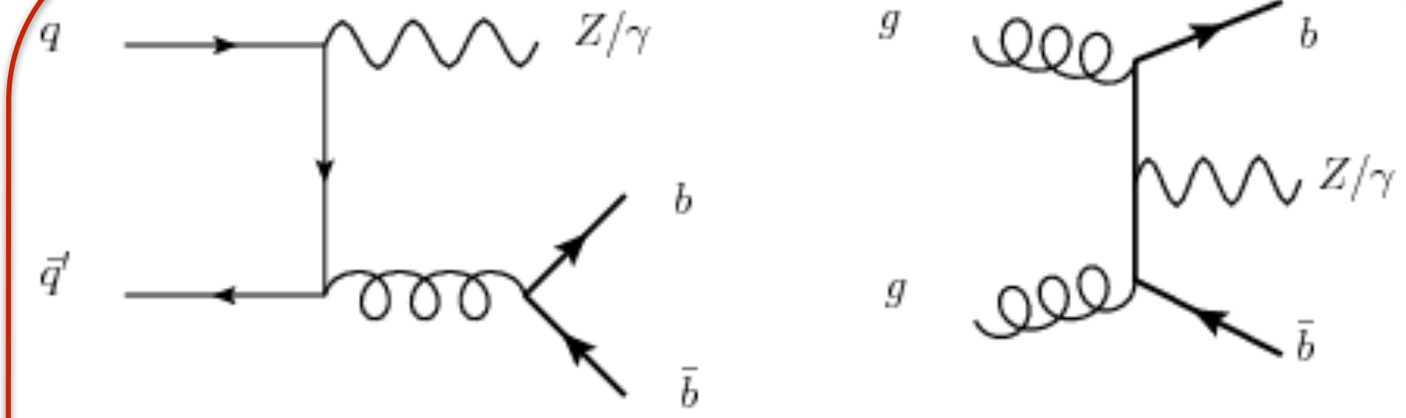

Z(→νν)+bb

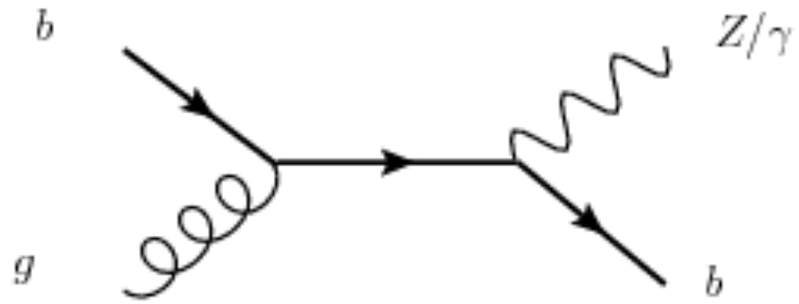

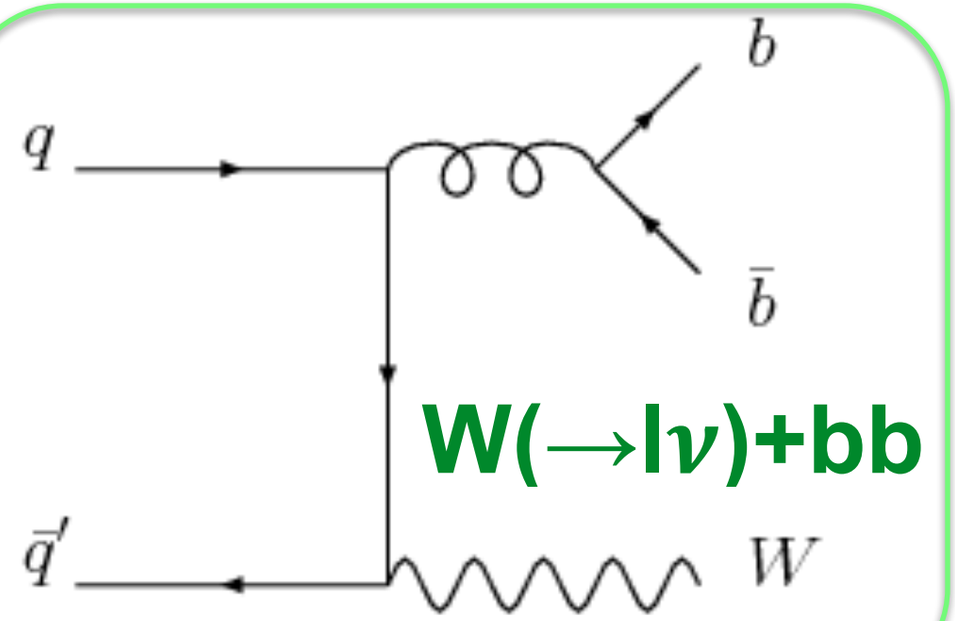

W(→lν)+bb

Other minor background includes:
Zh, diboson, single top, QCD

tt production

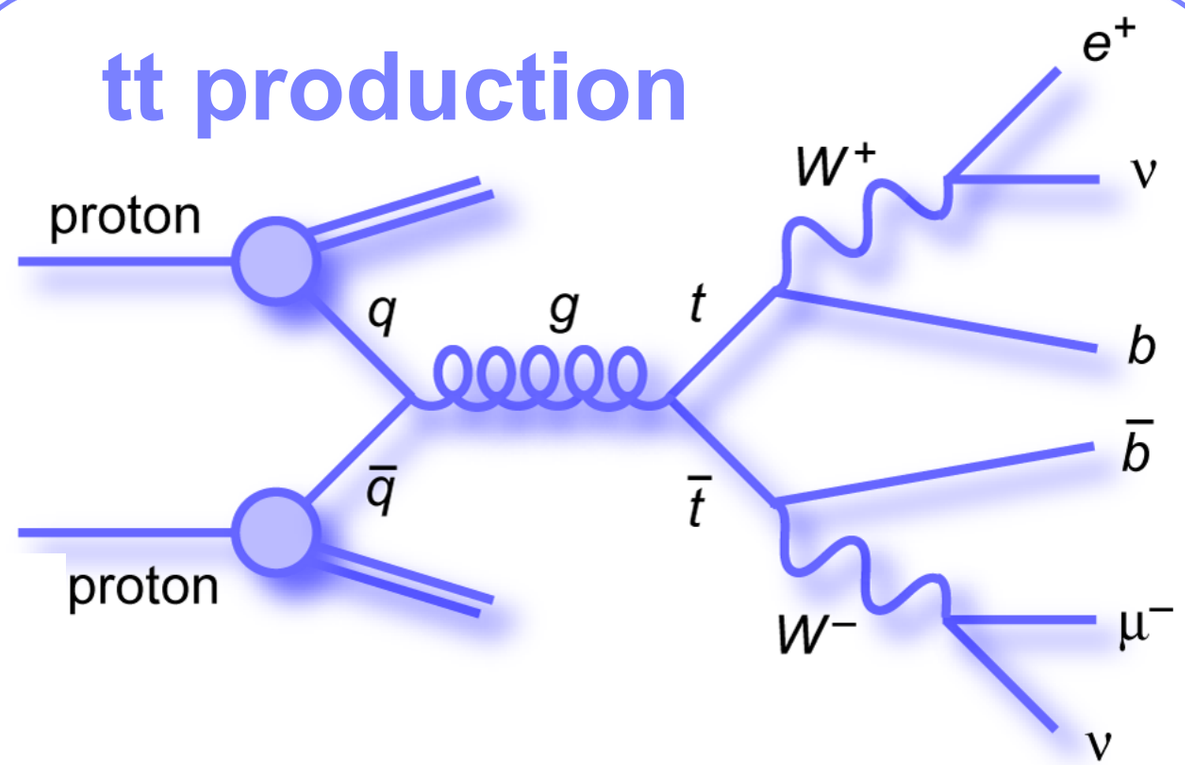

Mono H→bb: Control Regions

	Resolved	Boosted
1.	SR as described in Section 5	SR as described in Section 5
2.	mass side band regions dominated by Z($\to \nu\nu$)+jets events	mass side band regions dominated by Z($\to \nu\nu$)+jets events
3.	one additional lepton with no additional jets (W+jets dominated)	one additional lepton and no restrictions on the number of additional jets (combination of Top and W+jets)
4.	one additional lepton with at least one additional jet (Top dominated)	-

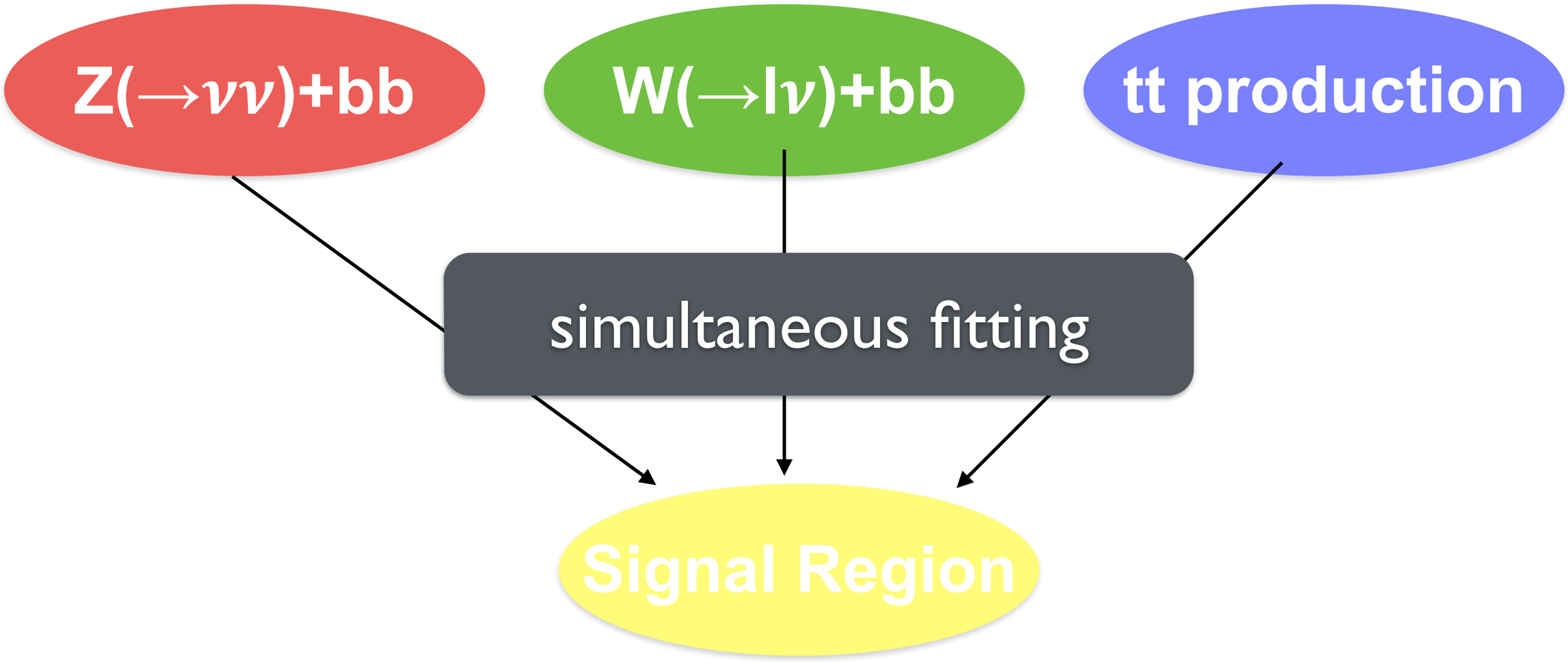

Mono H→bb: Control Regions (Resolved)

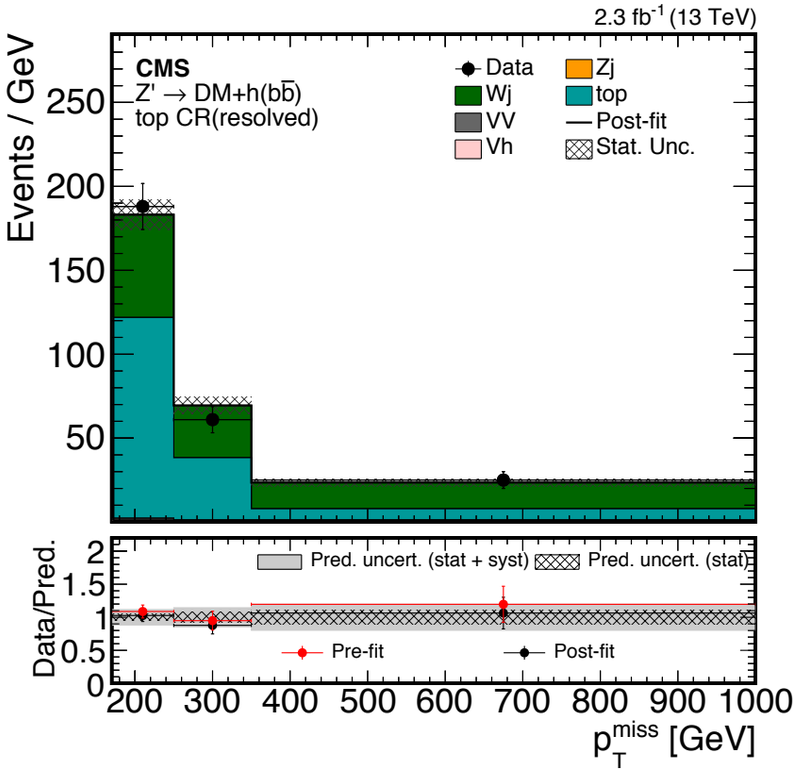

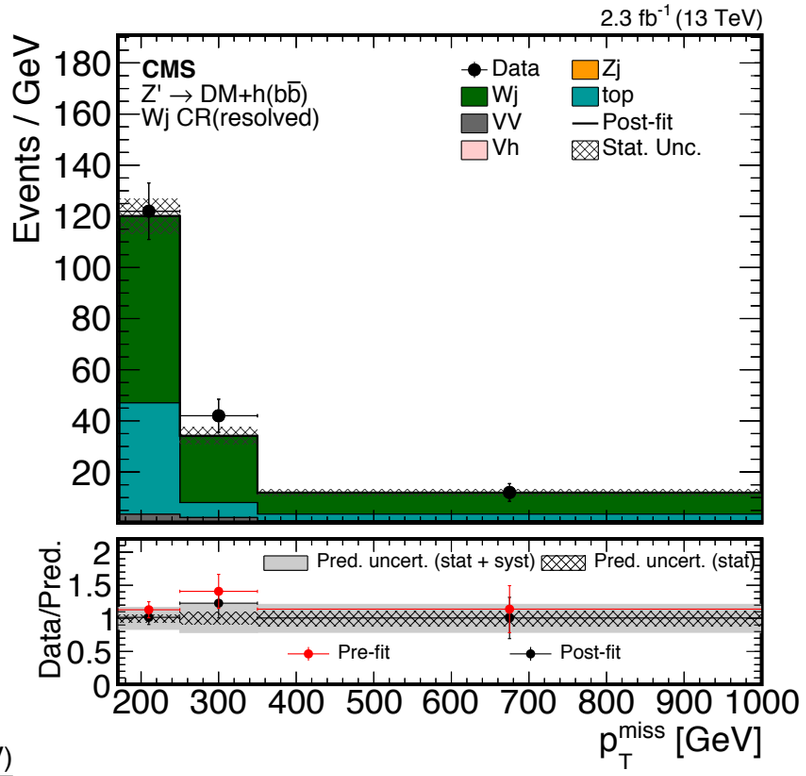

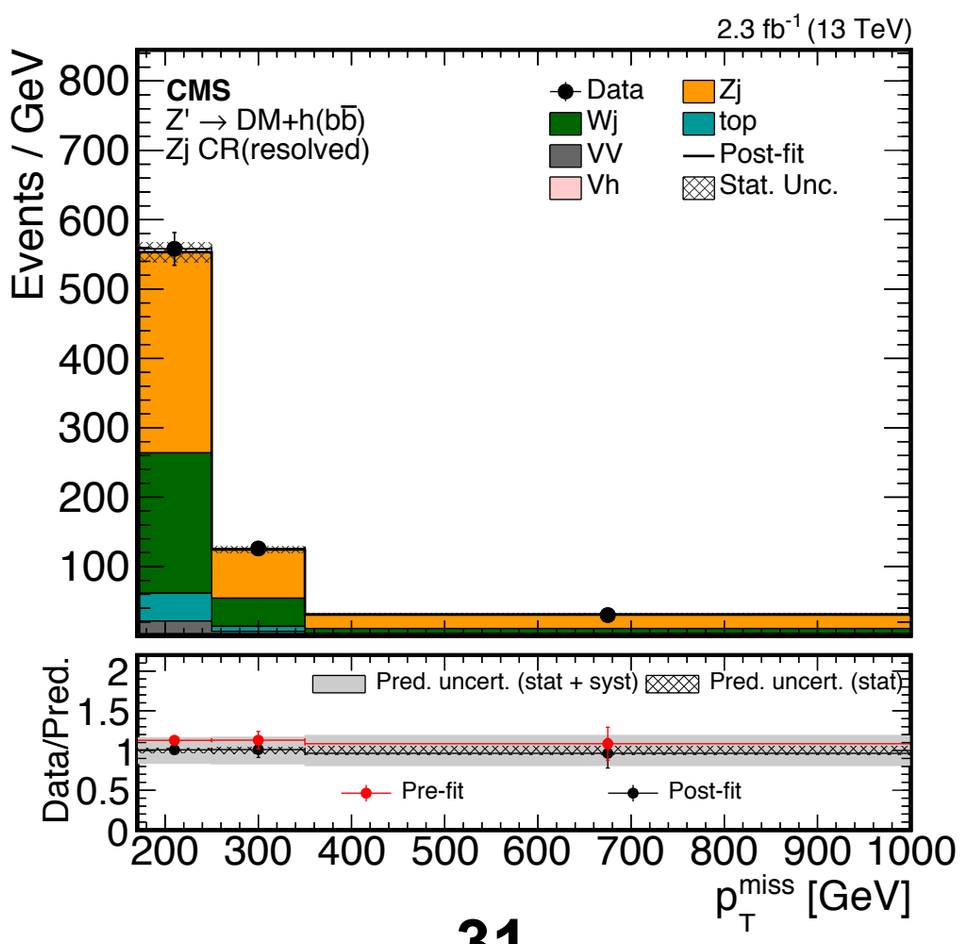

Mono H→bb: Control Regions (Boosted)

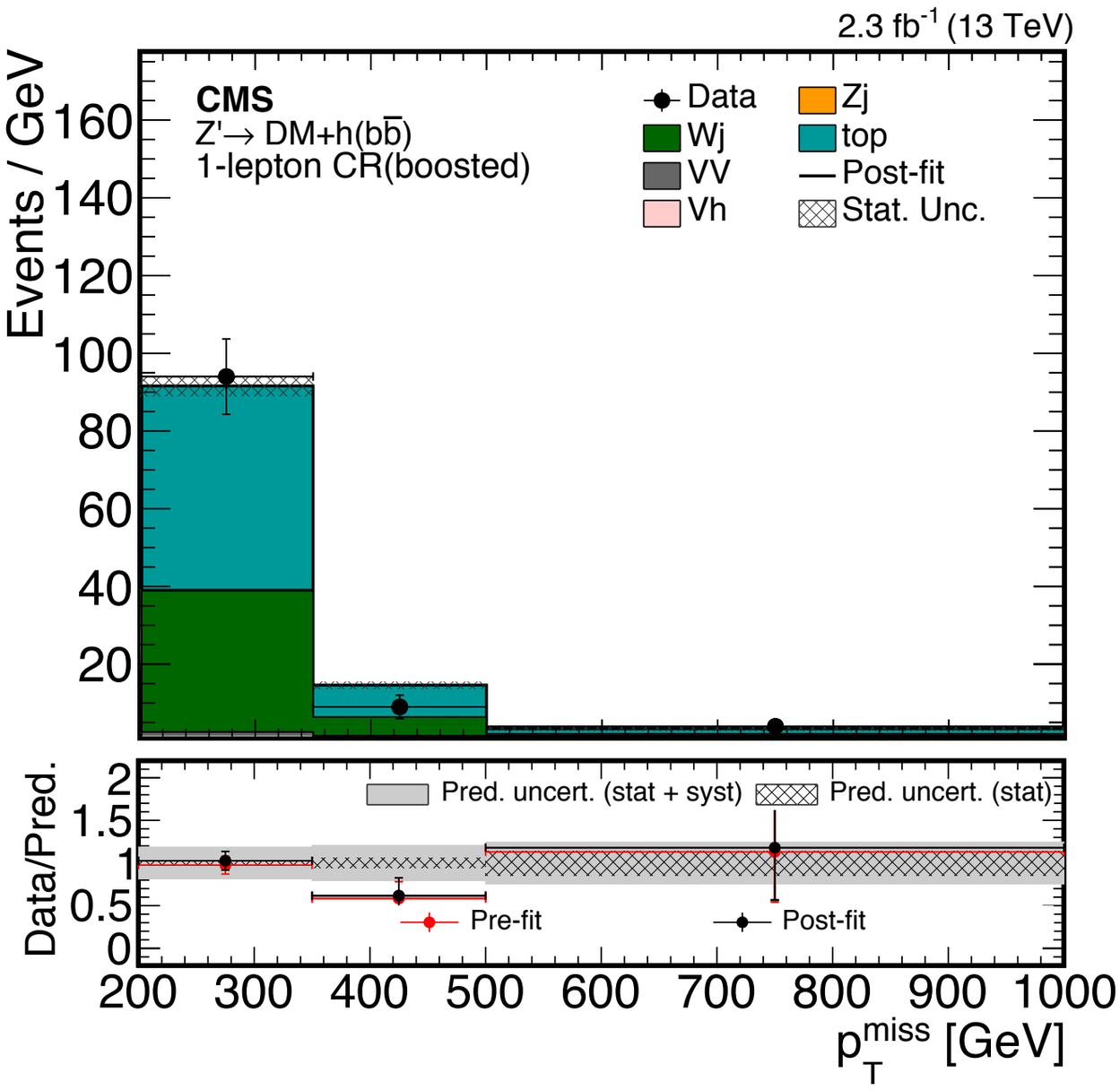

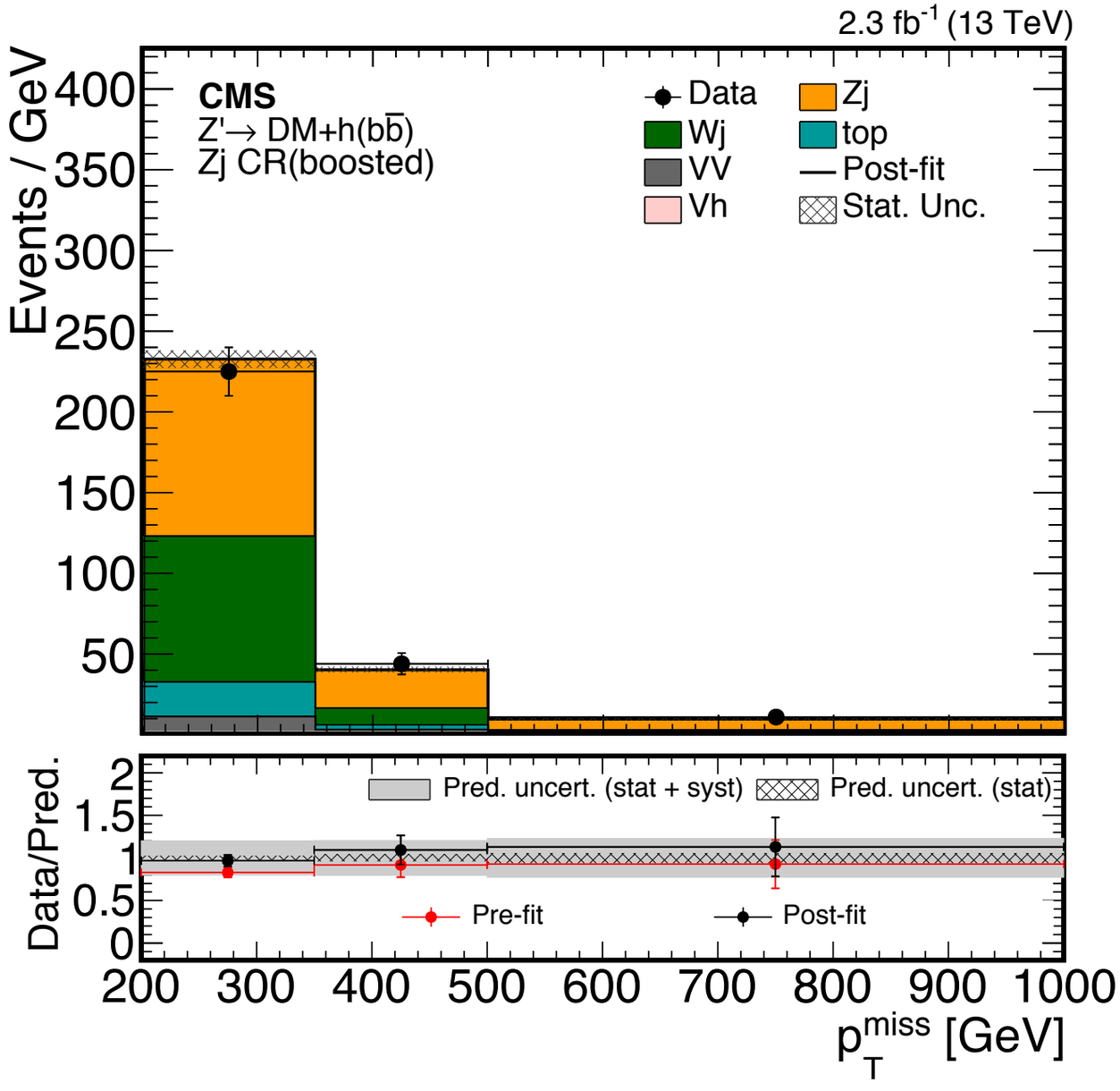

Mono H→bb: Signal Regions

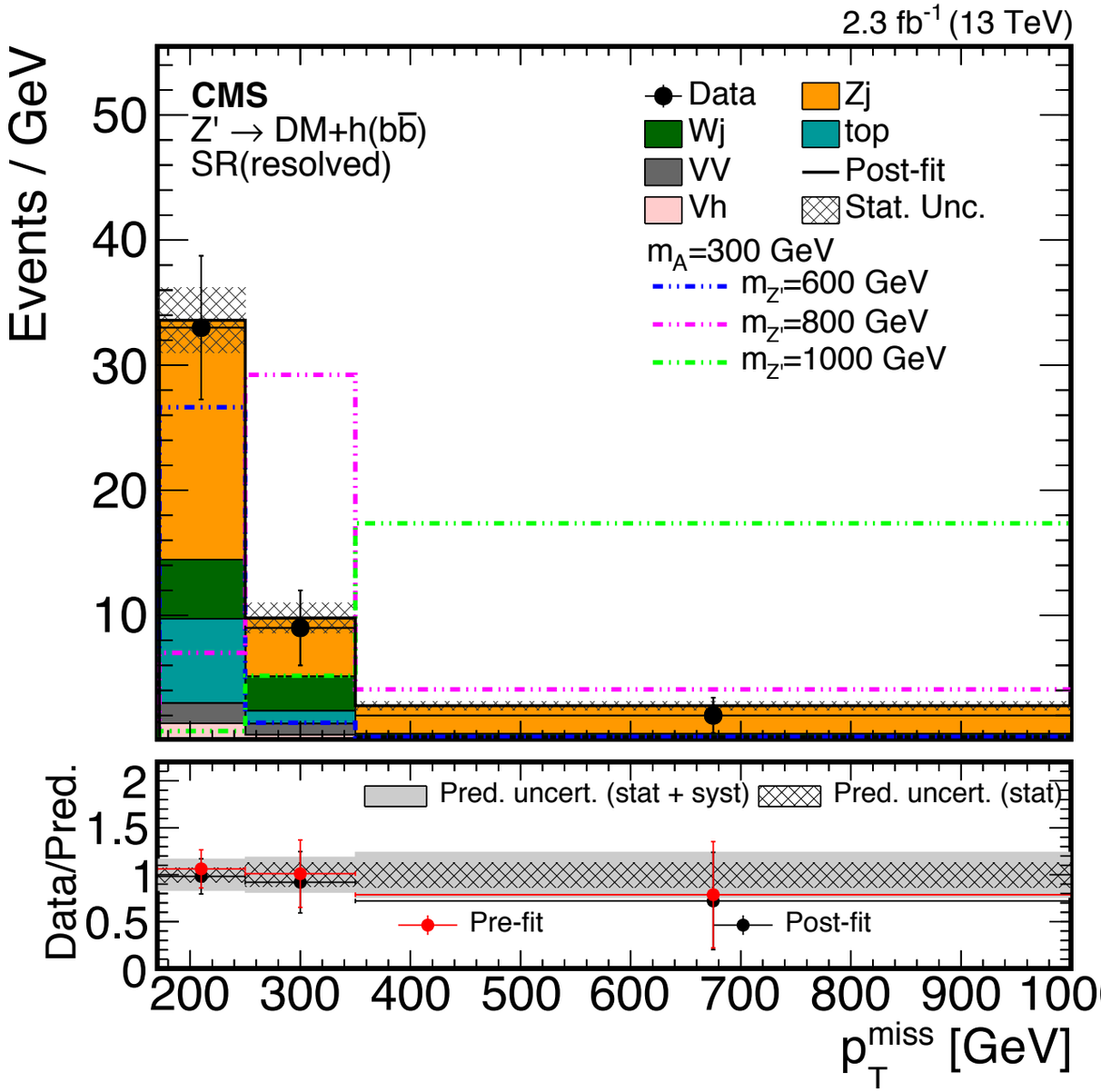

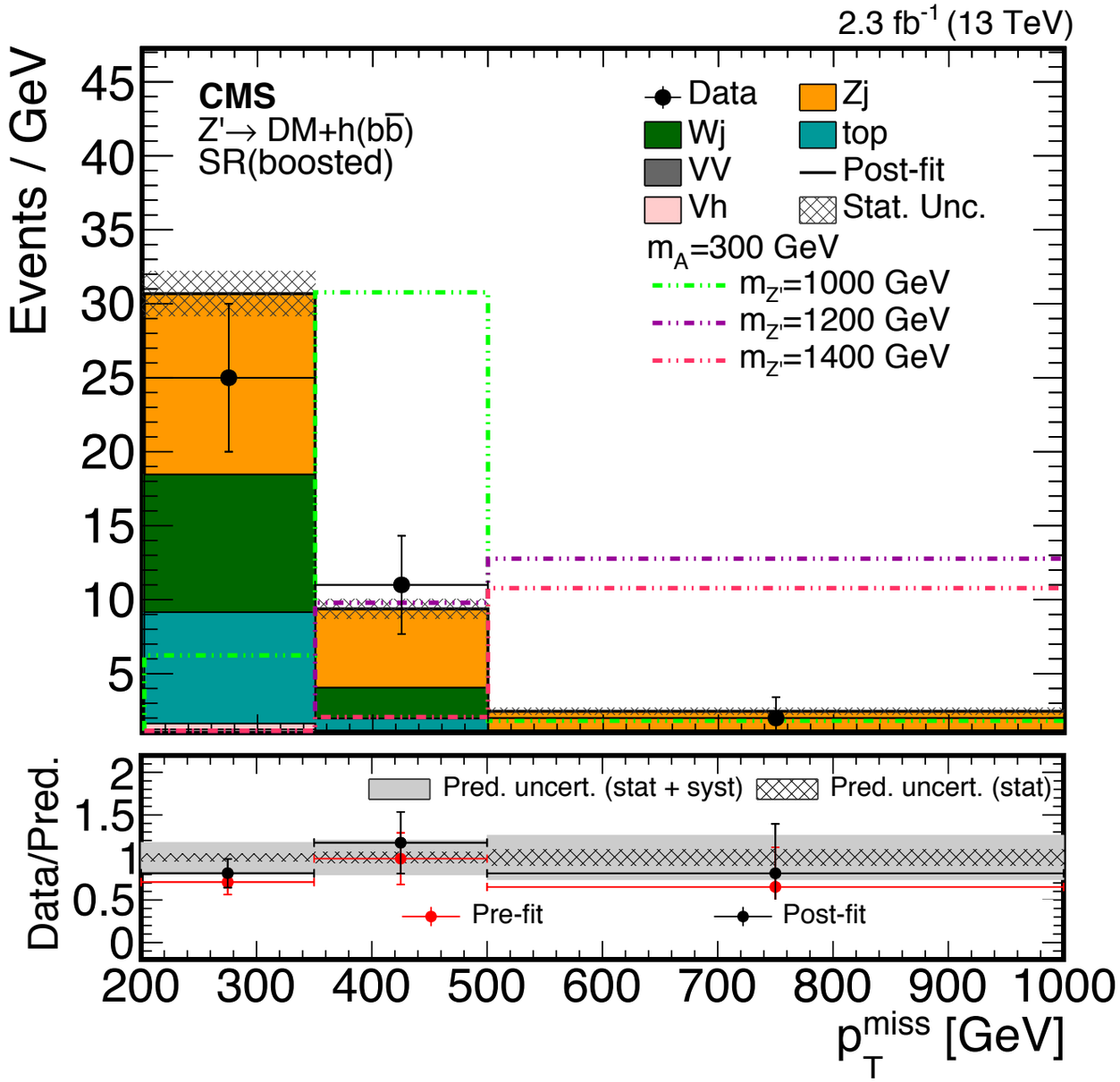

Mono H→bb: Event Display

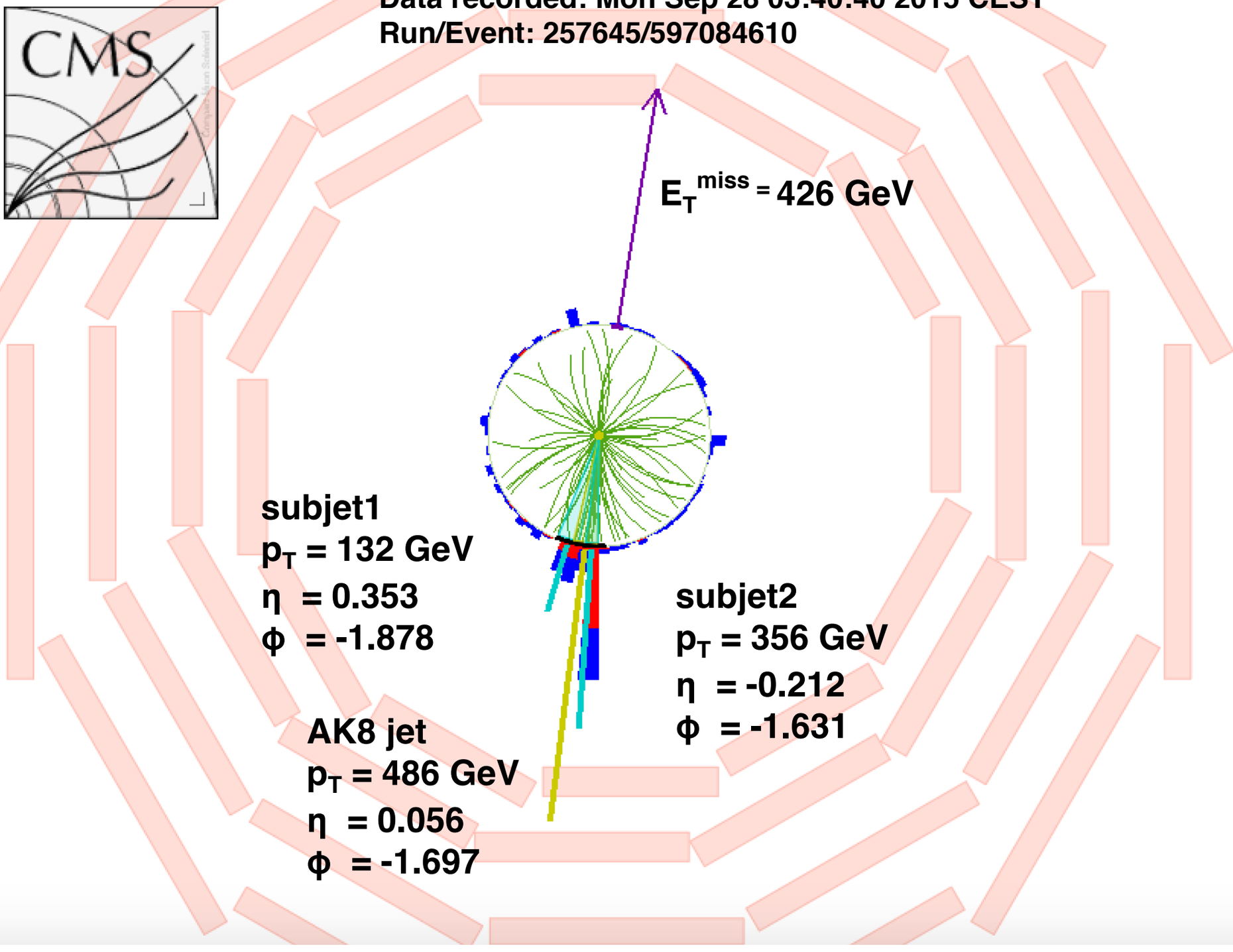

Mono H→$\gamma\gamma$: Event Selection

- Efficiency drops at large MZ' due to the isolation cut
  - $p_{\mathrm{T}\gamma\gamma} > 90$ GeV
  - $E_{\mathrm{T}}^{\mathrm{miss}} > 105$ GeV.
  - $p_{T1}/m_{\gamma\gamma} > 0.5$
  - $p_{T2}/m_{\gamma\gamma} > 0.25$

m_{A} [GeV]	300	400	500	600	700	800
$m_{Z'}$ [GeV]	$\mathrm{h} \to \gamma\gamma$					
600	0.317 ± 0.004	0.212 ± 0.003	—	—	—	—
800	0.399 ± 0.004	0.386 ± 0.003	0.348 ± 0.003	0.280 ± 0.003	—	—
1000	0.444 ± 0.004	0.437 ± 0.003	0.422 ± 0.003	0.402 ± 0.003	0.373 ± 0.003	0.330 ± 0.003
1200	0.474 ± 0.004	0.468 ± 0.003	0.461 ± 0.003	0.454 ± 0.003	0.438 ± 0.003	0.417 ± 0.003
1400	0.492 ± 0.004	0.493 ± 0.003	0.485 ± 0.003	0.481 ± 0.003	0.472 ± 0.003	0.465 ± 0.003
1700	0.493 ± 0.004	0.499 ± 0.003	0.504 ± 0.003	0.503 ± 0.003	0.499 ± 0.003	0.498 ± 0.003
2000	0.351 ± 0.004	0.373 ± 0.003	0.394 ± 0.003	0.421 ± 0.003	0.453 ± 0.003	0.488 ± 0.003
2500	0.213 ± 0.004	0.217 ± 0.003	0.227 ± 0.003	0.236 ± 0.003	0.254 ± 0.003	0.268 ± 0.003

Mono H→$\gamma\gamma$: Major Kinematic Distributions

Resonant background: estimated with simulation

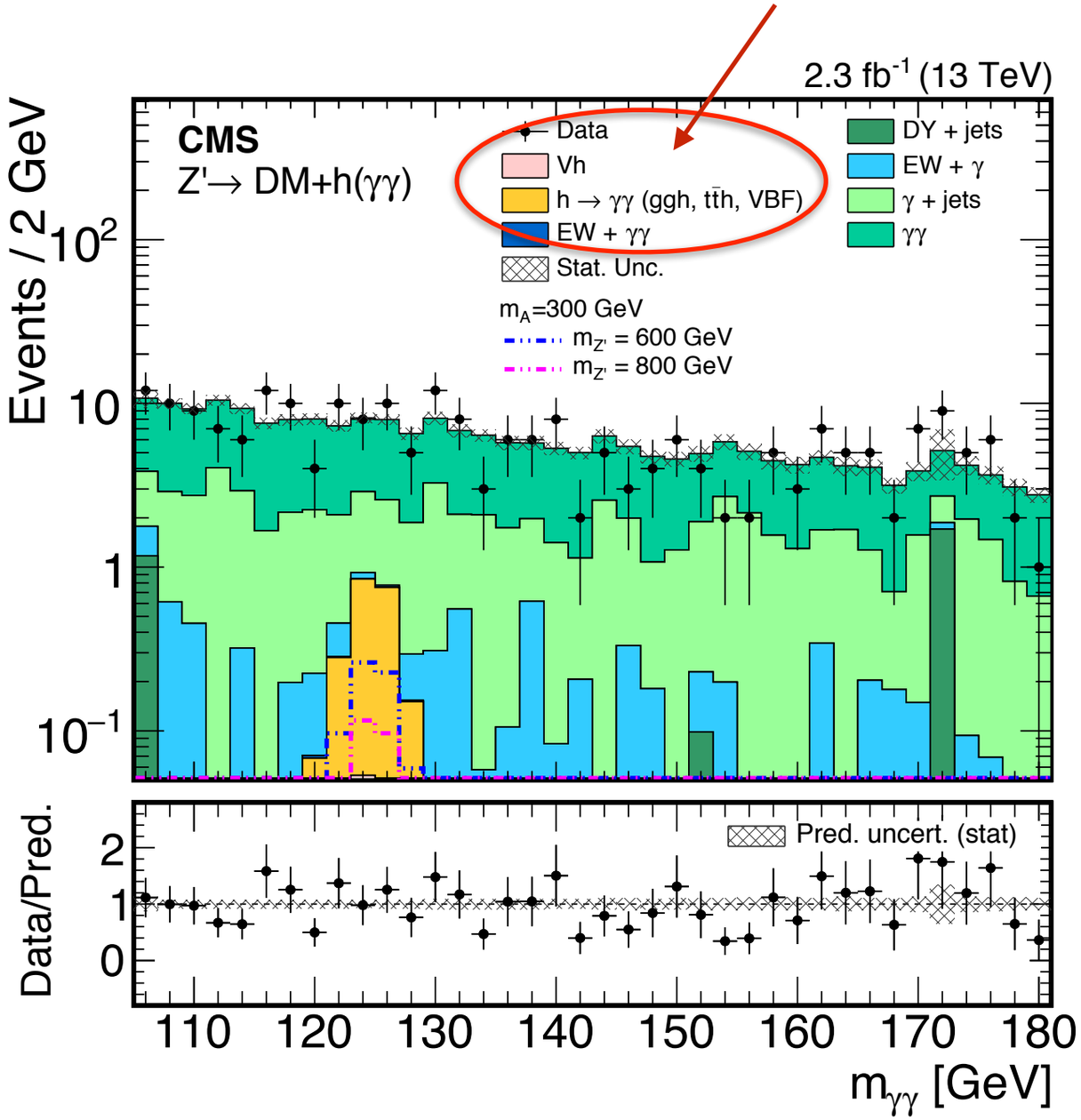

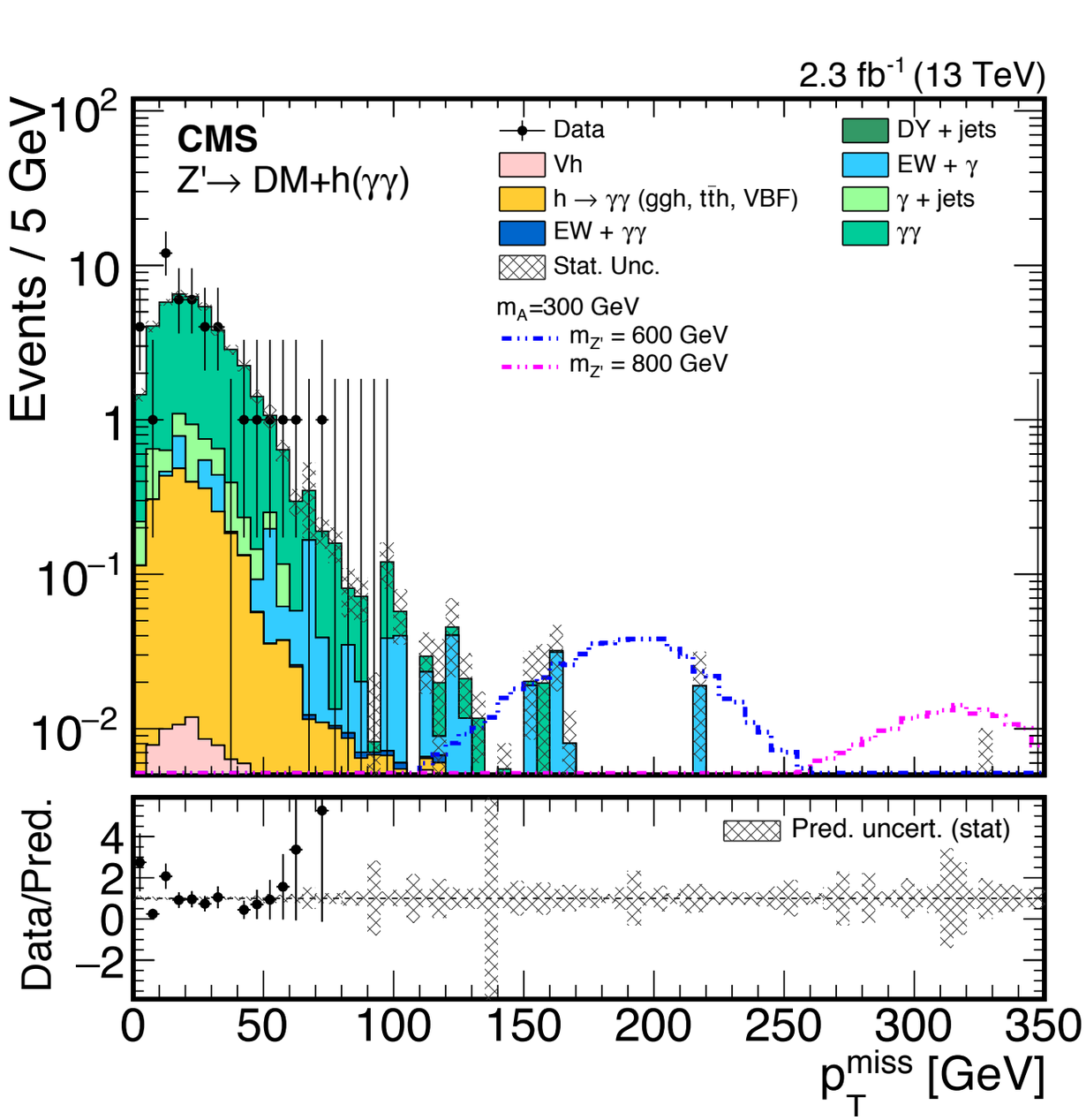

Mono H→$\gamma\gamma$: Non-Resonant Background

- Estimated from low MET (MET<105 GeV) control regions and diphoton mass sideband

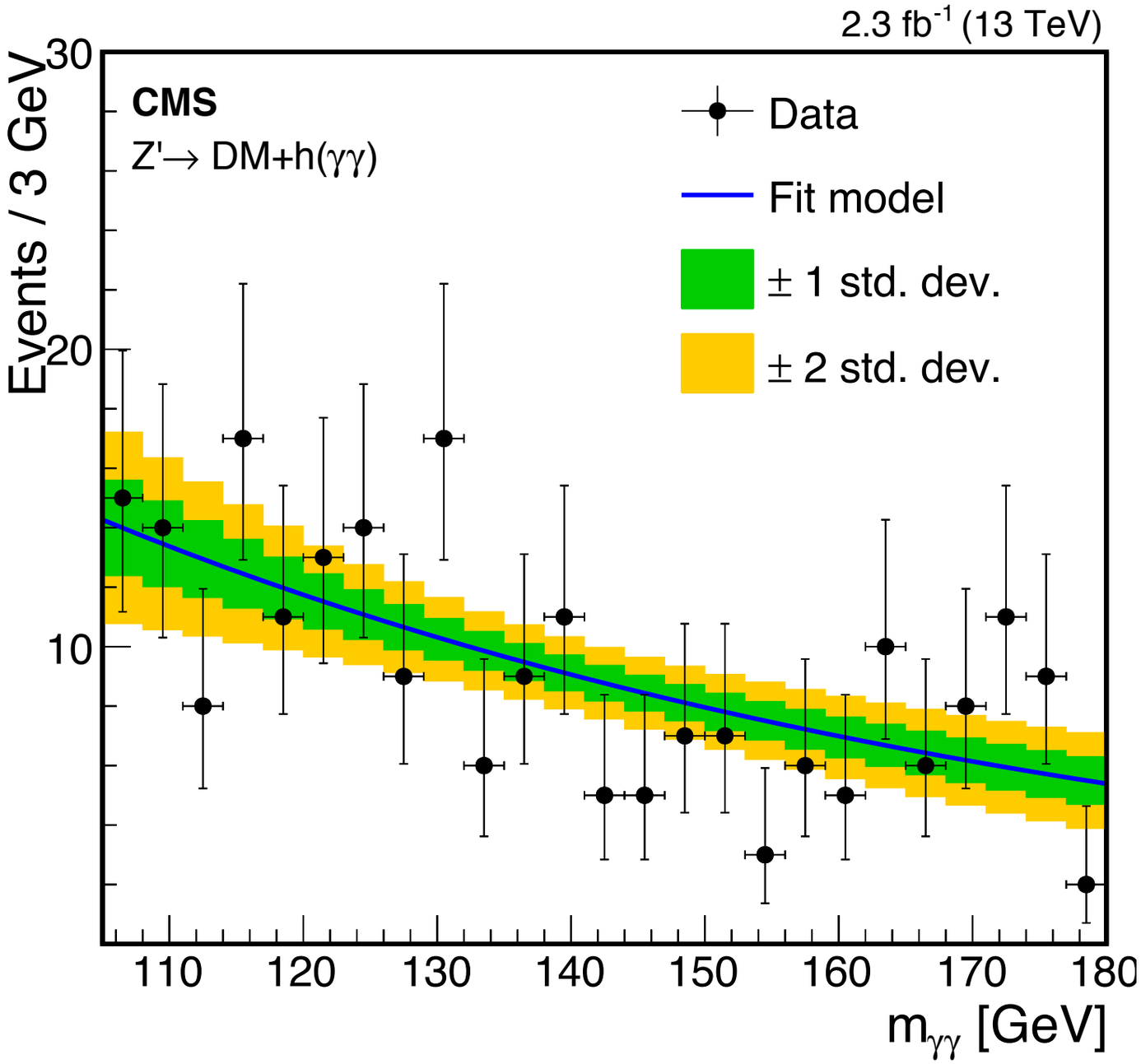

Mono H→$\gamma\gamma$: Non-Resonant Background

- Estimated from low MET (MET<105 GeV) control regions and diphoton mass sideband

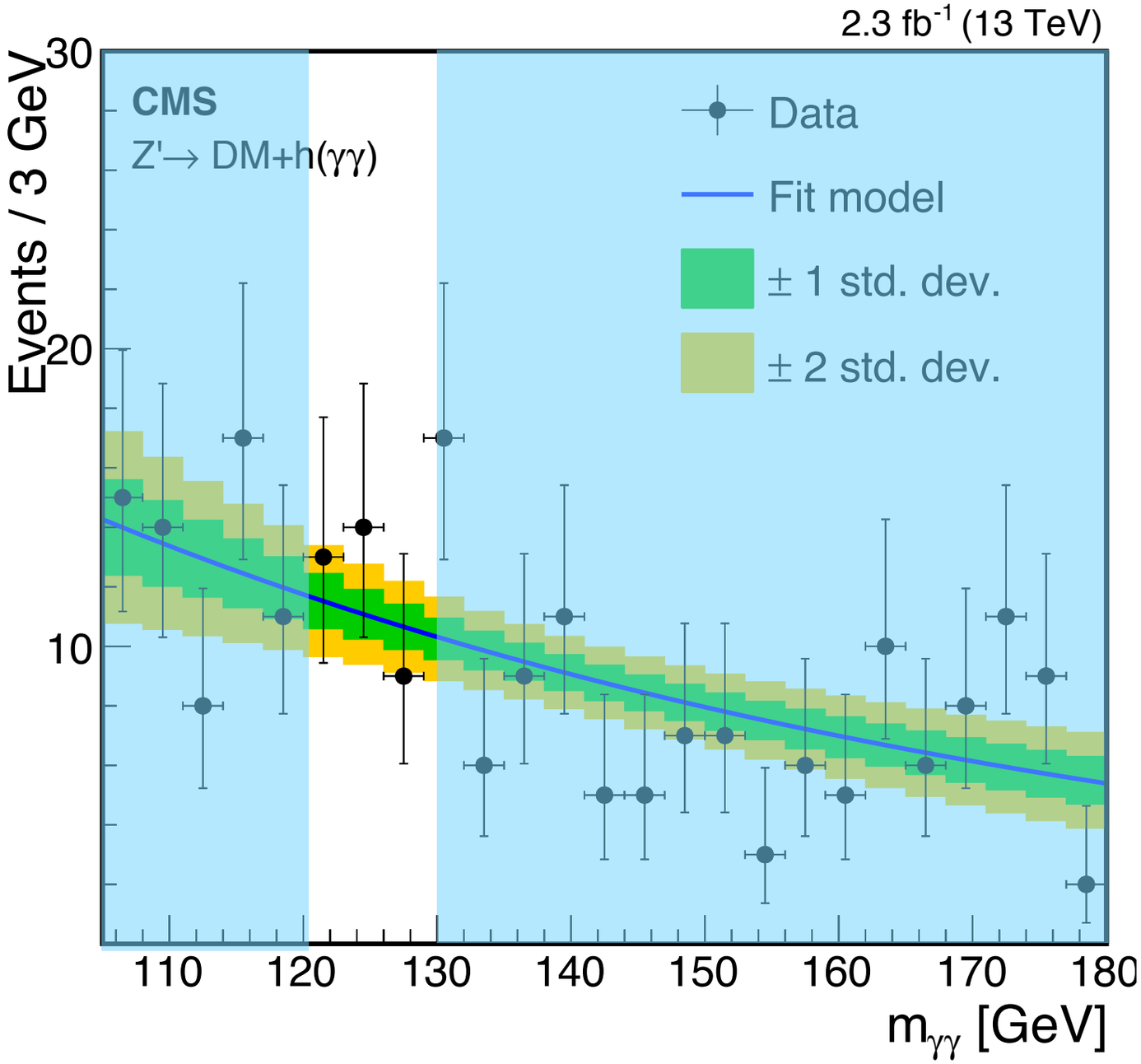

$$N_{\mathrm{SR}}^{\mathrm{bkg}} = \alpha N_{\mathrm{SB}}^{\mathrm{bkg}}$$

Mono H→$\gamma\gamma$: Non-Resonant Background

- Estimated from low MET (MET<105 GeV) control regions and diphoton mass sideband

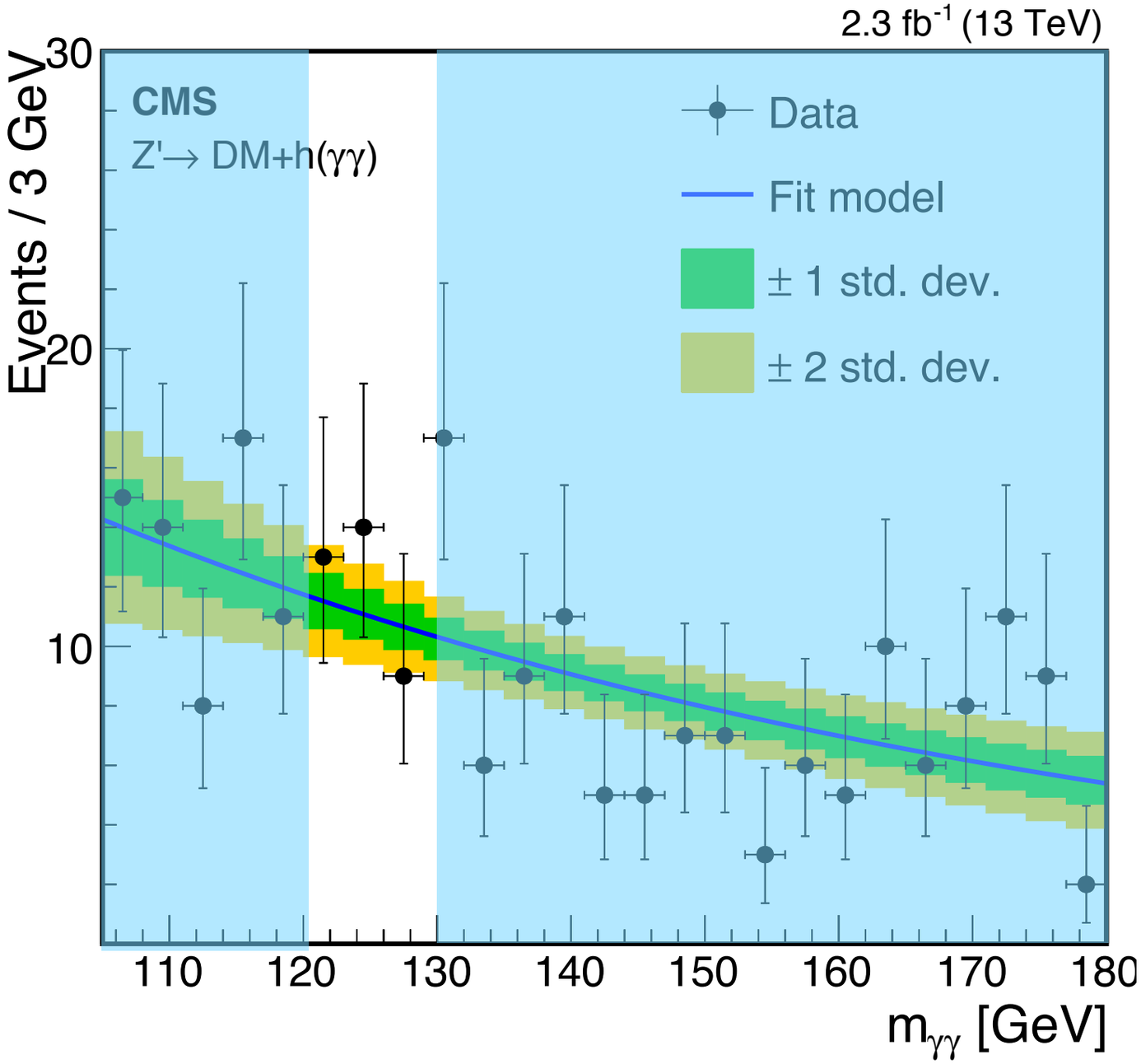

$$N_{\mathrm{SR}}^{\mathrm{bkg}} = \alpha N_{\mathrm{SB}}^{\mathrm{bkg}}$$

$$\alpha = \frac{\int_{\mathrm{SR}} f_{\mathrm{bkg}}(m_{\gamma\gamma})\mathrm{d}m_{\gamma\gamma}}{\int_{\mathrm{SB}} f_{\mathrm{bkg}}(m_{\gamma\gamma})\mathrm{d}m_{\gamma\gamma}}$$

Combining the Two Decay Channels

Resolved

Boosted

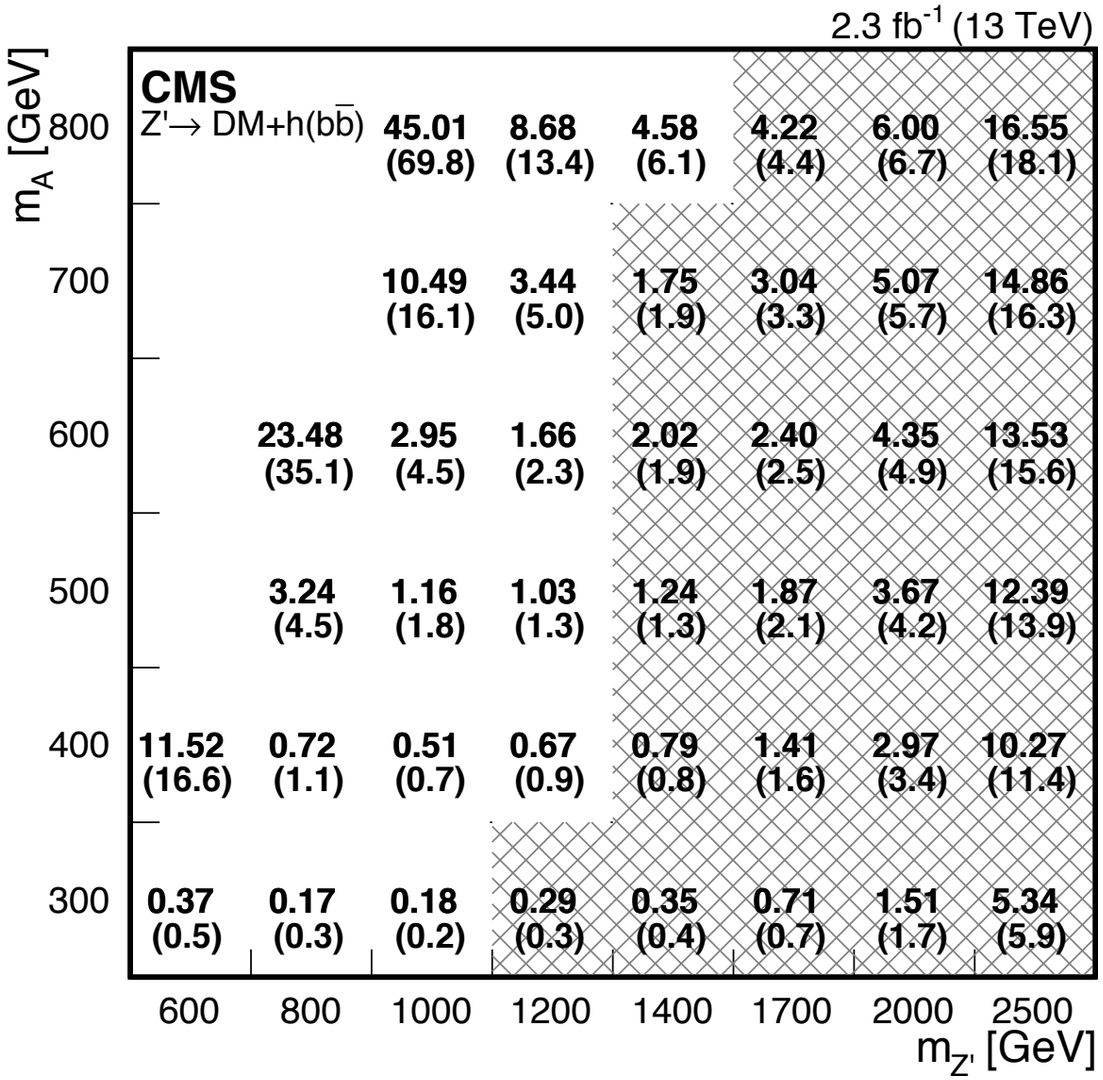

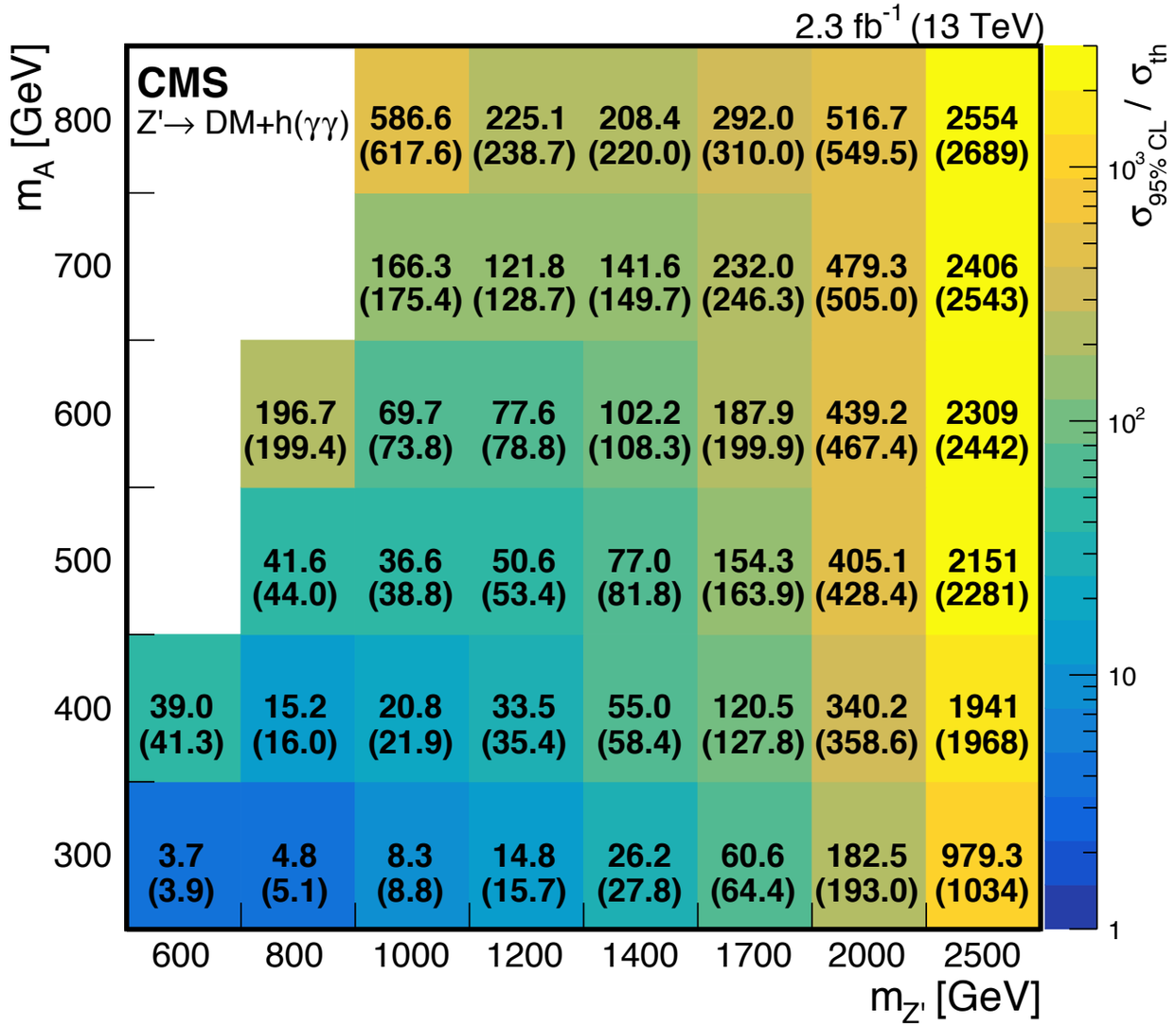

Combining the Two Decay Channels

- 600 (770) < mZ' < 1860 (2040) GeV excluded for $g_{Z'}$=0.8 (formula)

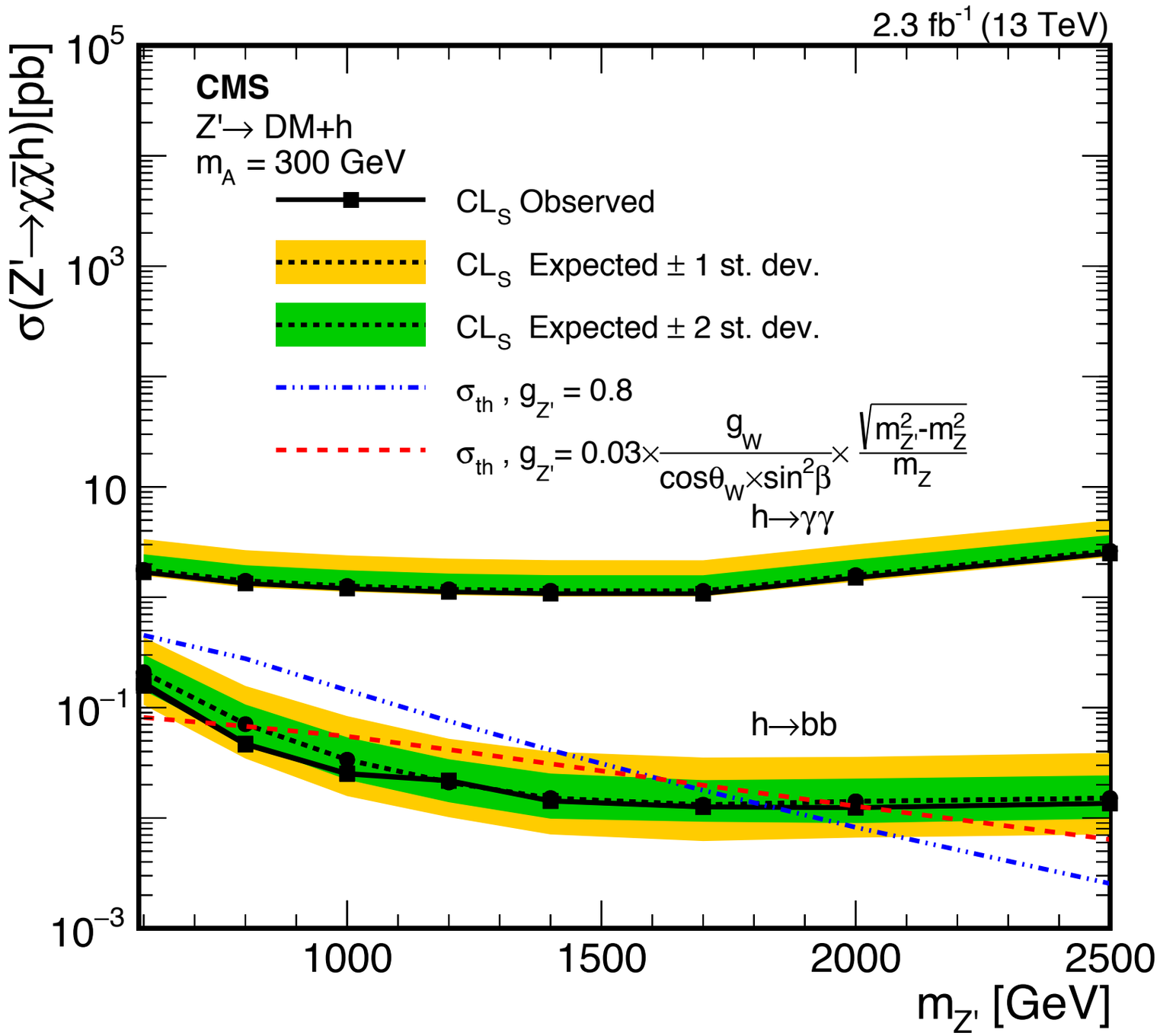

Expanding the Mass Of A

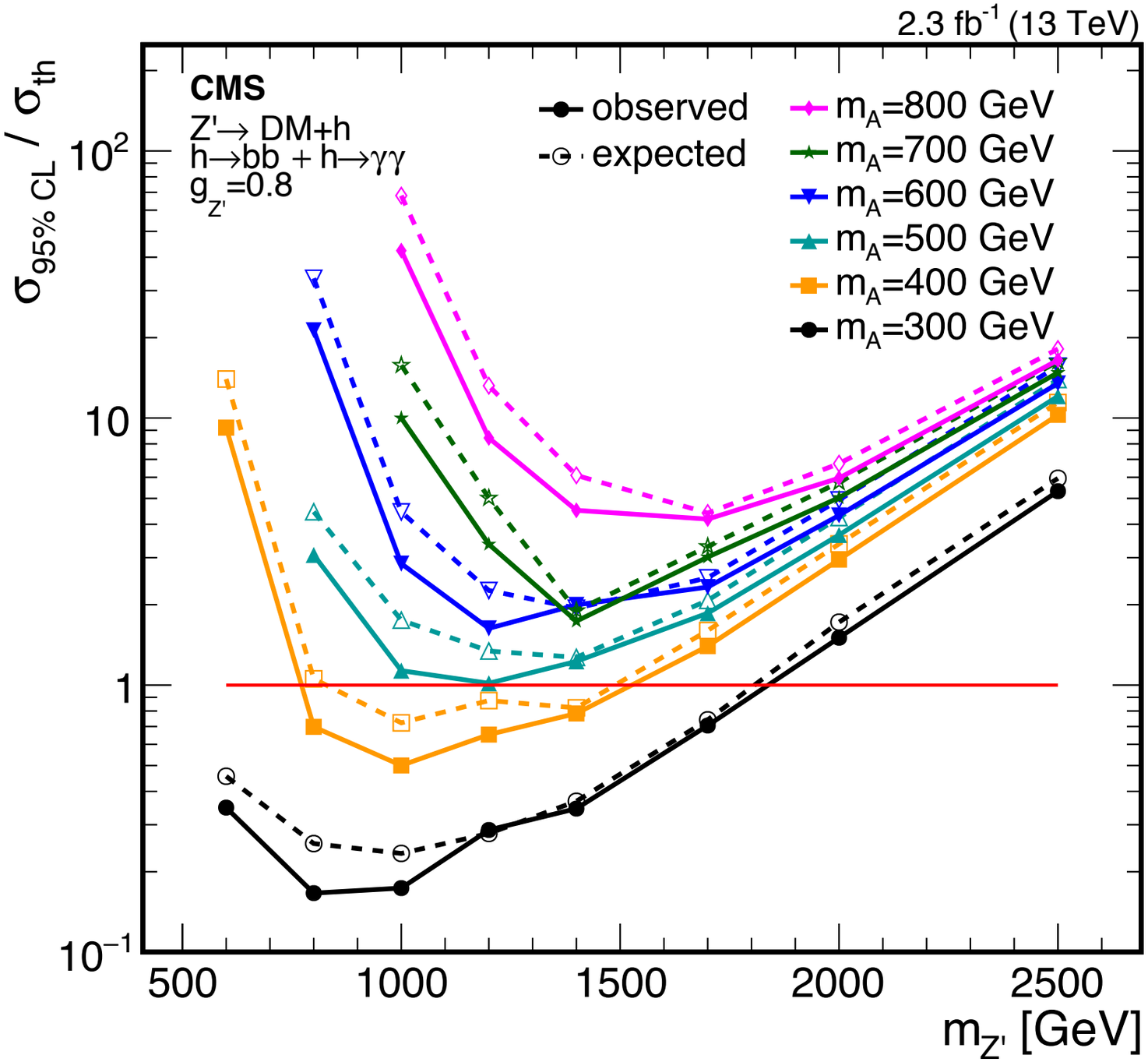

Mono-X With Vector/Axial Mediators

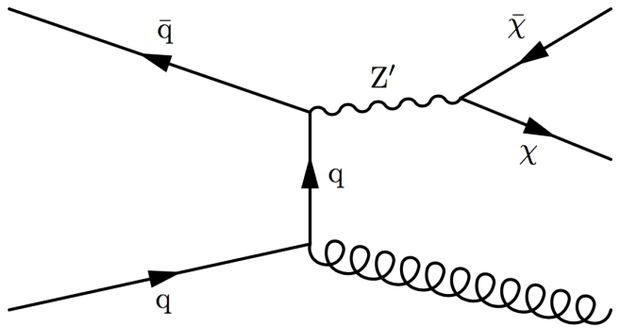

Mono-jet

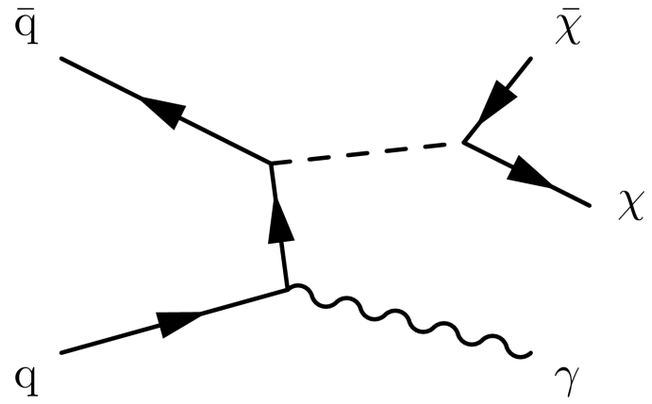

Mono-photon

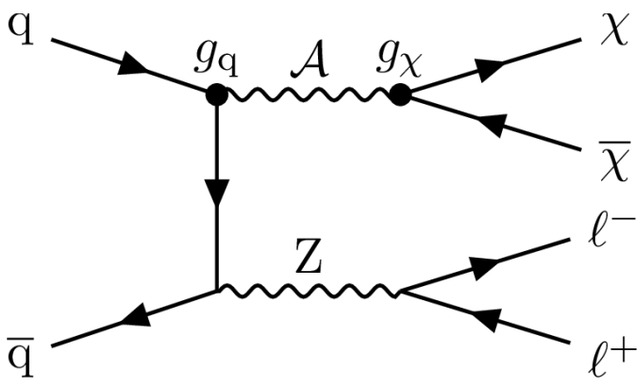

Mono-Z(leptonic)

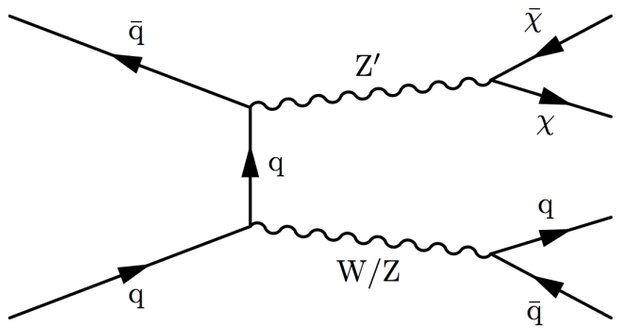

Mono-W/Z(hadronic)

Collider Results Only (Axial-Vector Mediator)

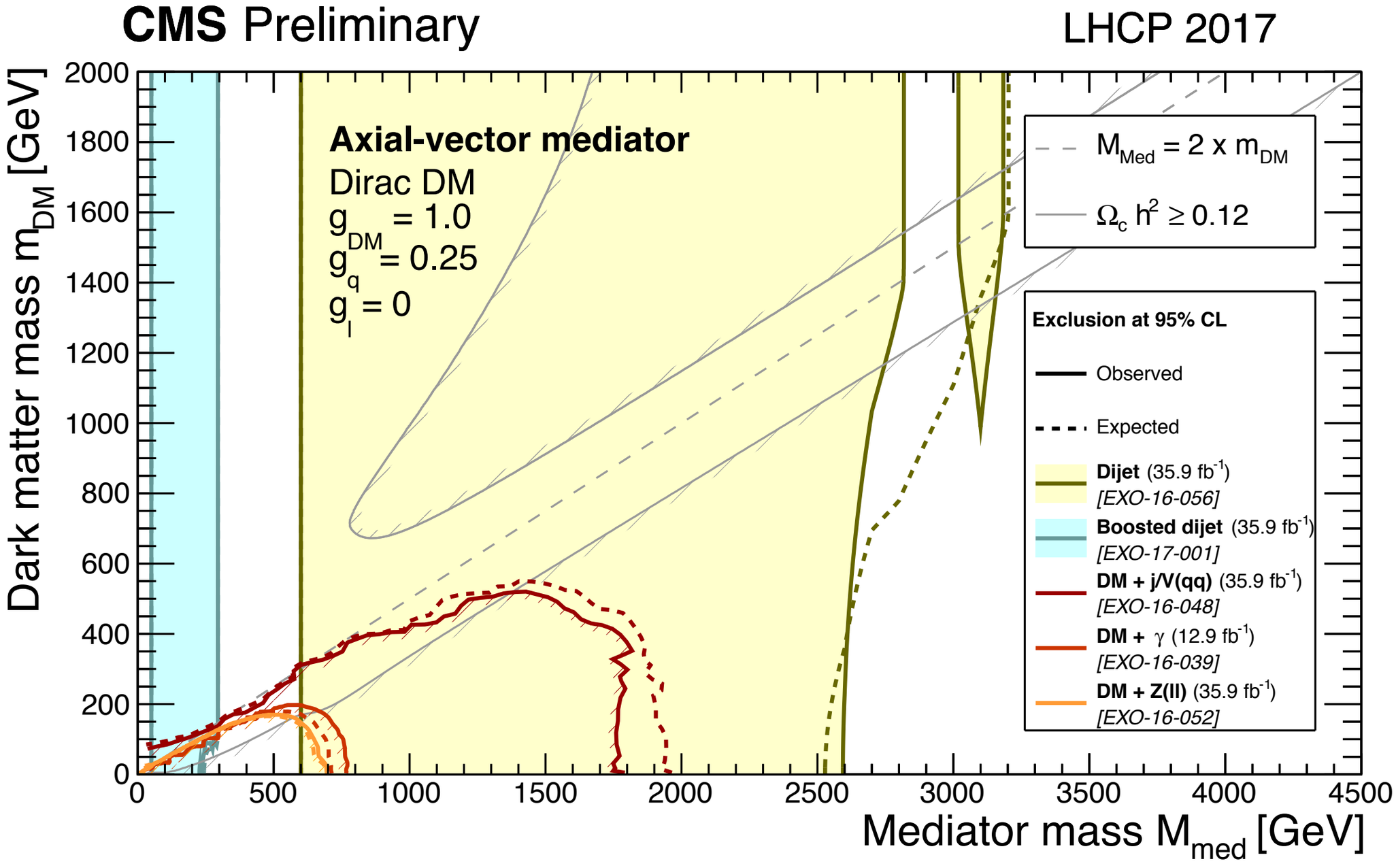

If We Use Different Parameter Values

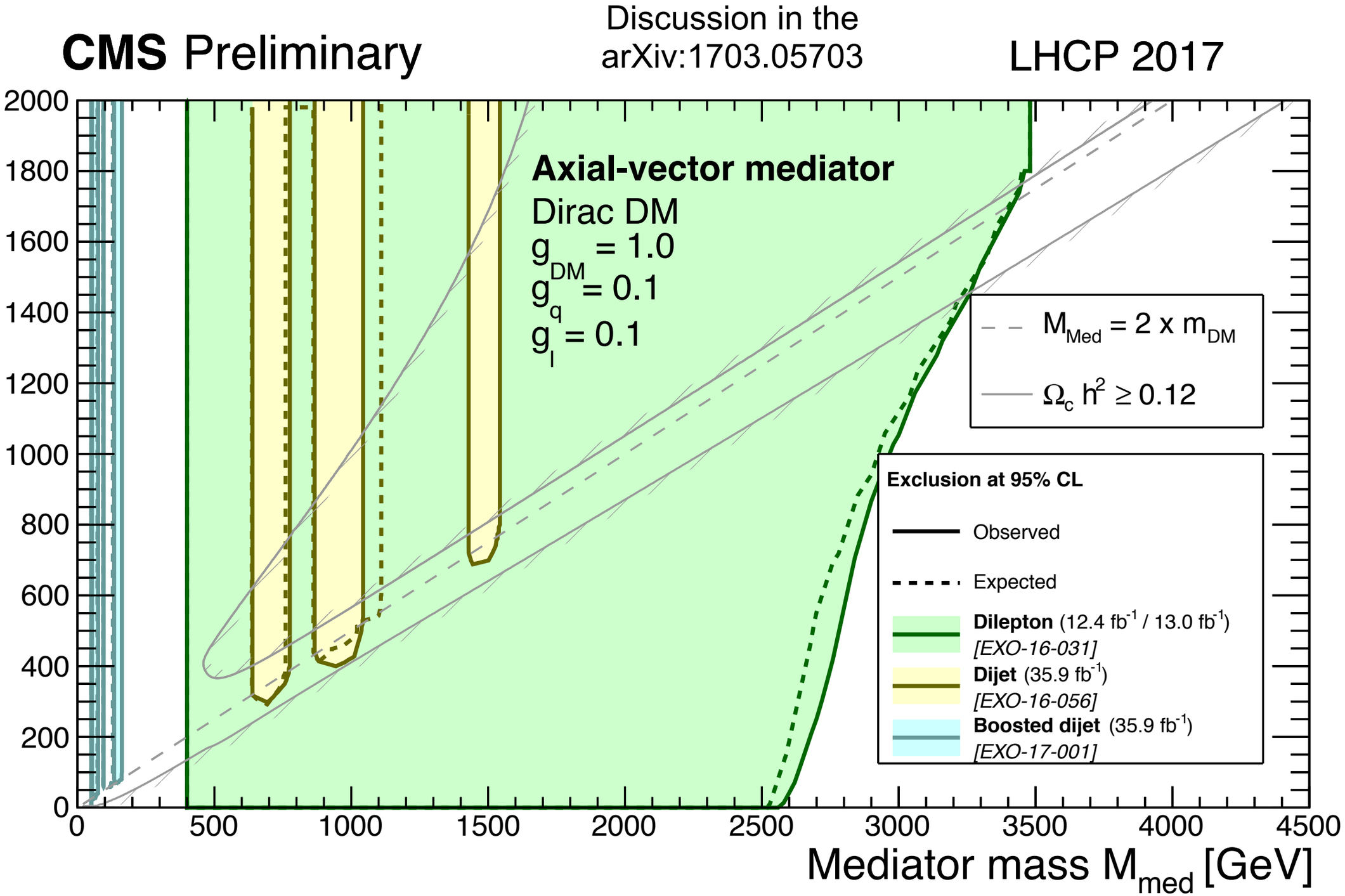

Collider v.s. Non-Collider Experiments (SI)

$$\sigma_{\mathrm{SI}}^{\mathrm{vector}} \simeq 6.9\times10^{-41}\,\mathrm{cm}^2 \left(\frac{g_q g_{\mathrm{DM}}}{0.25}\right)^2 \left(\frac{1\ \mathrm{TeV}}{M_{\mathrm{med}}}\right)^4 \left(\frac{\mu_{n\chi}}{1\ \mathrm{GeV}}\right)^2$$

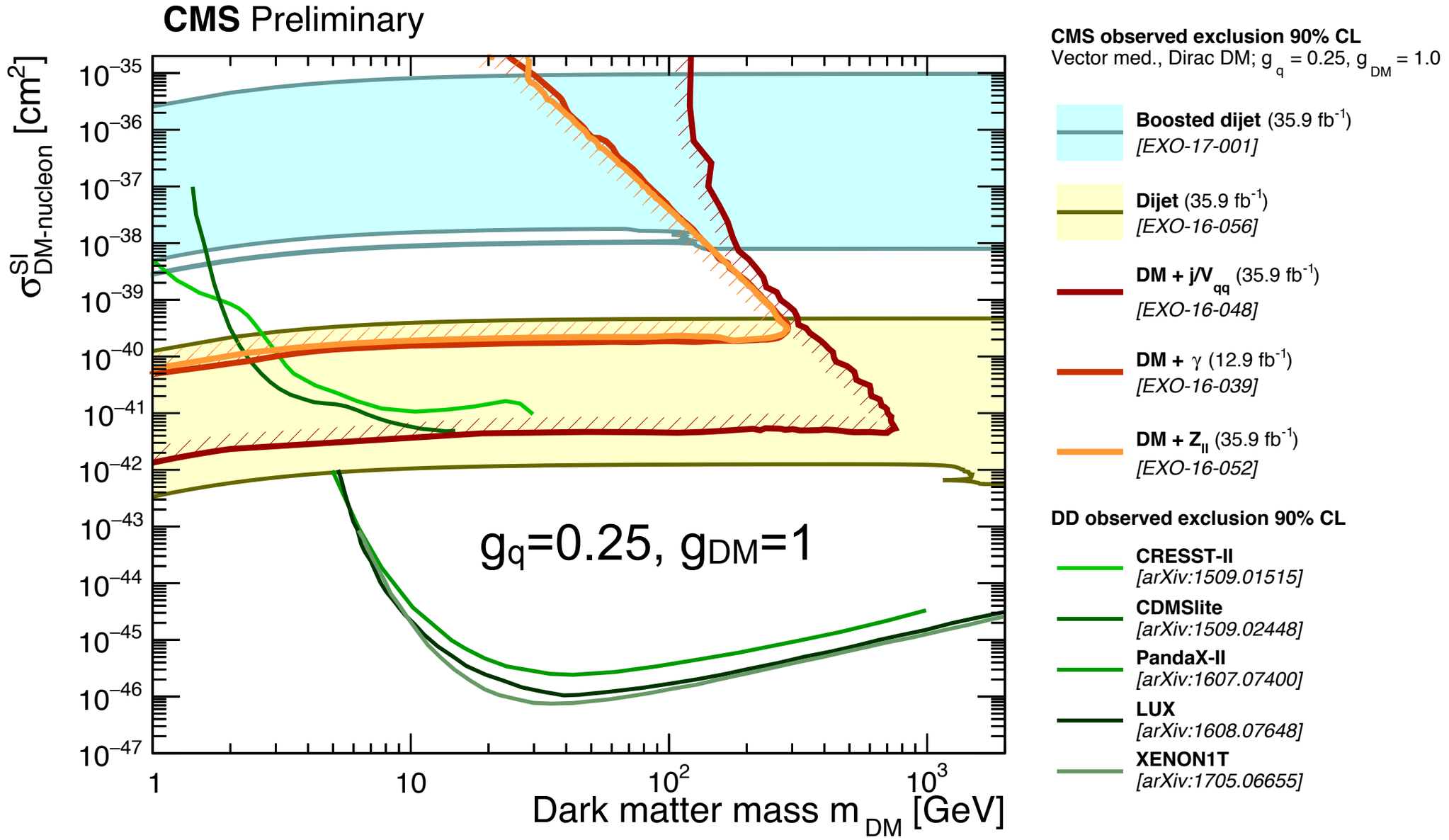

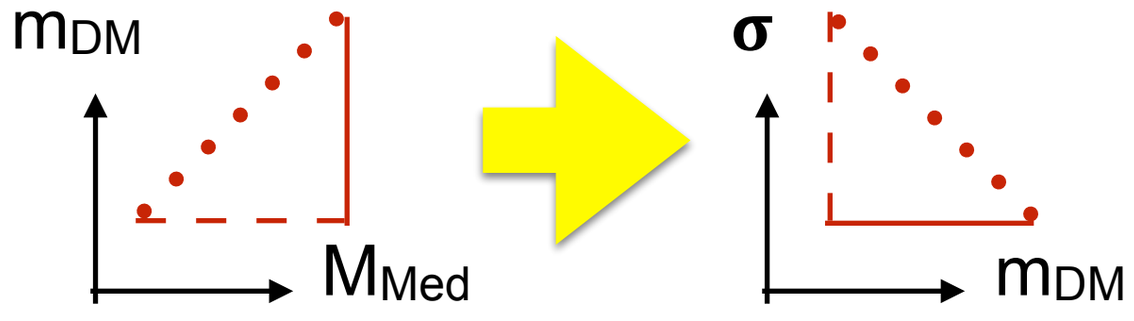

Collider v.s. Non-Collider Experiments (SI)

$$\sigma_{\mathrm{SI}}^{\mathrm{vector}} \simeq 6.9\times10^{-41}\,\mathrm{cm}^2 \left(\frac{g_q g_{\mathrm{DM}}}{0.25}\right)^2 \left(\frac{1\ \mathrm{TeV}}{M_{\mathrm{med}}}\right)^4 \left(\frac{\mu_{n\chi}}{1\ \mathrm{GeV}}\right)^2$$

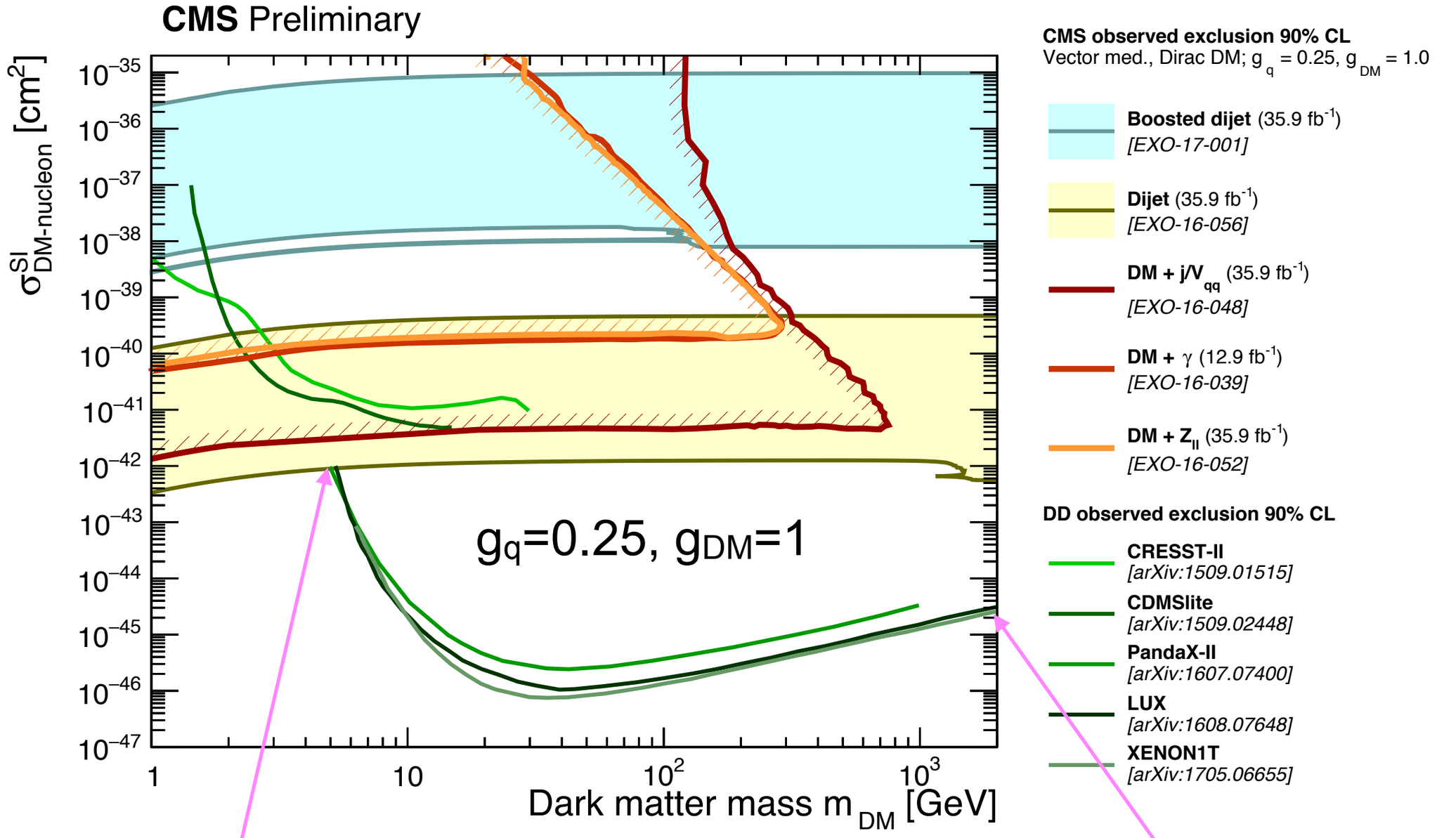

Experimental limit

No upper bound

Collider v.s. Non-Collider Experiments (SI)

$$\sigma_{\mathrm{SI}}^{\mathrm{vector}} \simeq 6.9\times10^{-41}\,\mathrm{cm}^2 \left(\frac{g_q g_{\mathrm{DM}}}{0.25}\right)^2 \left(\frac{1\ \mathrm{TeV}}{M_{\mathrm{med}}}\right)^4 \left(\frac{\mu_{n\chi}}{1\ \mathrm{GeV}}\right)^2$$

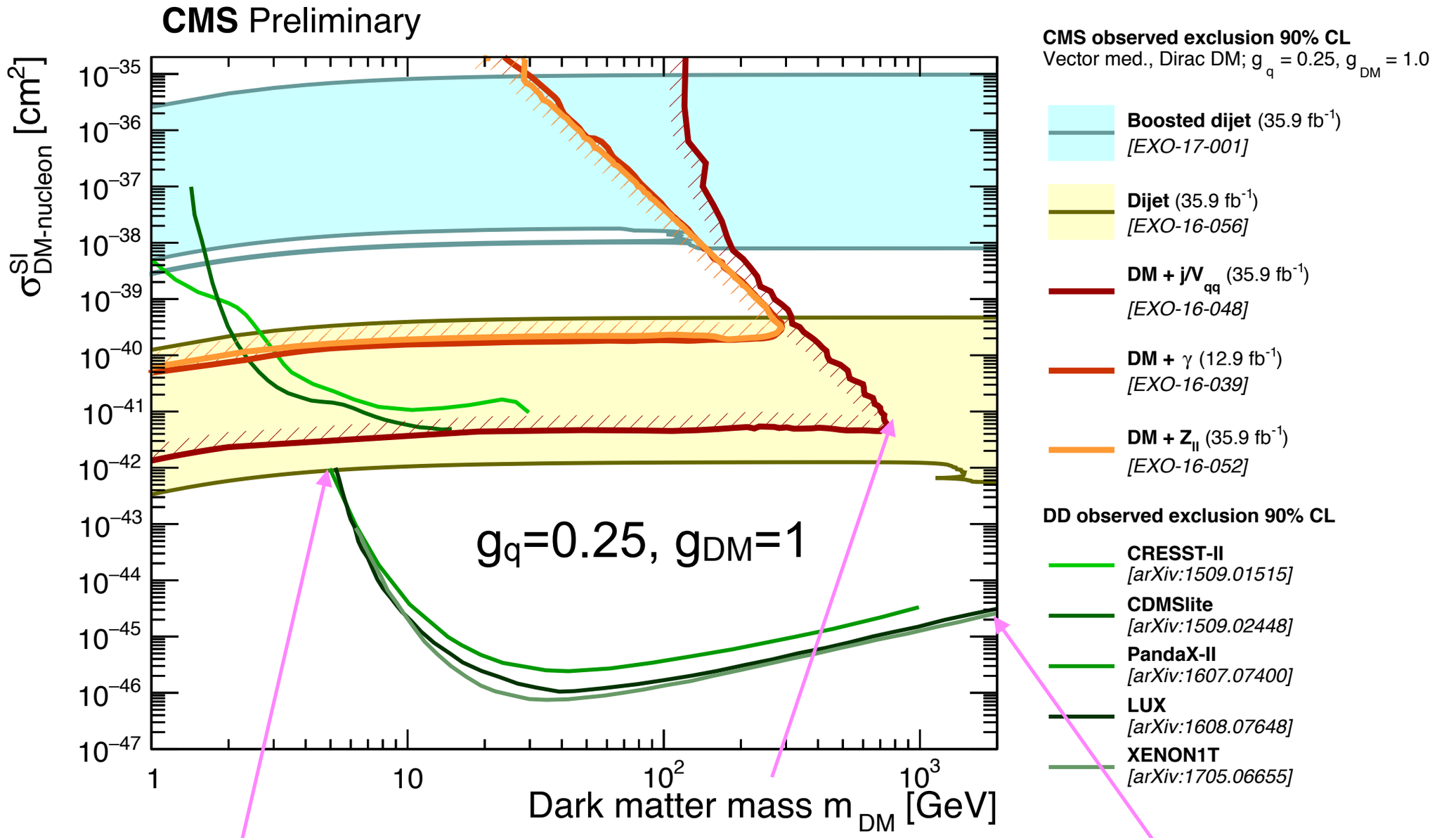

Experimental limit

Upper bound limited by mediator mass (collider energy)

No upper bound

Collider v.s. Non-Collider Experiments (SD)

$$\sigma_{\mathrm{SD}}^{\mathrm{axial}} \simeq 2.4\times10^{-42}\,\mathrm{cm}^2 \left(\frac{g_q g_{\mathrm{DM}}}{0.25}\right)^2 \left(\frac{1\ \mathrm{TeV}}{M_{\mathrm{med}}}\right)^4 \left(\frac{\mu_{n\chi}}{1\ \mathrm{GeV}}\right)^2$$

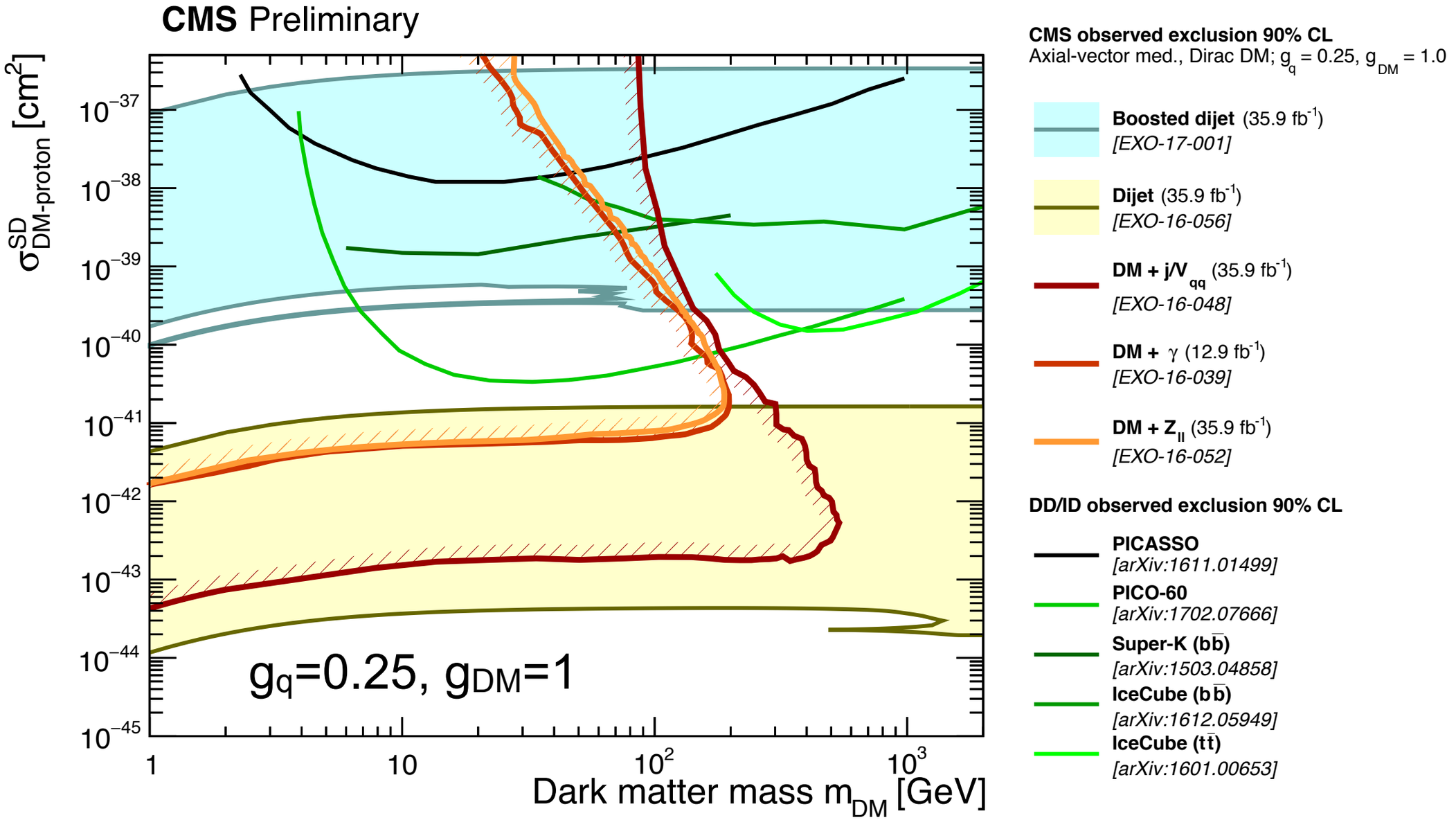

For the model parameters considered here, collider experiments can probe SD cross sections 2-3 orders of magnitude smaller than the non-collider experiments.

Mono-X with Scalar/Pseudo-Scalar Mediators

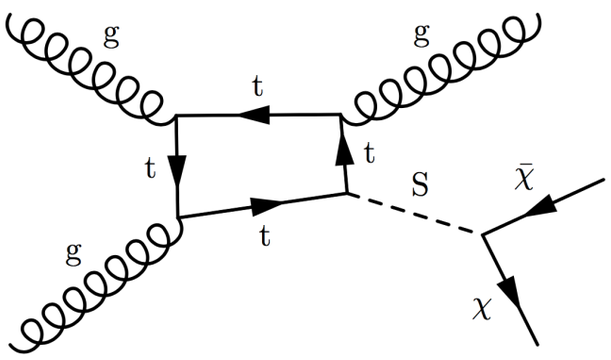

Mono-jet

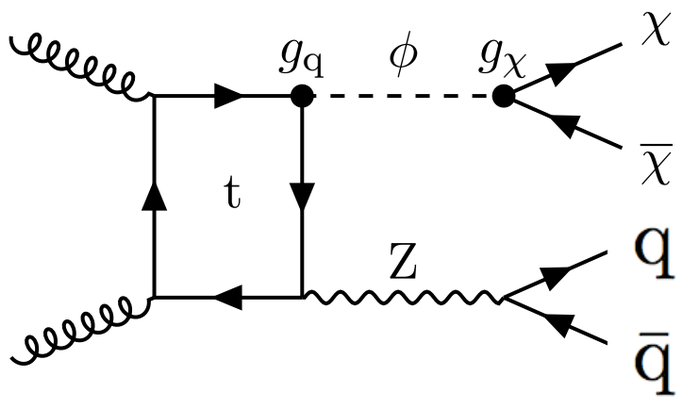

Mono-Z(hadronic)

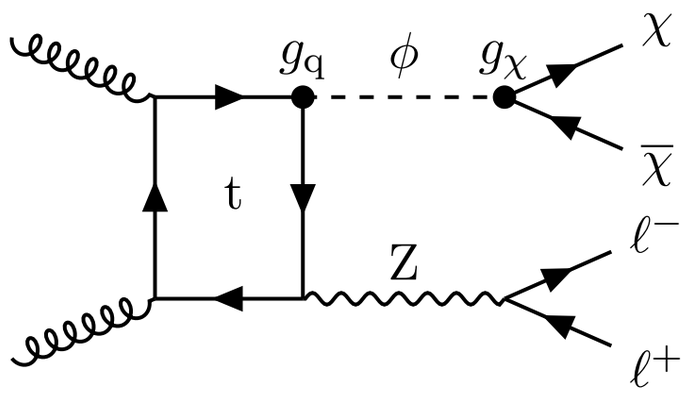

Mono-Z(leptonic)

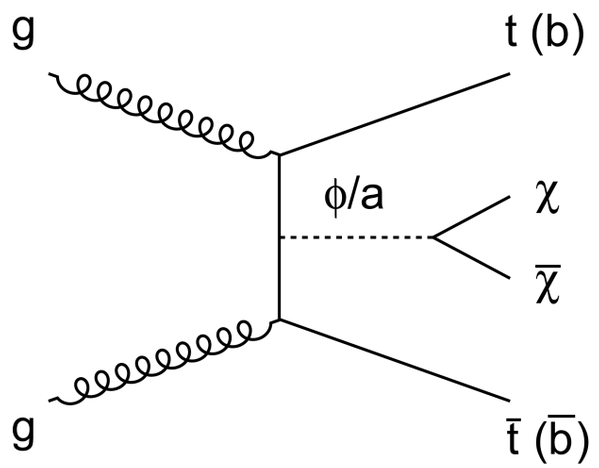

Mono-tt/bb

Collider Results for Scalar/Pseudo-Scalar

- For the mono-V channel, pseudo-scalar/scalar limits include ggZH diagrams only because VH generators do not yet include mixing with SM Higgs
- ttbar is the best at low-mass

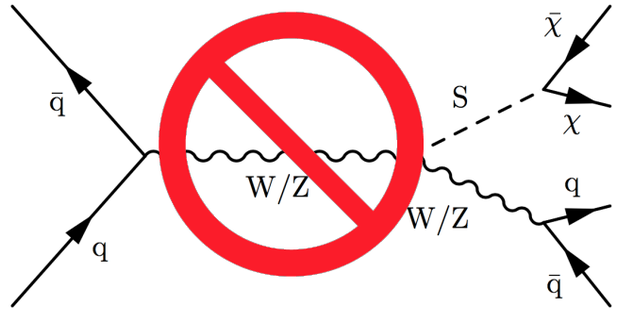

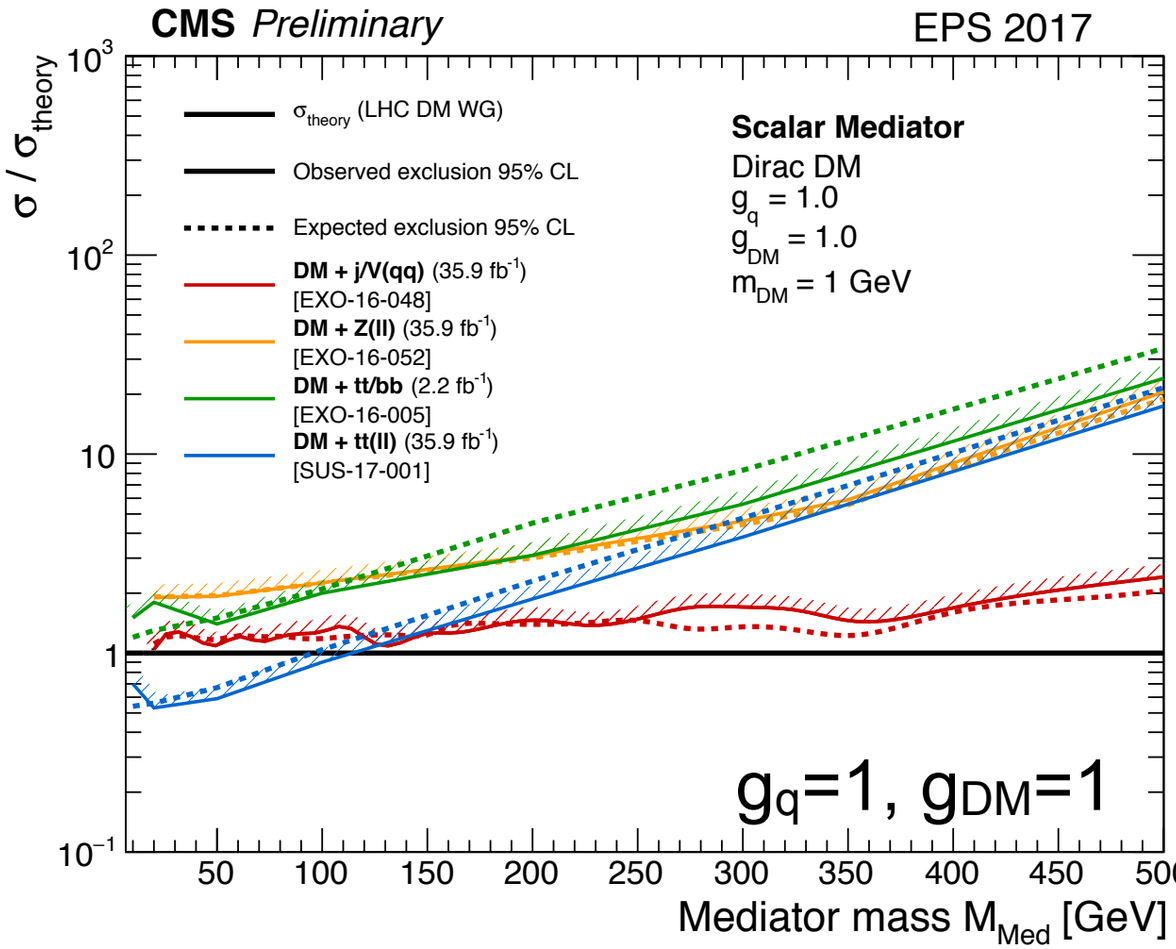

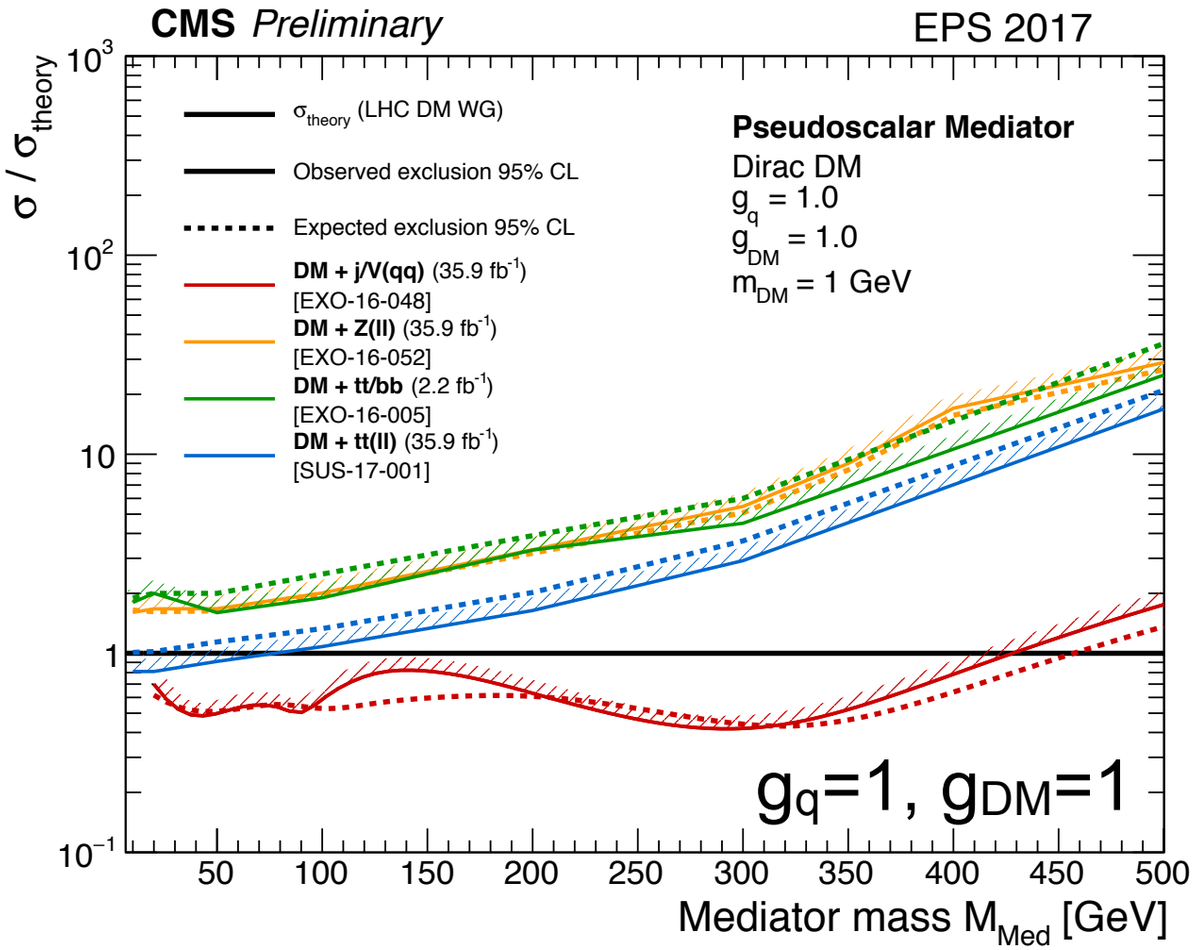

Possibility to Combine With Other Mono-X?

- The h in the Feynman diagram below could be replaced with a quark to give a mono-jet signature

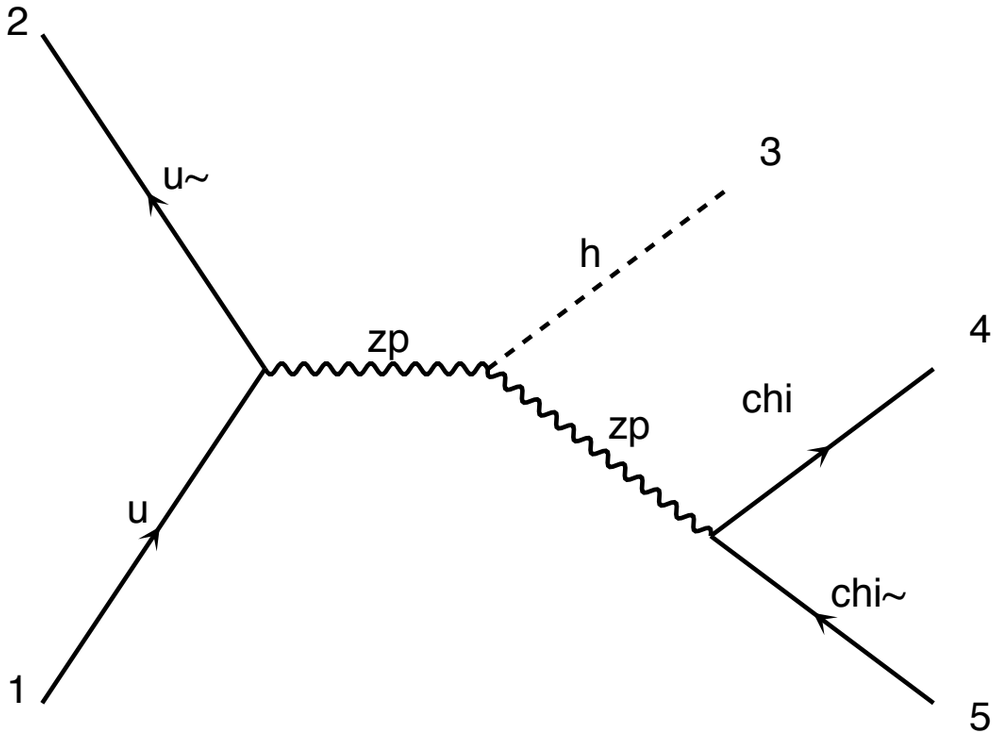

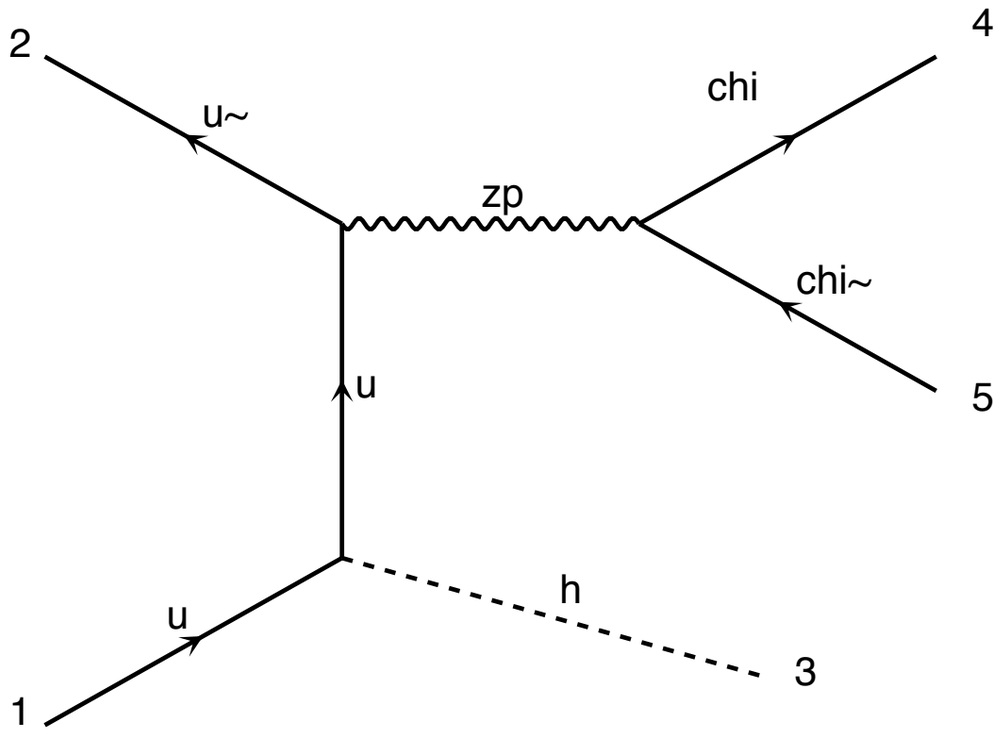

Conclusion And Outlook

- We have started a new dark matter channel at CMS and searched for associated production of dark matter with a Higgs boson decaying to bb or $\gamma\ \gamma$, using the 2015 13 TeV data
- For the bb channel, we are working on a completely different analysis method for the 2016 analysis
  - CA15 jet reconstruction, double-b tagging, mono-jet-like background estimation, more signal model interpretation, soft drop mass and better pileup removal
- Comparison/Combination with other mono-X channels is expected.

Backup Slides

Mono H→bb: Resolved and Boosted Jets

- For jets with pT > 500 GeV, the reconstruction efficiency of one AK8 jet is higher than that of two AK4 jets

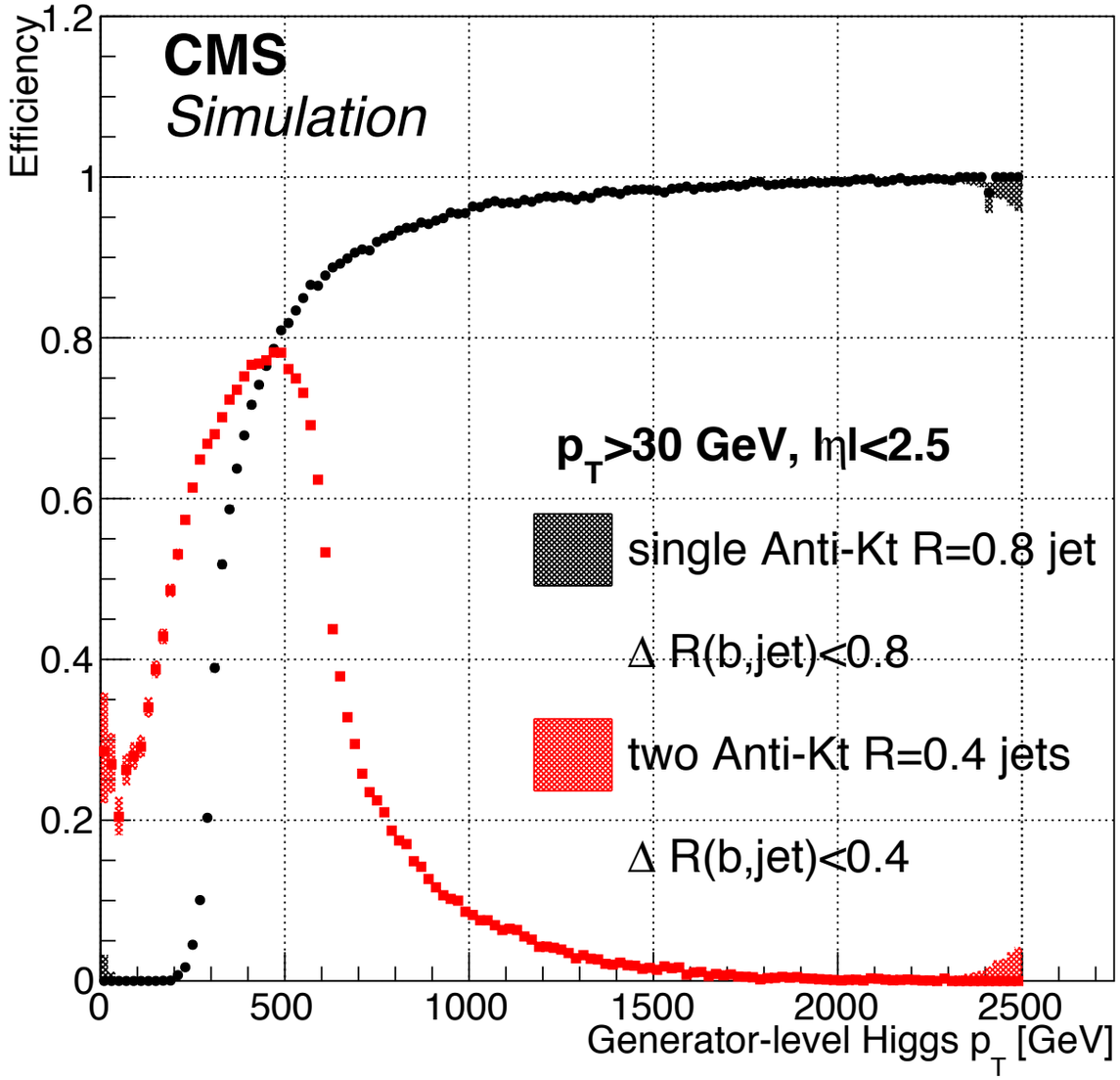

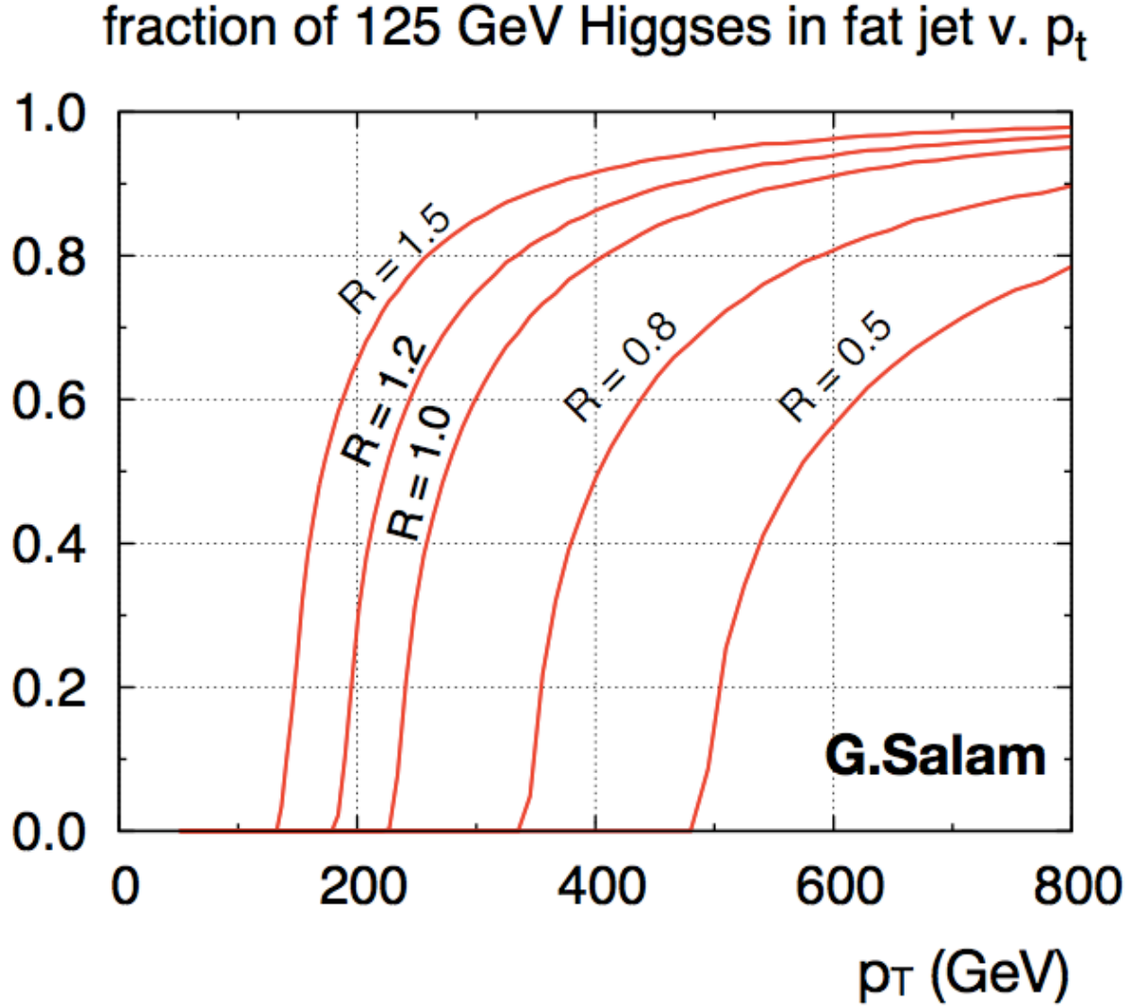

Mono H→bb: Expected Yields

$h \to b\bar{b}$ analysis	Number of events (in 2.3 fb^{-1})	
Process	Resolved	Boosted
$Z(\to \nu\bar{\nu})$+jets	29.6 ± 4.9	19.3 ± 2.0
top quark	7.3 ± 2.1	8.2 ± 2.3
W+jets	9.1 ± 2.2	10.7 ± 2.6
Diboson	2.7 ± 0.7	1.5 ± 0.5
Vh	2.0 ± 0.2	0.8 ± 0.2
Multijet	0.010 ± 0.002	0.02 ± 0.01
Total background	50.7 ± 5.4	40.5 ± 4.3
Data	44	38
$m_{Z'}$ [GeV]		
600	29.0 ± 3.5	—
800	40.4 ± 3.8	—
1000	23.3 ± 2.5	—
1200	—	23.6 ± 2.5
1400	—	13.1 ± 1.5
1700	—	5.6 ± 0.7
2000	—	2.3 ± 0.3
2500	—	0.24 ± 0.03

Re-Interpretation Of Dijet Searches

$$(g'_B)^2 = \frac{g_B^2}{2}\left(1+\sqrt{1+4\frac{\Gamma_{DM}}{\Gamma(g_B)}}\right)$$

$$\begin{aligned}
\sigma_0(g_B) &= \sigma_{DM}(g'_B, g_{DM}=1, m_{DM}) \\
&= \frac{(g'_B)^4}{\Gamma_q(g'_B)+\Gamma_{DM}}\frac{C}{M_{med}^4} \\
\rightarrow \frac{g_B^4}{\Gamma(g_B)} &= \frac{(g'_B)^4}{\Gamma_q(g'_B)+\Gamma_{DM}} \\
\rightarrow (g'_B)^2 &= \frac{g_B^2}{2}\left(1+\sqrt{1+4\frac{\Gamma_{DM}}{\Gamma(g_B)}}\right),
\end{aligned}$$

$$\Gamma_{\mathrm{V}}^{\chi\bar{\chi}} = \frac{g_{\mathrm{DM}}^2 M_{\mathrm{med}}}{12\pi}\left(1-4\frac{m_{\mathrm{DM}}^2}{M_{\mathrm{med}}^2}\right)^{1/2}\left(1+2\frac{m_{\mathrm{DM}}^2}{M_{\mathrm{med}}^2}\right) \quad ,$$

$$\Gamma_{\mathrm{AV}}^{\chi\bar{\chi}} = \frac{g_{\mathrm{DM}}^2 M_{\mathrm{med}}}{12\pi}\left(1-4\frac{m_{\mathrm{DM}}^2}{M_{\mathrm{med}}^2}\right)^{3/2} \quad ,$$

$$\Gamma_{\mathrm{V}}^{q\bar{q}} = \frac{g_q^2 M_{\mathrm{med}}}{4\pi}\left(1-4\frac{m_q^2}{M_{\mathrm{med}}^2}\right)^{1/2}\left(1+2\frac{m_q^2}{M_{\mathrm{med}}^2}\right) \quad ,$$

$$\Gamma_{\mathrm{AV}}^{q\bar{q}} = \frac{g_q^2 M_{\mathrm{med}}}{4\pi}\left(1-4\frac{m_q^2}{M_{\mathrm{med}}^2}\right)^{3/2} \quad ,$$

How To Translate (Vector)

arXiv: 1603.04156

In general, the SI DM-nucleon scattering cross section takes the form

$$\sigma_{\rm SI} = \frac{f^2(g_q) g_{\rm DM}^2 \mu_{n\chi}^2}{\pi M_{\rm med}^4} \,, \tag{4.1}$$

where $\mu_{n\chi} = m_n m_{\rm DM}/(m_n + m_{\rm DM})$ is the DM-nucleon reduced mass with $m_n \simeq 0.939\,\text{GeV}$

For the vector mediator,

$$f(g_q) = 3 g_q \,,$$

and hence

$$\sigma_{\rm SI} \simeq 6.9 \times 10^{-41}\ {\rm cm}^2 \cdot \left(\frac{g_q g_{\rm DM}}{0.25}\right)^2 \left(\frac{1\,\text{TeV}}{M_{\rm med}}\right)^4 \left(\frac{\mu_{n\chi}}{1\,\text{GeV}}\right)^2 .$$

How To Translate (Scalar)

In general, the SI DM-nucleon scattering cross section takes the form

$$\sigma_{\rm SI} = \frac{f^2(g_q) g_{\rm DM}^2 \mu_{n\chi}^2}{\pi M_{\rm med}^4}\,, \tag{4.1}$$

where $\mu_{n\chi} = m_n m_{\rm DM}/(m_n + m_{\rm DM})$ is the DM-nucleon reduced mass with $m_n \simeq 0.939\,\text{GeV}$

For the simplified model with scalar mediator exchange we follow the recommendation of ATLAS/CMS DM Forum [1] and assume that the scalar mediator couples to all quarks (like e.g. the SM Higgs). In general the formula for $f(g_q)$ is

$$f^{n,p}(g_q) = \frac{m_n}{v}\left[\sum_{q=u,d,s} f_q^{n,p} g_q + \frac{2}{27} f_{\rm TG}^{n,p} \sum_{Q=c,b,t} g_Q\right]\,. \tag{4.4}$$

these values, we find that numerically

$$f(g_q) = 1.16 \cdot 10^{-3}\, g_q\,,$$

and therefore the size of a typical cross section is

$$\sigma_{\rm SI} \simeq 6.9 \times 10^{-43}\ \text{cm}^2 \cdot \left(\frac{g_q\, g_{\rm DM}}{1}\right)^2 \left(\frac{125\,\text{GeV}}{M_{\rm med}}\right)^4 \left(\frac{\mu_{n\chi}}{1\,\text{GeV}}\right)^2\,.$$

How To Translate (Axial-Vector)

arXiv: 1603.04156

For the axial-vector mediator, the scattering is SD and the corresponding cross section can be written as

$$\sigma_{\rm SD} = \frac{3 f^2(g_q) g_{\rm DM}^2 \mu_{n\chi}^2}{\pi M_{\rm med}^4} \,. \tag{4.7}$$

In general $f^{p,n}(g_q)$ differs for protons and neutrons and is given by

$$f^{p,n}(g_q) = \Delta_u^{(p,n)}\, g_u + \Delta_d^{(p,n)}\, g_d + \Delta_s^{(p,n)}\, g_s \,, \tag{4.8}$$

Under the assumption that the coupling g_q is equal for all quarks, one finds

$$f(g_q) = 0.32 g_q \,, \tag{4.9}$$

and thus

$$\sigma^{\rm SD} \simeq 2.4 \times 10^{-42}\ {\rm cm}^2 \cdot \left(\frac{g_q g_{\rm DM}}{0.25}\right)^2 \left(\frac{1\,{\rm TeV}}{M_{\rm med}}\right)^4 \left(\frac{\mu_{n\chi}}{1\,{\rm GeV}}\right)^2 . \tag{4.10}$$

Mono Higgs (bb)

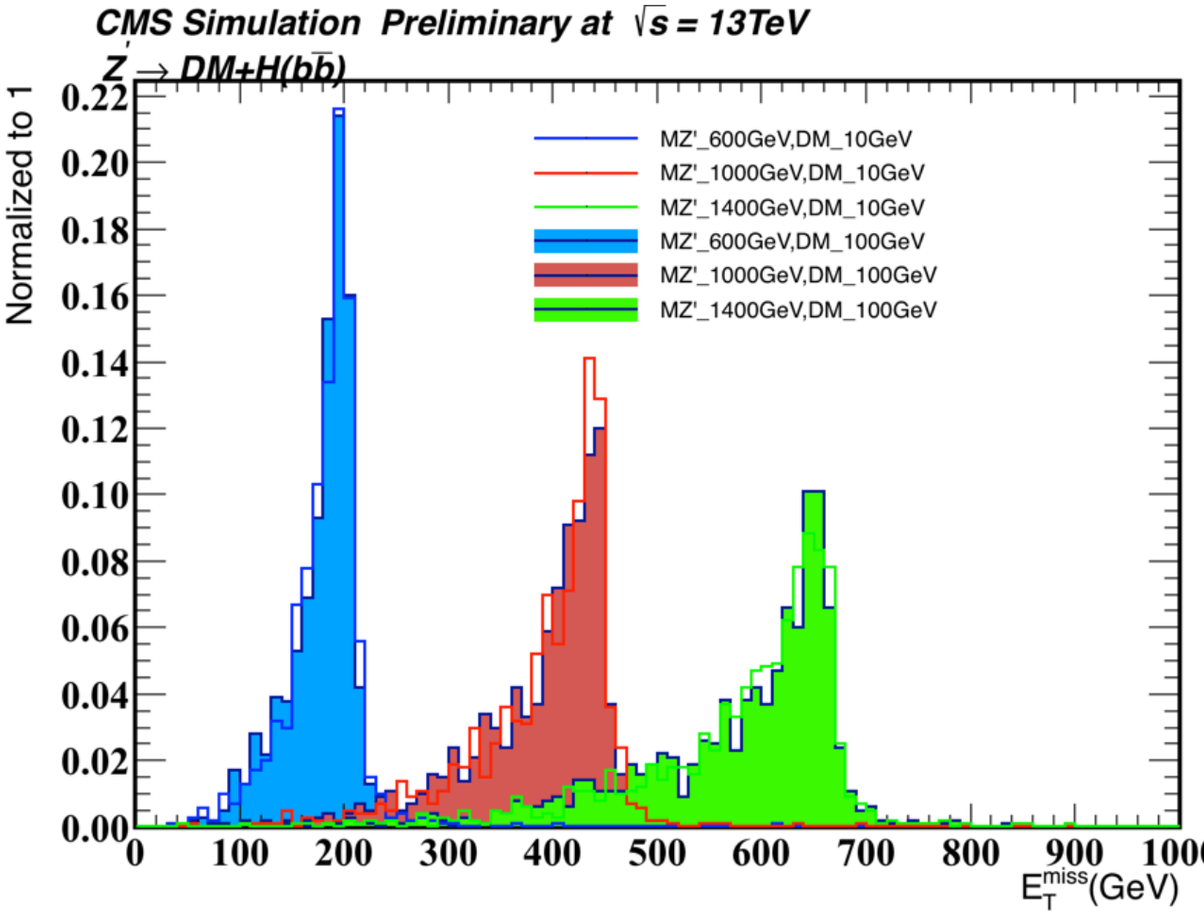

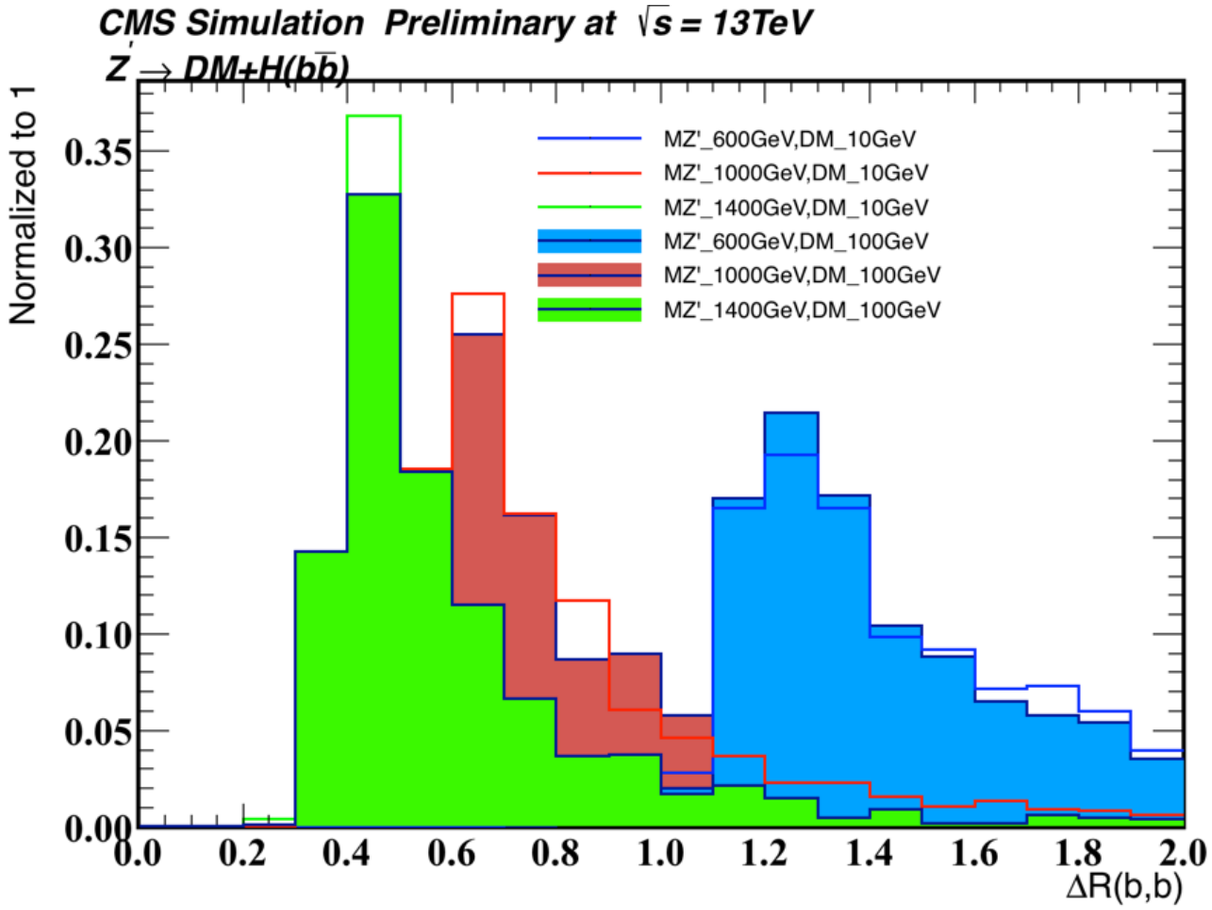

Mono Higgs (bb) Model

A Type-2 2HDM [5][6] is assumed, where Φ_u couples to up-type quarks and Φ_d couples to down-type quarks and leptons. The gauge symmetry of the SM is extended by a $U(1)_{Z'}$, with a new massive Z′ gauge boson. In this 2HDM model, only Φ_u and right-handed up-type quarks u_R are charged under the $U(1)_{Z'}$ while Φ_d and all the other SM fermions are neutral.

After electroweak symmetry breaking, the Higgs doublets attain vacuum expectation values v_u and v_d, and in unitary gauge the doublets are parametrized as

$$\Phi_d = \frac{1}{\sqrt{2}} \begin{pmatrix} -\sin\beta\, \mathrm{H}^+ \\ v_d - \sin\alpha\, \mathrm{h} + \cos\alpha\, \mathrm{H} - i \sin\beta\, \mathrm{A}^0 \end{pmatrix},$$

$$\Phi_u = \frac{1}{\sqrt{2}} \begin{pmatrix} \cos\beta\, \mathrm{H}^+ \\ v_u + \cos\alpha\, \mathrm{h} + \sin\alpha\, \mathrm{H} + i \cos\beta\, \mathrm{A}^0 \end{pmatrix},$$

where h and H are neutral CP-even scalars, $\mathrm{H}^\pm$ are charged scalars, and A^0 is a neutral CP-odd scalar. In this framework, $\tan\beta \equiv v_u/v_d$, and α is the mixing angle that diagonalizes the $\mathrm{h} - \mathrm{H}$ mass squared matrix. The α is assigned to be $\alpha = \beta - \pi/2$, in the limit where the h has SM-like couplings to fermions and gauge bosons, and $\tan\beta \geq 0.3$ as implied from the perturbativity of the top Yukawa coupling.

Mono Higgs (bb) Model

The model is described by six parameters, namely, (i) the pseudoscalar mass m_{A^0}, (ii) the DM mass m_χ, (iii) the Z′ mass $m_{Z'}$, (iv) $\tan\beta$, (v) the Z′ coupling strength $g_{Z'}$, and (vi) the coupling constant between A^0 and dark matter particles g_χ. However, only the masses m_{A^0} and $m_{Z'}$ affect the kinematic distributions and all the other parameters affect the cross sections and decay widths only, since the decay widths of A^0 and Z′ have a small effect on the kinematics. In addition, when the A^0 is on-shell, i.e. when $m_{A^0} > 2m_\chi$, the cross section has little dependence on the mass of dark matter particle m_χ. We considered a Z′ resonance mass between 600 and 2500 GeV, an A^0 mass of 300 GeV, and the mass of the DM particle is set to 100 GeV. The A^0 mass below 300 GeV is not considered due to the $b \to s\gamma$ constraints [6]. With the $\tan\beta$ and the g_χ fixed at unity, independent of the value of $g_{Z'}$, the branching ratio of decays to DM particles $\mathcal{B}(A^0 \to \chi\chi)$ is $\approx 100\%$ for an A^0 mass of 300 GeV and it starts to decrease as $m_{A^0} > 2m_t$ since the decay of $A^0 \to t\bar{t}$ becomes kinematically accessible. For example, for an A^0 mass of 400 GeV, the $\mathcal{B}(A^0 \to \chi\chi)$ reduces to 54%. The results in this document consider only the decays to DM particles. The signal model cross section is calculated using the benchmark model parameters $\tan\beta$ and g_χ set to 1 and for two different values of $g_{Z'}$:

1. the cross section is measured using the constraints from dijet searches and electroweak precision measurements [4], following:

$$g_{Z'} \leq 0.03 \times \frac{g_W}{\cos\theta_W \times \sin^2\beta} \times \frac{\sqrt{m_{Z'}^2 - m_Z^2}}{m_Z};$$

2. the cross section is obtained using a fixed coupling value $g_{Z'} = 0.8$ as considered in Ref. [7].

Mono Higgs (bb) Selection Efficiency

Cut Variable	Resolved	Boosted
AK4 Jet Kinematics	2 jets with $p_T > 30$ GeV and $\|\eta\| < 2.4$	-
AK8 Jet Kinematics	-	$p_T > 200$ GeV, $\|\eta\| < 2.4$
E_T^{miss}	> 170 GeV	> 200 GeV
p_T^{bb}	> 150 GeV	-
b tagging	Medium WP for both jets	Loose WP for two subjets
$m_{corrected}^{pruned}$	-	100 to 150 GeV
m_{bb}	100 to 150 GeV	-
$\Delta\phi$(AK4 Jet,E_T^{miss})	> 0.4	> 0.4
$\Delta\phi(\vec{p}_T^{miss}, E_T^{miss})$	< 0.7	-
additional isolated lepton (e, μ, τ_h)	0	0
additional AK4 jet	not more than one	not more than one
additional AK4 b jet	0	0

Table 1: Signal region event selections for resolved and boosted regimes.

The product of detector acceptance and full selection efficiency described above for the signal varies from 16% to 33% depending on the $m_{Z'}$ for $m_{A^0} = 300$ GeV. The average E_T^{miss} increases with $m_{Z'}$. Therefore, the selection efficiency also increases with increase in $m_{Z'}$.

Mono Higgs (bb) Fit To The E_T^{miss}

In the final fit, one nuisance parameter for the event yield of each major background, W+jets, $Z(\rightarrow \nu\nu)$+jets and Top, is allowed to change the corresponding normalizations. During the simultaneous fit of SR and CRs, the data-to-simulation scale factors for these backgrounds are constrained in such a way that the data and simulation match in the CRs and SR at the same time. The normalization of the diboson and VH backgrounds are kept fixed during the fit. The simultaneous fit of signal and background enhanced CRs allows to correlate normalization and systematic uncertainties and helps in reducing the final uncertainty. The measured data-to-simulation scale factors are close to unity. In particular, for the resolved regime these are 1.23 ± 0.17 for for $Z(\rightarrow \nu\nu)$+jets, 1.33 ± 0.19 for W+jets and 1.13 ± 0.17 for Top, while for the boosted analysis these are 0.77 ± 0.15 for $Z(\rightarrow \nu\nu)$+j, 0.95 ± 0.19 for W+jets and Top.

The results of this search are interpreted in terms of upper limit on the production cross section of DM candidates in association with a Higgs boson decaying to a pair of bottom-anti-bottom quark via $Z' \rightarrow A^0H \rightarrow \chi\bar{\chi}b\bar{b}$. The upper limits are computed at 95% confidence level using a modified frequentist method [35] computed with an asymptotic approximation [36]. A profile likelihood ratio is used as the test statistic in which systematic uncertainties are modeled as nuisance parameters. These limits are obtained as a function of $m_{Z'}$.

Figure 5 shows the expected and observed exclusion upper limit on the dark matter production cross section. The $m_{Z'}$ mass range 600 to 1777 GeV is expected to excluded with 95% CL when the signal model cross section is calculated using $g_{Z'} = 0.8$ and the observed data exclude the mass range of 600 to 1863 GeV. When the signal model cross section is calculated using constrained $g_{Z'}$ the expected exclusion range is 826 to 1890 GeV, and with the observed data exclusion range is 768 to 2036 GeV. The results are compatible with the recent results from ATLAS experiment in E_T^{miss} + H ($b\bar{b}$) decay mode [7].

Mono Higgs (bb) Systematic Uncertainties

- **Trigger**: the parameters describing the trigger efficiency curve have been varied within their statistical uncertainties. An uncertainty of 2% is estimated on the signal yield for $E_{\mathrm{T}}^{\mathrm{miss}}$ above 170 GeV.
- **Jet energy scale (JES)**: the JES for each jet is varied within one standard deviation as a function of p_{T} and η, and the efficiency of the analysis selection is recomputed to assess the variation on the normalization and $E_{\mathrm{T}}^{\mathrm{miss}}$ shape for signal and backgrounds. The effect of JES is studied on the corrected pruned mass for boosted analysis and measured to be 2%.
- **Jet energy resolution**: an uncertainty of 2% is considered due to jet energy resolution uncertainty, by recomputing the signal acceptance after smearing the energy resolution for each jet.
- **b tagging**: the b tagging scale factors are applied consistently to jets in signal and background events. An average systematic uncertainty of 6% per b jet, 12% per c jet, and 15% per light quarks and gluons is used to account for the normalization uncertainty [27].
- **Pruned mass**: The pruned mass distribution of AK8 jet is not well reproduced by simulation and different hadronizers (PYTHIA8 and HERWIG++) gives slightly different shapes, therefore, an uncertainty of 10% is used to account for the difference between hadronizers and 5% uncertainty to account for data and simulation mismatch in the high statistics W+jets CR.

Mono Higgs (bb) Systematic Uncertainties

- **Relative contribution of W+jets and Top backgrounds**: For the boosted regime, same background normalization scale factor is used for W+jets and Top backgrounds. Therefore, an uncertainty of 30% is used for these processes to take care of relative normalization of these two processes.
- **Unclustered** $E_{\mathrm{T}}^{\mathbf{miss}}$: the systematic uncertainty on the calibration of unclustered $E_{\mathrm{T}}^{\mathrm{miss}}$ (i.e. $E_{\mathrm{T}}^{\mathrm{miss}}$ associated with particles not clustered into jets) is propagated as normalization and shape uncertainty on $E_{\mathrm{T}}^{\mathrm{miss}}$.
- **Lepton efficiency and acceptance**: an uncertainty of 2% is measured by varying PDFs and the lepton efficiency scale factors within one standard deviation and recomputing the signal selection efficiency.
- **Heavy flavor**: in order to minimize the systematic uncertainty for light flavor over heavy flavor mismodeling in the simulation samples the b tag selection is kept same in SR and CRs. The remaining potential problematic issue is the uncertainty on the amount of W+gluon (with the gluon splitting to a pair of bottom and anti-bottom quarks) in the W+heavy flavor jets sample, which can be different with or without the mass cut on the Higgs boson candidate. In order to measure the size of this uncertainty, W+gluon events are estimated using two different showering models (PYTHIA8 and POWHEG+HERWIG) in the simulation. This is achieved by matching geometrically ($\Delta R < 0.3$) the reconstructed Higgs boson decay products to b hadrons. The W+gluon composition is found to be 20% different in the two samples, and this is considered as an upper limit of the uncertainty for this systematic effect.

Mono Higgs (bb) Systematic Uncertainties

- **Luminosity**: an uncertainty of 2.7% is used for the normalization of simulated samples in order to reflect the uncertainty on the integrated luminosity measurement in 2015 [33].

- **Factorization and renormalization scales**: for W+jets, Z($\rightarrow \nu\nu$)+jets and Top the alternative variations of renormalization and factorization scale is propagated which directly affect the normalization and shape of the $E_{\mathrm{T}}^{\mathrm{miss}}$.
- **Parton density function (PDF)**: The uncertainty on the signal acceptance and $E_{\mathrm{T}}^{\mathrm{miss}}$ shape due to the choice of PDF is measured following the method described by

Mono Higgs (bb) Systematic Uncertainties

PDF4LHC [34].

- **Electroweak corrections**: The effect of electroweak corrections is studied by recomputing the normalization and $E_{\mathrm{T}}^{\mathrm{miss}}$ shape for W+jets and Z($\rightarrow \nu\nu$)+jets backgrounds by varying the size of electroweak corrections by one standard deviation.
- **Backgrounds taken directly from simulation prediction**: an uncertainty of 20% is assumed for the normalization of single top (the uncertainty on the measured cross section), SM Higgs and diboson.
- **Simulation samples Statistics**: The finite size of the signal and background simulated samples are included in the normalization uncertainties and shape, such that it affects each bin of the final fitted distributions independently from the other bins.

In summary, a mixture of uncertainties related to the data-driven methods, simulation, and theory inputs is estimated to be 20% on the backgrounds in the SR. The uncertainty on the major backgrounds (W+jets, Z($\rightarrow \nu\nu$)+jets and Top) in the SR is reduced by constraining the normalization of these processes in data with the simultaneous fit of $E_{\mathrm{T}}^{\mathrm{miss}}$ shape in signal and background enriched regions. The major source of systematics which effect the fit are statistical uncertainty on Z($\rightarrow \nu\nu$)+jets, W+jets background and heavy flavor, JES and b tagging. The effect of remaining uncertainities is found to be tiny on the final fit.

Mono-H (AA)

Mono Higgs (γγ)

$\alpha = 0.190 \pm 0.035$ (stat) 20% systematic

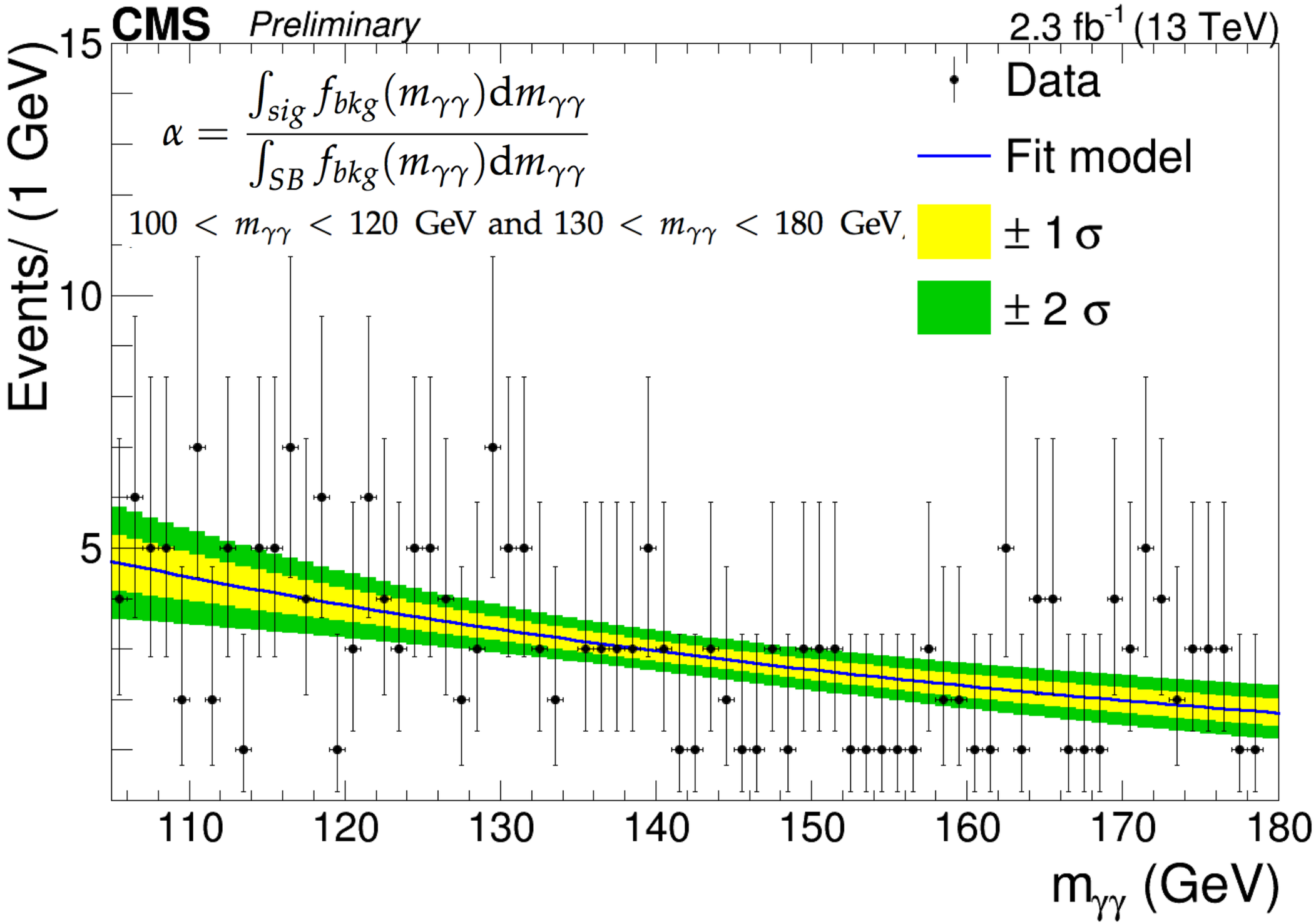

Mono Higgs (γγ)

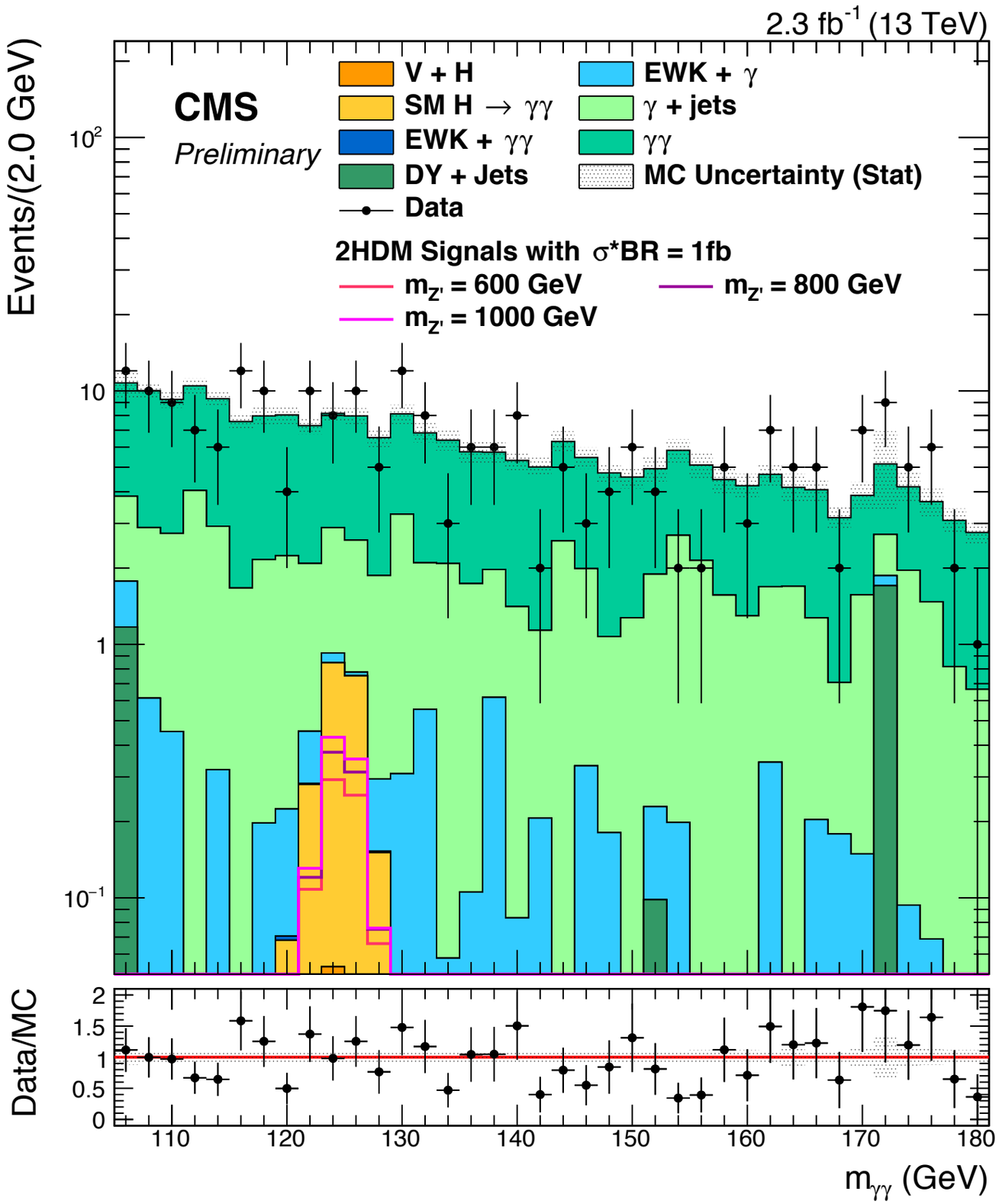

Mono Higgs (γγ): Selection And Efficiency

Table 1: Maximum allowable value of each variable used in barrel and endcap photon identification [22]. The p_T used in these formulas is expressed in GeV.

Variable	Barrel Selection	Endcap Selection
H/E	< 0.05	< 0.05
$\sigma_{i\eta i\eta}$	< 0.0102	< 0.0274
Iso_{Ch} [GeV]	< 3.32	< 1.97
ρ corrected Iso_{Neu} [GeV]	$< 1.92 + 0.14 p_T + 0.000019 (p_T)^2$	$< 11.86 + 0.0139 p_T + 0.000025 (p_T)^2$
ρ corrected Iso_{γ} [GeV]	$< 0.81 + 0.0053 p_T$	$< 0.83 + 0.0034 p_T$

$m_{Z'}$ [GeV]	Signal $A \cdot \epsilon$
600	$0.317 \pm 0.004(stat) \pm 0.026(syst)$
800	$0.399 \pm 0.004(stat) \pm 0.026(syst)$
1000	$0.444 \pm 0.004(stat) \pm 0.026(syst)$
1200	$0.474 \pm 0.004(stat) \pm 0.026(syst)$
1400	$0.492 \pm 0.004(stat) \pm 0.026(syst)$
1700	$0.493 \pm 0.004(stat) \pm 0.026(syst)$
2000	$0.351 \pm 0.004(stat) \pm 0.026(syst)$
2500	$0.213 \pm 0.004(stat) \pm 0.026(syst)$

Mono Higgs (γγ) Selection And MC

- $p_{T1}/m_{\gamma\gamma} > 0.5$
- $p_{T2}/m_{\gamma\gamma} > 0.25$
- $p_{T\gamma\gamma} > 90$ GeV
- $E_{\mathrm{T}}^{\mathrm{miss}} > 105$ GeV.

The photons in the barrel (i.e. photons with $\eta_{SC} \leq 1.4442$) and photons in the endcap ($1.556 \leq \eta_{SC} \leq 2.5$) have different selection criteria. The efficiency corresponding to the working point chosen for this analysis is 90.4% (90.0%) efficient in the barrel(endcap), while the misidentified photon rejection efficiency for the barrel(endcap) is 83.8% (81.3%), as evaluated for simulated photons with p_T above 20 GeV. The photon selection is detailed in Tab. 1. In addition to the

Jets are used in this analysis for additional cleaning of the $E_{\mathrm{T}}^{\mathrm{miss}}$ distribution. A large mismeasured $E_{\mathrm{T}}^{\mathrm{miss}}$ contribution can arise in events where jets are mismeasured. In order to suppress the QCD background the $min|\Delta\phi(jet, E_{\mathrm{T}}^{\mathrm{miss}})|$, the minimum azimuthal difference between the $E_{\mathrm{T}}^{\mathrm{miss}}$ and all jets in the event with $p_T > 50$ GeV, must be greater than 0.5. This avoids events where mismeasured jets give rise to mismeasured $E_{\mathrm{T}}^{\mathrm{miss}}$ in the event. The residual discrepancy

Mono Higgs (γγ) Selection And MC

There are several backgrounds relevant to this analysis. There is an irreducible background from the associated production of a Higgs boson and a W or Z boson (VH). Then the Z boson decays to two neutrinos or the W boson decays to a lepton and neutrino. There are additionally "resonant" but reducible backgrounds that are peaked in the invariant mass range of the Higgs boson from the other production modes of the SM Higgs boson: gluon fusion (ggH) , vector boson fusion (VBF) and production in association with top quarks (ttH). All of these resonant backgrounds are modelled at next-to-leading order in simulation. VH and VBF simulated samples are generated using POWHEG [11], while ggH and ttH samples were generated with MADGRAPH 5 and MC@NLO [12]. Additionally, there are several non-resonant background sources that can mimic the signal when they have mismodelled $E_{\mathrm{T}}^{\mathrm{miss}}$ and happen to reconstruct two photons with an invariant mass close to the mass of the Higgs boson. These include contributions from dijet and multijet events (QCD), electroweak (EWK) processes such as Z, ZZ, t, $t\bar{t}$ or W boson produced in association with 1 or 2 photons, $\gamma\gamma$, γ + jet, Drell-Yan production in association with jets with the Z boson decaying to electron pairs and neutrinos. The ZZ sample is generated with POWHEG [11] package. All other background samples are generated using MADGRAPH 5 and MC@NLO generators [12]. Parton showering is simulated in PYTHIA 8 [13].

Mono Higgs (γγ) Background Estimation

As explained in Equation 2, the predicted number of background events in the signal region is evaluated from the number of observed events in the $m_{\gamma\gamma}$ sidebands in the high-$E_{\mathrm{T}}^{\mathrm{miss}}$ region (N_{SB}^{bkg}) multiplied by a transfer factor α obtained fitting the $m_{\gamma\gamma}$ distribution in the low-$E_{\mathrm{T}}^{\mathrm{miss}}$ control region. Therefore we need to assign two different systematic uncertainties to this procedure, one on N_{SB}^{bkg} and one on α. The first one takes into account the fact that N_{SB}^{bkg} is statistically limited. This uncertainty is modeled using the gamma distribution, following the procedure in Ref. [26]. If we take N_{sig}^{bkg} as number of expected background events in the signal region (i.e. $N_{sig}^{bkg} = \alpha \cdot N_{SB}^{bkg}$), then the dispersion is $\alpha \cdot \sqrt{(N_{SB}^{bkg})^2 + 1}$. For $N_{SB}^{bkg} = 1$ the associated uncertainty is approximately 70%. As mentioned above, a 20% systematic uncertainty is also assigned to reflect the imperfect knowledge of the background $m_{\gamma\gamma}$ shape in the low-$E_{\mathrm{T}}^{\mathrm{miss}}$ region, hence on the knowledge of the α factor.

Mono Higgs (γγ) Background Estimation

The systematic uncertainty from mismeasured $E_{\mathrm{T}}^{\mathrm{miss}}$ is evaluated, following the method of Ref. [1], by comparing data and MC in a control sample which looks similar (in terms of $E_{\mathrm{T}}^{\mathrm{miss}}$) to the Higgs signal events. It has been first checked that non-resonant SM background events have a $E_{\mathrm{T}}^{\mathrm{miss}}$ distribution which looks almost identical to that of the SM $\mathrm{H} \to \gamma\gamma$ MC. Then, it has been verified that the same level of agreement holds for a control sample enriched in $\gamma +$ jet events defined by inverting the photon identification requirements on the second photon and applying a tight set of identification criteria on the first one. Finally, data and MC are compared in the $\gamma +$ jet enriched sample and the efficiency of the $E_{\mathrm{T}}^{\mathrm{miss}}$ selection in the $\gamma +$ jet control region for both data and MC is calculated. We take the scale factor among data and MC efficiency (90%) as a systematic uncertainty to be associated to mismeasured $E_{\mathrm{T}}^{\mathrm{miss}}$ tails in simulation. It is worth mentioning however that at the end of the selection the contribution of simulated background with mismeasured $E_{\mathrm{T}}^{\mathrm{miss}}$ that enter in the statistical analysis is less than 10^{-3} and comes only from the VBF and the ttH SM $\mathrm{H} \to \gamma\gamma$ production modes. The dominant background contribution coming from non-resonant processes, is estimated from data, as described in Sec 5.2.1, and is affected only by the systematic uncertainty on α.

Mono Higgs (γγ) Systematic Uncertainty

- **Trigger uncertainty**: extracted from $Z \to e^+e^-$ events using the tag-and-probe technique; its size is approximately 1%.
- **Photon energy scale uncertainty**: A 1% energy scale uncertainty is assigned. This number was derived to take into account the knowledge of the energy scale at the Z peak and of its extrapolation to higher masses.
- **Photon resolution uncertainty**: The uncertainty on the resolution corrections factors is evaluated summing and subtracting 0.5% in quadrature from the estimated additional Gaussian smearing measured at the Z peak.
- **Photon identification uncertainty**: taken as the uncertainty in the data/simulation scale factors, can be as large as 2%, depending on the p_T and the η of the photon.